NUMERICAL SIMULATIONS OF BLACK HOLE BINARIES: SECOND ORDER SPECTRAL METHODS

A Dissertation

Presented to the Faculty of the Graduate School

of Cornell University

in Partial Fulfillment of the Requirements for the Degree of

Doctor of Philosophy

by

Nicholas W. Taylor

February 2010

NUMERICAL SIMULATIONS OF BLACK HOLE BINARIES:

SECOND ORDER SPECTRAL METHODS

Nicholas W. Taylor, Ph.D.

Cornell University 2010

Current spectral simulations of Einstein's equations require writing the system in first-order form, potentially introducing instabilities and inefficiencies. This work presents a new penalty method for pseudo-spectral evolutions of second order in space wave equations. The penalties are constructed as functions of Legendre polynomials and are added to the equations of motion everywhere, not only on the boundaries as is typical in first-order formulations. Semi-discrete stability of the new method is proved using energy arguments for the scalar wave equation in flat space, and the generalization to the scalar wave on a curved background is derived. Evolutions of the second order Einstein equations in generalized harmonic form are also explored. Numerical results for multi-domain second order scalar wave and single black hole evolutions demonstrate stability and convergence . The application of the new techniques to the evolution of a 16 orbit, equal mass black hole binary is currently underway. Preliminary results are discussed, which at this time show good performance for approximately the first 10 orbits, after which the evolutions become unstable. However, the findings suggest that these difficulties can be overcome, and that the new second order penalty method will soon become a viable alternative to first order spectral evolutions of Einstein's equations.

BIOGRAPHICAL SKETCH

Nicholas William Taylor was born on March 23, 1975 in Detroit, Michigan in the United States of America. Growing up primarily in the mountains of western North Carolina, he excelled at an early age at building forts in the woods and playing with fire. He kept snakes and spiders as pets and once had four chickens, until they were eaten by the dogs. He graduated from Polk County High School in Columbus, North Carolina in June 1993, sold his three-cylinder Saab, and moved to Coesfeld, Germany. There he spent a year as a foreign exchange student getting up at 5 a.m. to ride a bicycle to the local baker and fetch Brötchen for the family. At the University of North Carolina at Chapel Hill, he contemplated a major in philosophy for a semester before deciding to study physics and mathematics. He graduated with highest distinction in May 1998. He then spent a year at Princeton University in Princeton, New Jersey studying physics until being overtaken by restlessness in Spring 2000. In August 2001, he entered the graduate physics program at Cornell University in Ithaca, New York. After exploring a number of different research topics, he began working under the supervision of Saul Teukolsky on numerical relativity in the Fall of 2005. He enjoys ice skating, sailing, and occasionally getting thrown from horses.

For my mother.

ACKNOWLEDGEMENTS

I would like to thank my advisor Saul Teukolsky for his tremendous wisdom, support, and patience during the past few years. Enthusiastic thanks also to Larry Kidder for his invaluable help with the work and especially with the SpEC code. I am indebted to Jim Alexander for giving me the opportunity to work on an experimental project earlier in my graduate career and for his guidance and encouragement while searching for a research topic. I thank Jimmy York for being a mentor and friend, and for his engaging general relativity lectures. Thanks also to Eanna Flanagan for insightful questions and comments about the work and for serving on my committee. I am grateful to Larry Kidder, Harald Pfeiffer, and Mark Scheel, the three primary authors of the indispensable SpEC code, which I used to perform the great majority of simulations in this research. Finally, I would like to express my gratitude to the many others with whom I have had many interesting and helpful discussions, often over coffee or the occasional ice skating outing, including particularly Christopher Mayes, Abdul Mroué, and Manuel Tiglio.

TABLE OF CONTENTS

LIST OF FIGURES

CHAPTER 1

INTRODUCTION

Gravitational wave observatories such as the Laser Interferometer Gravitational-Wave Observatory (LIGO) in the United States and Virgo in Italy are on the threshold of detecting gravitational waves for the first time, an event that will mark the beginning of a new era of observational astronomy [1, 2, 3]. Not only will such observations provide a probe into phenomena and regions of the Universe that are inaccessible to ordinary electromagnetic scrutiny, but they will also afford new tests of the validity of general relativity in the strong-field regime [4]. The most likely sources for detection of gravitational waves are compact binaries of neutron stars and black holes [5]. The coalescence of these objects presents a fascinating area of physics to explore, containing rich dynamics such as spin flips and momentum kicks [6, 7, 8, 9, 10, 11].

The quintessential example of a gravitational wave source is a binary black hole system, which evolves through three distinct phases: inspiral, merger, and ringdown. The inspiral phase is by far the longest, during which the binary slowly loses energy through radiated gravitational energy. Analysis of the inspiral can be performed using post-Newtonian methods, which approximate the black holes as point masses and assume the gravitational field is weak and velocities are small compared with the speed of light. Eventually, as the black holes near each other, these assumptions break down: The inspiral rate increases rapidly, and the black holes merge. After merger, the single distorted remnant black hole undergoes oscillations as it rings down to its final state. Although the ringdown can be modeled using perturbation techniques, no known analytical method exists for the final stage of the inspiral and the merger in general. In

this regime, gravity is described by the full nonlinear Einstein equations, and one must turn to numerical simulations [12].

Numerical relativity enables the investigation of dynamics in the strong-field regime while also providing calibrations of post-Newtonian and perturbation methods [13, 14, 16]. There is, however, another important benefit of numerical studies. The anticipated gravitational wave signal arriving at a detector is extremely small. Consequently, techniques such as matched filtering must be used to extract the waveform [15]. Matched filtering relies on cross-correlation of the signal with a catalog of template waveforms to improve the signal-to-noise ratio. The templates are parametrized expressions based on various analytical approximations, with parameters and functional forms chosen by comparison with exact results [17]. It is therefore important to have a large variety of high accuracy numerical waveforms in order to improve the detection likelihood. Unfortunately, binary black hole simulations are computationally expensive, typically requiring weeks of runtime on a supercomputer for even modest accuracy [16]. Finding the most efficient and accurate methods is thus one of the primary goals of numerical relativity.

Einstein's equations consist of a set of coupled, second order, hyperbolic partial differential equations with constraints. At the continuum level, these constraints must be satisfied for any solution to the equations. In a numerical simulation, the constraints can be satisfied in the initial data, but because of numerical errors during the evolution (truncation, discretization, etc.), it is impossible for them to remain satisfied exactly. One of the greatest difficulties in numerical relativity has been the search for formulations of the equations that are stable in the presence of constraint violations [12]. Of course, a formulation

that is ill-suited for numerical methods may have other inherent instabilities as well. For this reason, one of the primary features that has been sought after in a formulation of Einstein's equations is symmetric hyperbolicity, because it guarantees (for first-order systems) certain nice properties of the solutions, including existence, uniqueness, and well-posedness (roughly, stability) [18].

Once a formulation is in hand, there are essentially two methods of numerical implementation that have been used: finite difference and spectral. Roughly speaking, finite difference methods approximate the equations by replacing (spatial) derivatives with algebraic differences over grid points. They have the advantage of simplicity and robustness and are comparatively easy to stabilize. They are also tolerant of poorly formulated boundary conditions. Finite difference methods have the disadvantage, however, of inefficiency and slow convergence as the numerical resolution is increased. Spectral methods, on the other hand, approximate the solutions to the equations as truncated expansions in basis functions (e.g. a finite Fourier series). They are, roughly speaking, comparatively less forgiving of badly posed boundary conditions and relatively more difficult to implement. However, spectral methods have the advantage of superior efficiency and accuracy [18, 19, 20].

The most successful formulations of Einstein's equations to date are the generalized harmonic and Baumgarte-Shapiro-Shibata-Nakamura (BSSN) systems [16, 21, 22, 23, 24, 25]. In the generalized harmonic system, the equations take a particularly simple form that is manifestly (symmetric) hyperbolic. It was this formulation, with finite difference methods, that Pretorius used recently in his groundbreaking binary black hole simulations to obtain the first successful merger [21]. By contrast, the BSSN system is significantly more complicated,

and the robustness it seems to provide is not well understood. Nevertheless, groups at UT Brownsville (now at RIT) and the NASA Goddard Space Flight Center, also utilizing finite difference techniques, have had remarkable success in recent years with the BSSN system and the moving punctures method [22, 23]. A first-order version of the generalized harmonic system has been implemented more recently, using spectral methods, with significant success by the Cornell-Caltech group [16, 24, 25]. Since solutions to the vacuum Einstein equations are mathematically smooth (provided pathological coordinates are not chosen), spectral methods should be optimal in terms of efficiency and accuracy [19].

Even though Einstein's equations are naturally second order, they must generally be rewritten as a (fully) first-order system when using spectral methods. The reason for this is that there is little mathematical theory underlying the proper formulation of second order hyperbolic systems, and it is accordingly unclear how to evolve the second-order equations spectrally in a stable and consistent manner. On the other hand, there is an extensive literature on first-order systems, which includes theorems concerning the well-posedness of the equations and ways to impose stable boundary conditions for hyperbolic systems [18, 19, 20].

Reducing the order of the equations is usually done by introducing new variables defined as first-order time and space derivatives. The disadvantage of this is that the definitions (at least for spatial derivatives) become constraints that the solution must satisfy and thus new possible sources of instability in the system. Furthermore, each new variable must be evolved with the system, increasing the number of equations and the computational cost of the simulations. In the case of the generalized harmonic form of the equations, for example, the reduc-

tion to first order in space requires the introduction of 30 additional variables, more than doubling the number of equations and constraints in the system [24]. Since the simulations are so computationally expensive, even a small fractional increase in the cost can be a significant detriment.

Being able to evolve Einstein's equations spectrally in second-order (in space) form would avoid these additional constraints and equations, potentially allowing for greater efficiency and stability. Recently, there has been some progress toward understanding the properties of second-order systems. Gundlach and Martín-García have proposed and analyzed definitions of symmetric hyperbolicity for a general class of second order in space systems [26, 27, 28]. They have also shown how one may define characteristic modes in the second-order system and hence formulate stable boundary conditions at the continuum level. However, there is still the problem of how to impose the boundary conditions in the discrete system in a stable and consistent way.

Even for the second order in space wave equation, the simplest representative hyperbolic system, naive attempts to impose boundary conditions in the same way as in a first-order formulation generally fail. In this work, I present a new method for imposing boundary conditions in the second-order wave equation that is robust, stable, and convergent. Since the generalized harmonic form of Einstein's equations appears as ten nonlinear coupled wave equations, the extension of the scalar wave methods to this case is straightforward. While some stability problems in the second-order binary black hole evolutions remain, the results are promising and I believe the methods presented here will soon become a viable alternative to first-order spectral evolutions of Einstein's equations. It is also likely that this work will ultimately allow other formula-

tions of Einstein's equations, such as the BSSN formulation, to be treated by spectral methods without reduction to first-order form.

In Chapter 2, I discuss the new second-order method in the context of scalar waves, starting with the simplest system: the one-dimensional wave equation. Beginning with a typical spectral method for the fully first-order form of the equations, I review how penalty methods [29] can be used to impose boundary conditions and how stability can be proved using energy methods [18, 20]. In Section 2.2.3, I present the new penalty method for the one-dimensional second order in space wave equation and prove stability of the semi-discrete system. I then generalize the method to three dimensions and derive the necessary modifications for the case of a scalar wave on a curved background. Numerical results indicate that the new second-order method is at least as efficient and significantly more accurate than the equivalent first-order formulation, while also being completely stable.

In Chapter 3, I investigate the application of the method to Einstein's equations, beginning with a review of the first and second order generalized harmonic formulations. I then apply the new penalty method to the case of a single black hole and discuss solutions to the problems that arise. The single black hole evolutions display excellent convergence and stability, as well as significantly improved efficiency over the first-order code. Finally, I present preliminary results from the evolution of an equal mass, 16 orbit black hole binary. These evolutions are unfortunately not yet as successful: Although the lower resolutions show remarkably good agreement with the first-order results for as much as 15 orbits, stability and convergence issues arise at high resolution, which have not yet been resolved.

I use geometric units where appropriate, which includes the scalar wave on a curved background and all cases of Einstein's equations. In these units, the speed of light $c = 1$, which implies that [length] = [time] and [energy] = [mass]. Also, these units set $G = 1$, implying that [length] = [mass]. As is customary, all times and lengths are measured in units of the black hole mass M_1 (for the equal mass binaries I consider, this is taken to be the irreducible mass of one black hole). It is convenient to express the mass in units of km, recalling that the mass of the sun in these units is $M_\odot \simeq 1.48\,\mathrm{km}$. To convert to conventional units of mass or time, one can divide by the following factors:

$$c \simeq 3.0 \times 10^5\,\mathrm{km/s},$$

$$G/c^2 \simeq 7.42 \times 10^{-31}\,\mathrm{km/kg}.$$

For example, the 16 orbit binary black hole simulation discussed in Chapter 3 takes a total time of about $10{,}000\,\mathrm{M}_1$ to reach merger. Supposing that the black holes each have a mass of $M_1 = 10\,M_\odot$, we can divide the inspiral time in units of km by c to get the time in conventional units. In this case, the inspiral lasts about 0.5 seconds.

CHAPTER 2

SPECTRAL METHODS FOR THE WAVE EQUATION IN SECOND-ORDER FORM

2.1 Introduction

Recent advances [21, 22, 23] in numerical simulations of black holes in general relativity have led to many interesting results. Most of these simulations have been carried out with finite-difference methods. However, the vacuum Einstein equations have mathematically smooth solutions (unless pathological coordinates are chosen). Accordingly, one expects that spectral methods should be optimal in terms of efficiency and accuracy.

Einstein's equations are a hyperbolic system involving second derivatives in space and time. However, the numerical solution of hyperbolic systems using spectral methods is normally performed with a fully first-order formulation, even when the equations are naturally higher order. Reducing the order of the equations is usually achieved by introducing new variables defined as first-order time or space derivatives. The basic impetus for this first-order reduction is that there exists a well-established body of mathematical literature for first-order hyperbolic systems [18, 19, 20], which includes methods for analyzing the well-posedness of the equations and the proper way to impose stable boundary conditions in terms of characteristic variables.

The obvious disadvantage of the first-order reduction is the introduction of additional variables, whose definitions (at least for spatial derivatives) become constraints the solution must satisfy and thus new possible sources of instability

in the system. Furthermore, each new variable must be evolved, increasing the number of equations and the computational cost of the simulations. In some cases, this can be a substantial increase.

Successful simulations of Einstein's equations using spectral methods have thus far been implemented only as first-order reductions of the second-order system [24, 16]. In the case of the generalized harmonic form of the equations, the reduction to first order in space proceeds by introducing 30 additional variables, more than doubling the number of equations and constraints in the system [24]. These simulations typically require significant computational time, upwards of a hundred CPU-weeks for high resolution runs [16].

A first order in time, second order in space system has the potential to reduce the constraint-violating instabilities and the computational expense of the simulations. However, the mathematical knowledge underlying the proper formulation for such systems is much less developed. Recently, Gundlach and Martín-García have proposed and analyzed definitions of symmetric hyperbolicity for a general class of second order in space systems [26, 27]. They have also shown how one may define characteristic modes in the second-order system and thereby formulate stable boundary conditions at the continuum level.

There still remains the problem of how to impose the boundary conditions in the discrete system (using spectral methods). Even for the second order in space wave equation, the simplest representative hyperbolic system, naive attempts to impose boundary conditions in the same way as in a first-order formulation generally fail. In this work, we present a new method for imposing boundary conditions in the second-order wave equation that is robust, stable, and convergent.

Since the generalized harmonic form of Einstein's equations appears as ten nonlinear coupled wave equations, this work provides a foundation for solving Einstein's equations directly in second-order form using spectral methods. This application will appear in Chapter 3. It is likely that the work presented here will also allow other formulations of Einstein's equations, such as the BSSN (Baumgarte-Shapiro-Shibata-Nakamura) formulation, to be treated by spectral methods without reduction to first-order form.

In Section 2.2.1 we review a typical spectral method for evolving the fully first-order form of the one-dimensional wave equation. We review how boundary conditions can be imposed using penalty methods [29], and how stability of the system can be analyzed with energy methods [18, 20]. In Section 2.2.3 we present the new penalty method for the one-dimensional second order in space wave equation and prove stability of the system using energy arguments. In Section 2.3 we generalize the method to three dimensions, and in Section 2.4 we apply the method to the case of a scalar wave on a curved background.

2.2 One-Dimensional Wave Equation

We begin with the one-dimensional wave equation in flat, two-dimensional spacetime

$$\ddot{\psi} = \psi'', \tag{2.1}$$

where $\psi = \psi(x,t)$. As is typical, dots denote differentiation with respect to t, while primes denote differentiation with respect to x. We will first review a typical first-order pseudo-spectral method for evolving this equation before discussing the second-order formulation.

2.2.1 First-Order System

The wave equation in Eq. (2.1) reduces to first order by introducing the variables π and ϕ, where

$$\pi \equiv -\dot{\psi}, \tag{2.2}$$

$$\phi \equiv \psi'. \tag{2.3}$$

The negative sign in the first equation is purely a matter of convention. The first-order representation of the one-dimensional wave equation is thus

$$\dot{\psi} = -\pi, \tag{2.4}$$

$$\dot{\pi} = -\phi', \tag{2.5}$$

$$\dot{\phi} = -\pi'. \tag{2.6}$$

Equation (2.4) is just the definition of π, while the definition of ϕ in Eq. (2.3) amounts to the addition of a constraint $C = 0$, where

$$C \equiv \psi' - \phi. \tag{2.7}$$

The system of Eqs. (2.4)-(2.6) is an example of a symmetric hyperbolic system, which we now define.

A general first-order system of quasi-linear evolution equations (in any number of space dimensions) can be written as

$$\dot{\mathbf{u}} + P^i(\mathbf{u})\,\partial_i \mathbf{u} = Q(\mathbf{u}), \tag{2.8}$$

where $\mathbf{u}$ represents a vector of variables and P^i are square matrices. In the present case, for example, $\mathbf{u} = \{\psi, \pi, \phi\}$. Consider a domain Ω with boundary $\partial\Omega$ and let n^i be the outward-directed normal vector to the boundary. The system

of Eq. (2.8) is called symmetric hyperbolic if there exists a symmetric, positive-definite matrix S such that SP^n is symmetric for any direction n^i, where $P^n \equiv n_i P^i$. The system of Eqs. (2.4)-(2.6) trivially satisfies this condition, since P^x is already symmetric. As will be discussed below, symmetric hyperbolic systems have the advantage of permitting the definition of a conserved energy with boundary flux that can be written in terms of characteristic variables. These variables in turn provide the appropriate form of boundary conditions.

A characteristic variable U with speed λ is defined to be a linear combination of the variables $\mathbf{u}$, such that $U \equiv \xi \cdot \mathbf{u}$, where ξ is a left eigenvector of P^n with eigenvalue λ. The characteristic variables (also called modes) satisfy approximate advection equations

$$\partial_t U = -\lambda\, n^i \partial_i U + \ldots, \tag{2.9}$$

where the dots represent derivatives transverse to the boundary in addition to lower order terms. One can therefore think of characteristic modes as propagating into or out of the domain with respect to a particular boundary, depending on the sign of λ. Boundary conditions must be correspondingly supplied on the incoming modes at each boundary, which are those with speed $\lambda < 0$.

For the one-dimensional wave equation of Eqs. (2.4)-(2.6), the characteristic variables and speeds are

$$U_\psi = \psi, \qquad \lambda = 0, \tag{2.10}$$

$$U_\pm = \pi \pm n^x \phi, \qquad \lambda = \pm 1. \tag{2.11}$$

Here, n^x is the unit outgoing normal vector to the boundary, which in one dimension is just $n^x = \pm 1$. With this definition, U_- is incoming ($\lambda < 0$) at each boundary.

For a symmetric hyperbolic system, there exists a (not necessarily unique) conserved, positive definite energy

$$E = \int_{\Omega} \epsilon \, dV, \tag{2.12}$$

which is conserved in the sense that

$$\dot{\epsilon} = \partial_i F^i. \tag{2.13}$$

Note that this is a mathematical energy (or norm), which is not necessarily equal to the physical energy of the system. The time derivative of the energy is given by the flux through the boundary,

$$\dot{E} = \int_{\partial\Omega} F^n \, dA, \tag{2.14}$$

where $F^n \equiv n_i F^i$. For general quasi-linear systems such as Eq. (2.8), the energy is only strictly conserved when coefficients $P^i(\mathbf{u})$ in the equations are approximated as constant (in time and space) and lower order terms $Q(\mathbf{u})$ are neglected.

For the one-dimensional wave equation of Eqs. (2.4)-(2.6), the conserved energy density is

$$\epsilon = \frac{1}{2}(\pi^2 + \phi^2). \tag{2.15}$$

Using Eqs. (2.13), (2.5), (2.6), and (2.11), we get

$$F^x = -\pi\,\phi = \frac{n^x}{4}(U_-^2 - U_+^2). \tag{2.16}$$

If we consider our domain to be the interval $[-1, 1]$, then

$$\dot{E} = \frac{1}{4}\sum_{x=\pm 1}(U_-^2 - U_+^2). \tag{2.17}$$

For well-posedness and stability, one requires that the growth of the energy be controlled by specifying boundary conditions for the positive terms in $\dot{E}$. Therefore, a boundary condition must be supplied on the incoming mode U_-. For

example, with a homogeneous condition specifying $U_- = 0$ (or more generally $U_- = \kappa U_+$ for $|\kappa| \leq 1$), it follows that $\dot{E} \leq 0$. Together with the positive definiteness of the energy, this ensures that the system is stable. If instead the incoming mode is a prescribed function $U_- = f$, then we still have stability in the sense of controlling the energy with a bound that involves f.

The definition of energy given by Eq. (2.15) is not unique, but is motivated in part by a desire to obtain a sharp energy bound. For example, we could have defined the energy density with a term $a^2\psi^2$ as

$$\epsilon = \frac{1}{2}(a^2\,\psi^2 + \pi^2 + \phi^2). \tag{2.18}$$

In this case, we would obtain the additional term in $\dot{E}$

$$-\int_\Omega a^2\,\psi\,\pi\,dV \leq \frac{a}{2}\int_\Omega (a^2\psi^2 + \pi^2)\,dV, \tag{2.19}$$

where we have used the inequality $2\,uv \leq u^2 + v^2$ for any (real) u, v. We would thus arrive at the weaker estimate

$$\dot{E} \leq \frac{1}{4}\sum_{x=\pm 1}(U_-^2 - U_+^2) + a\,E. \tag{2.20}$$

With a condition on the incoming mode to control the boundary term, the system is still well-posed (i.e. energy growth no faster than exponential) in this case [18], but it is no longer stable in the sense that $\dot{E} \leq 0$.

In the semi-discrete problem, one considers the discretization in space but not time. We choose to impose boundary conditions in the semi-discrete system via penalties added to the equations on the boundaries. A penalty method imposes conditions "weakly"—that is, approximately, without completely replacing the equation of motion on the boundary [29]. Heuristically, the rationale for this is that it is not necessary to enforce boundary conditions exactly, while solving the differential equations only approximately. All that is required is that the

discrete solution converges to the continuum solution with the correct boundary conditions as the resolution is increased. We find that these methods generally yield smoother solutions and superior convergence. Furthermore, they have the advantage of making it very easy to impose arbitrary boundary conditions.

The penalty boundary conditions are added to the equations on the boundary in the form $(U_-^{\rm BC} - U_-)$, so that if the condition is satisfied then the penalties vanish. The appropriate penalty (up to an overall coefficient) for each equation can be found by projecting the boundary conditions in terms of characteristic variables to fundamental variables [31]. In other words, we first transform to characteristic variables in the first-order system Eqs. (2.4)-(2.6) on the boundary and add penalties:

$$\dot{U}_\psi = -\frac{1}{2}(U_+ + U_-), \tag{2.21}$$

$$\dot{U}_+ = -n^x U'_+, \tag{2.22}$$

$$\dot{U}_- = +n^x U'_- + c\,(U_-^{\rm BC} - U_-). \tag{2.23}$$

Only the equation for $\dot{U}_-$ has a penalty term, since there is no boundary condition on U_ψ or U_+. We then transform back to fundamental variables to obtain the first-order equations with penalties:

$$\dot{\psi}_i = -\pi_i, \tag{2.24}$$

$$\dot{\pi}_i = -\phi'_i + \frac{c}{2}\,(\delta_{i0} + \delta_{iN})(U_-^{\rm BC} - U_-), \tag{2.25}$$

$$\dot{\phi}_i = -\pi'_i - \frac{c}{2}\,n^x(\delta_{i0} + \delta_{iN})(U_-^{\rm BC} - U_-). \tag{2.26}$$

Here we have explicitly denoted grid values with a subscript i. The Kronecker delta terms $\delta_{i0} + \delta_{iN}$ indicate that penalties are applied only on the boundaries at $i = 0, N$. For a pseudo-spectral method one chooses the nodes of a Gaussian quadrature rule as collocation points. The $N + 1$ grid points x_i run from $x_0 = -1$

to $x_N = +1$. Differentiation is implemented by matrix multiplication, as in $\pi_i' \equiv \sum_j D_{ij}^{(1)} \pi_j$, with $D_{ij}^{(1)}$ the first-order differentiation matrix. The penalty coefficients should satisfy $c \to \infty$ as $N \to \infty$, in order to ensure that the continuum equations and boundary conditions are recovered in the limit [29].

The exact range of allowed values for the penalty factor c in Eqs. (2.25)-(2.26) can be determined from a semi-discrete energy analysis, which we will now show. For ease in obtaining analytical results, we choose *Gauss-Legendre-Lobatto* collocation points (see Appendix A for details). The basis functions for this choice are the Legendre polynomials $P_n(x)$ on $[-1, 1]$. We begin by writing the semi-discrete energy corresponding to Eq. (2.15):

$$E = \frac{1}{2} \left[\langle \pi, \pi \rangle + \langle \phi, \phi \rangle \right], \tag{2.27}$$

where $\langle \cdot, \cdot \rangle$ represents a discrete inner product, as in

$$\langle \pi, \pi \rangle \equiv \sum_{i=0}^{N} \omega_i \pi_i^2. \tag{2.28}$$

Here π_i are the grid values of the function π, and ω_i are the quadrature weights (see Appendix A). Taking the time derivative of the semi-discrete energy in Eq. (2.27), we obtain

$$\dot{E} = -\pi_i \phi_i \Big|_{i=0}^{N} + \frac{c}{2} \langle \pi, (\delta_{i0} + \delta_{iN}) \delta U_- \rangle - \frac{c}{2} \langle \phi, (\delta_{i0} + \delta_{iN}) n^x \delta U_- \rangle, \tag{2.29}$$

where we have used summation by parts (the discrete analogue of integration by parts) in the first term and introduced the notation $\delta U_- \equiv U_-^{\mathrm{BC}} - U_-$ in the penalty terms. The first term in Eq. (2.29) is similar to the continuum result of Eq. (2.17):

$$-\pi_i \phi_i \Big|_{i=0}^{N} = \frac{1}{4} \sum_{i=0,N} (U_-^2 - U_+^2). \tag{2.30}$$

Evaluating the discrete inner products in the latter two terms of Eq. (2.29) yields

$$\dot{E}_{\text{penalties}} = \frac{c\,\omega}{2} \sum_{i=0,N} U_- \delta U_-, \tag{2.31}$$

where we have written ω for the quadrature weight $\omega_0 = \omega_N$ at $x = \pm 1$. Noting that

$$U_- \delta U_- = \frac{1}{2}(U_-^{\mathrm{BC}2} - U_-^2 - \delta U_-^2), \tag{2.32}$$

we put things together to find

$$\dot{E} = \frac{1}{4} \sum_{i=0,N} [(1 - c\,\omega) U_-^2 - U_+^2 + c\,\omega\,(U_-^{\mathrm{BC}2} - \delta U_-^2)]. \tag{2.33}$$

The condition on the penalty factor c for stability depends on the boundary condition we impose on U_-^{BC}. Requiring $\dot{E} \leq 0$, we find:

$$U_-^{\mathrm{BC}} = 0 \qquad \Rightarrow \quad c \geq \frac{1}{\omega}, \tag{2.34}$$

$$U_-^{\mathrm{BC}} = \kappa\, U_+ \quad \Rightarrow \quad \frac{1}{\omega\,\kappa^2} \geq c \geq \frac{1}{\omega}, \tag{2.35}$$

where $|\kappa| \leq 1$. The strictest condition is obtained by insisting that the energy be bounded by the continuum result of Eq. (2.17) for arbitrary U_-^{BC}:

$$\dot{E} \leq \dot{E}_{\mathrm{continuum}} \iff c = \frac{1}{\omega}. \tag{2.36}$$

The situation is slightly different when considering the semi-discrete energy for a multi-domain problem. For example, suppose we consider the interval $[-2, 2]$ with an inner boundary at $x = 0$. The energy calculation up to Eq. (2.33) is identical on each subdomain. The key difference is that now the incoming mode at the interface boundary is supplied by the adjacent subdomain. If we denote the intervals $[-2, 0]$ and $[0, 2]$ with subscripts 1 and 2, respectively, then at $x = 0$:

$$U_{1-}^{\mathrm{BC}} = U_{2+}, \tag{2.37}$$

$$U_{2-}^{\mathrm{BC}} = U_{1+}. \tag{2.38}$$

The terms in $\dot{E}$ at $x = 0$ are then:

$$\begin{aligned}(1 - c\,\omega)U_{1-}^2 - (1 - c\,\omega)U_{1+}^2 - c\,\omega\,\delta U_{1-}^2 \\ + (1 - c\,\omega)U_{2-}^2 - (1 - c\,\omega)U_{2+}^2 - c\,\omega\,\delta U_{2-}^2.\end{aligned} \tag{2.39}$$

This quadratic form is negative semi-definite if and only if $c = 1/\omega$. On a multi-domain problem the value of c required for stability is therefore fixed, regardless of what boundary condition one imposes at the external boundaries. Note that we have assumed that the penalties at the interface boundary enforce conditions on the incoming modes only. It is possible to penalize arbitrary combinations of the variables at interfaces and thereby to obtain different stability conditions (see e.g. [32]), but we do not consider this refinement here.

On an arbitrary domain, the definition of the discrete inner product must be modified. For instance, if we want to solve the problem on a domain Ω, and we have a mapping $\mu : [-1, 1] \to \Omega$, then the Jacobian of the mapping is inherited from the continuum inner product:

$$\langle f, g\rangle \equiv \sum_{i=0}^{N} \omega_i\, f_i\, g_i\, \mu_i'. \tag{2.40}$$

Since the penalty terms in Eq. (2.29) contain Kronecker deltas that pick out specific terms from the sums, the values of c we arrive at are modified by a Jacobian factor: $c \to c/\mu'$. For simplicity we will assume that we are dealing with the fundamental interval $[-1, 1]$ unless otherwise stated, so that no Jacobians are needed.

Although we derived the semi-discrete energy estimate on Legendre points, this is not a limitation. One could implement the system on Gauss-Chebyshev-Lobatto points using, for example, the Chebyshev-Legendre method [33]. With the Chebyshev-Legendre method, one uses the equations as defined on Legendre grid points and implements them on a Chebyshev grid by interpolating the

penalty functions to the new grid points. In this way, one is still implementing the equations with the same penalty functions, albeit evaluated at different grid points. However, this is in fact not necessary: in practice the system works well without modification on a Chebyshev grid by simply using the same grid values of the penalties as derived for Legendre points.

It is also worth noting that stability conditions derived from strict energy arguments can generally be relaxed to a degree. The penalty factor c, which was found to be $1/\omega = N(N+1)/2$ for Legendre methods, can be optimized by trial and error to obtain the least restrictive *Courant-Friedrichs-Lewy* (CFL) condition while maintaining stability. This is discussed, for example, in [34].

Stability of the *fully* discrete problem can be explored by examining eigenvalues. One writes the entire system as $\dot{y} = Ay$, a form suitable for a time-stepping algorithm, where the vector y represents the grid values of all the fields. The eigenvalues of the matrix A can then be plotted in the complex plane and compared with the stability region of the time-stepper of choice. One must use care when computing such eigenspectra, as they can be very sensitive to round-off error, and surprisingly high precision must sometimes be used. In general, positive real parts of the eigenvalues imply instability, while the spectral radius (maximum amplitude of eigenvalues) is roughly inversely proportional to the maximum allowed time-step [18] (the exact relation depends on the time-stepping algorithm being used).

A typical eigenspectrum for the system in Eqs. (2.24)-(2.26) on two subdomains is shown in Fig. 2.1. Curiously, the large amplitude conjugate pair of eigenvalues on Chebyshev points is absent on the Legendre grid. This implies that there is a less restrictive CFL condition for the system on Legendre grid

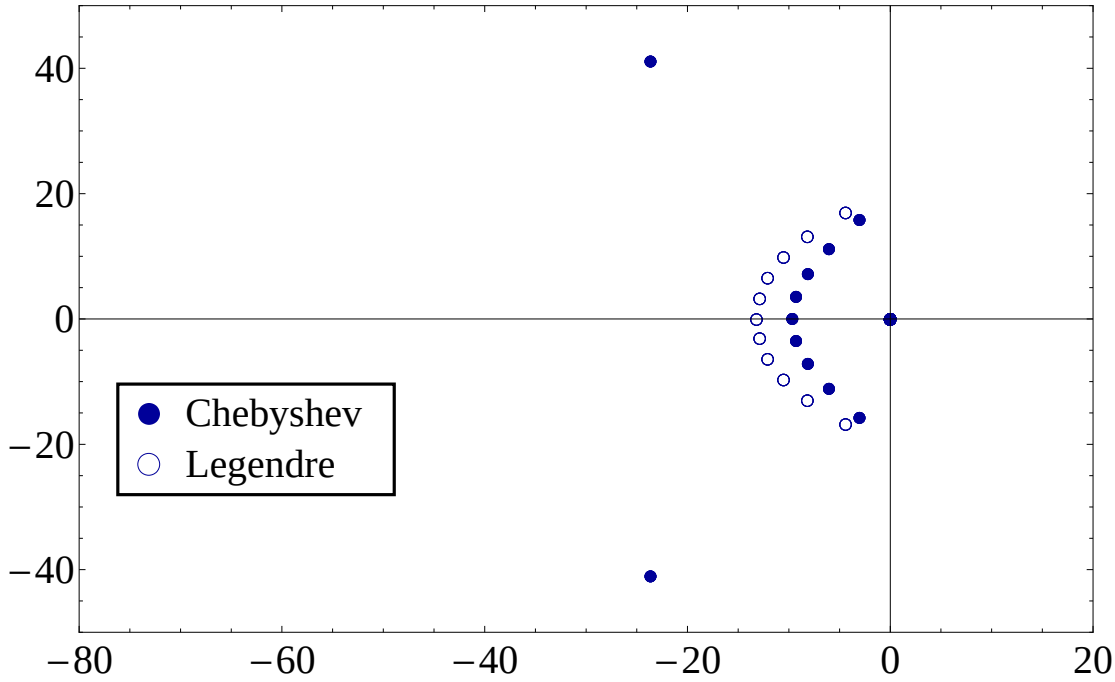

Figure 2.1: Eigenvalues in the complex plane of the first-order system Eqs. (2.24)-(2.26). This eigenspectrum is for a two-domain problem on [-1,1], with an inner boundary at $x = 0$, penalty factors $c = N(N + 1)/2$, outer boundary conditions $U_{-}^{\mathrm{BC}} = 0$, and $N + 1 = 11$ grid points per subdomain. Results for Legendre- and Chebyshev-Lobatto grids are shown for comparison.

points, and this is indeed the case for this particular system. However, it is unlikely that this difference carries over to more general systems [20]. For instance, we find no significant difference in time-stepping conditions on Chebyshev or Legendre grids for the *three-dimensional* wave equation (in flat or curved space). It is also worth noting that eigenvalue stability is insufficient to prove that the system is actually stable and convergent, but it is suggestive [20].

2.2.2 Second Order in Space

The second order in space system is

$$\dot{\psi} = -\pi, \tag{2.41}$$

$$\dot{\pi} = -\psi''. \tag{2.42}$$

The characteristic variables are the same as those of the first-order reduction with $\phi \to \psi'$:

$$U_\psi = \psi, \qquad \lambda = 0, \tag{2.43}$$

$$U_\pm = \pi \pm n^x \psi', \qquad \lambda = \pm 1, \tag{2.44}$$

The energy and flux are the same as well:

$$\epsilon = \frac{1}{2}(\pi^2 + \psi'^2) \quad \Rightarrow \quad \dot{E} = \frac{1}{4}\sum_{x=\pm 1}(U_-^2 - U_+^2). \tag{2.45}$$

The difficulty arises in the semi-discrete case when we try to find appropriate penalties by projecting from characteristic variables, as was done in the first-order system. The boundary condition $\delta U_- \equiv U_-^{\rm BC} - U_- = 0$ is now a *differential* as opposed to an *algebraic* condition:

$$\pi - n^x \psi' = U_-^{\rm BC}. \tag{2.46}$$

One therefore obtains a condition on ψ' at the boundary, but not on ψ itself (there is no boundary condition on U_ψ).

The system one would arrive at by naively following the same procedure as in the first-order case is

$$\dot{\psi}_i = -\pi_i, \tag{2.47}$$

$$\dot{\pi}_i = -\psi_i'' + c\,(\delta_{i0} + \delta_{iN})\,\delta U_-. \tag{2.48}$$

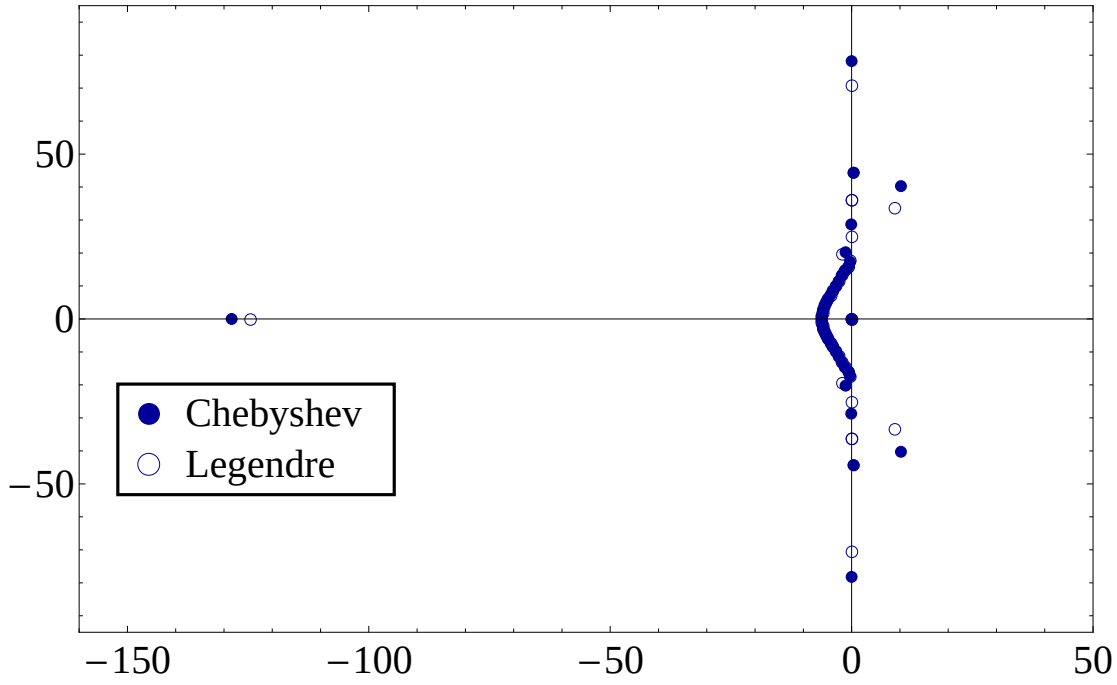

Figure 2.2: Eigenvalues of a typical unstable second-order system Eqs. (2.47)-(2.48). This eigenspectrum is for a two-domain problem on [-1,1], with an inner boundary at $x = 0$, penalty factors $c = N(N+1)/2$, outer boundary conditions $U_-^{\rm BC} = 0$, and $N + 1 = 11$ grid points per subdomain. Results for Legendre- and Chebyshev-Lobatto grids are shown for comparison.

We might try applying a penalty to Eq. (2.47) also:

$$\dot{\psi}_i = -\pi_i + c_1(\delta_{i0} + \delta_{iN})\,\delta U_-, \tag{2.49}$$

$$\dot{\pi}_i = -\psi_i'' + c_2\,(\delta_{i0} + \delta_{iN})\,\delta U_-. \tag{2.50}$$

These equations are generally unstable, particularly when evolved on multiple subdomains with at least one interface boundary. The penalty factors c_1, c_2 can be fine-tuned by trial and error to obtain approximately stable evolutions in some cases, but not robustly so. The error in ψ tends to grow exponentially, ruining the evolutions within a few hundred crossing times. Figure 2.2 shows a typical eigenspectrum for the system in Eqs. (2.47)-(2.48) on two subdomains. The eigenvalues with positive real parts clearly indicate instability.

2.2.3 Second Order Penalty Method

We will now derive a way to impose penalty boundary conditions for the second-order system that yields a robust, stable result. For the semi-discrete problem, we once again choose Gauss-Legendre-Lobatto collocation points. We begin by writing the second-order equations in the form

$$\dot{\psi}_i = -\pi_i + p, \tag{2.51}$$

$$\dot{\pi}_i = -\psi_i'' + q, \tag{2.52}$$

where p and q represent as yet undetermined penalties. The semi-discrete energy is

$$E = \frac{1}{2}\left[\langle \pi, \pi \rangle + \langle \psi', \psi' \rangle\right]. \tag{2.53}$$

Taking the time derivative, we find

$$\dot{E} = -\psi_i' \pi_i \Big|_0^N + \psi_i' \, p_i \Big|_0^N + \langle \pi, q \rangle - \langle \psi'', p \rangle, \tag{2.54}$$

where we have used summation by parts in the first two terms. The first term is like the continuum result for the first-order system in Eq. (2.17):

$$-\psi_i' \pi_i \Big|_0^N = \frac{1}{4} \sum_{i=0,N} (U_-^2 - U_+^2). \tag{2.55}$$

Since the projection of boundary conditions from characteristic to fundamental variables is unambiguous in the variable π, we will write the penalty q as in Eq. (2.48):

$$q = \frac{a}{\omega} \left(\delta_{i0} + \delta_{iN}\right) \delta U_-, \tag{2.56}$$

where a is an undetermined constant and ω is the quadrature weight at $x = \pm 1$. The factor $1/\omega$ is explicitly written in anticipation of its cancellation when evaluating the third term in Eq. (2.54):

$$\langle \pi, q \rangle = a\pi_0 \, \delta U_-^0 + a\pi_N \delta U_-^N. \tag{2.57}$$

If we also choose the penalty p in Eq. (2.51) to have a similar value on the boundary

$$p = -a\,\delta U_-, \tag{2.58}$$

then the second and third terms in Eq. (2.54) combine to form the expression

$$\psi_i' \, p_i \Big|_0^N + \langle \pi, q \rangle = \frac{a}{2} \sum_{i=0,N} (U_-^{\mathrm{BC}\,2} - U_-^2 - \delta U_-^2). \tag{2.59}$$

Note that we do not define p on the boundary with a factor of $1/\omega$, because the second term in Eq. (2.54) arises out of summation by parts as opposed to being picked out from the discrete sum by a Kronecker delta.

The difficulty in the energy analysis is the last term in Eq. (2.54), whose appearance is inevitable because of the derivatives in the definition of energy in Eq. (2.53). Such a term did not arise in the first-order energy estimate, precisely because the first-order energy in Eq. (2.27) did not contain any derivatives. Fortunately, it turns out we can eliminate the inner product $\langle \psi'', p \rangle$ by allowing the penalty p to be non-zero throughout the domain and by constructing it to be orthogonal to ψ''.

The scalar field ψ in the semi-discrete solution is an interpolating N^{th}-order polynomial [19]. Therefore, ψ'' is an N–2 order polynomial, and the product $\psi'' p$ is at most a polynomial of order $2N-2$. It follows that the quadrature integral is exact:

$$\langle \psi'', p \rangle = \int_{-1}^{1} \psi''(x) p(x)\, dx. \tag{2.60}$$

This inner product will automatically vanish if the penalty p is a linear combination of the Legendre polynomials $P_N(x)$ and $P_{N-1}(x)$, which are orthogonal to any polynomial of degree $N-2$ or less. We are therefore provided with two degrees of freedom for constructing the function p, which is sufficient to sat-

isfy the boundary values defined in Eq. (2.58). We make use of the following polynomials, constructed to take the values 0 or 1 at $x = \pm 1$:

$$f(x) = \frac{1}{2}(-1)^N \left[P_N(x) - P_{N-1}(x)\right], \tag{2.61}$$

$$g(x) = \frac{1}{2}\left[P_N(x) + P_{N-1}(x)\right]. \tag{2.62}$$

If we now define the penalty p to be

$$p = p_0\, f(x) + p_N\, g(x), \tag{2.63}$$

where p_0 and p_N represent the endpoint values of Eq. (2.58), then the penalty function p will have the correct boundary values while also satisfying

$$\langle \psi'', p \rangle = 0. \tag{2.64}$$

Putting things together, we find

$$\dot{E} = \frac{1}{4} \sum_{i=0,N} \left[(1-2a)U_-^2 - U_+^2 + 2a(U_-^{\mathrm{BC}2} - \delta U_-^2)\right], \tag{2.65}$$

which is just like Eq. (2.33) for the first-order system with $2a \leftrightarrow c\,\omega$. The conclusions reached previously for c therefore carry over: a multi-domain problem with arbitrary outer boundary conditions is stable only if $a = 1/2$. Hence, the second-order system with penalties is

$$\dot{\psi}_i = -\pi_i - \frac{1}{2}\left[f(x)\,\delta U_+^0 + g(x)\,\delta U_+^N\right], \tag{2.66}$$

$$\dot{\pi}_i = -\psi_i'' + \frac{1}{2\omega}\left[\delta_{i0}\,\delta U_+^0 + \delta_{iN}\,\delta U_+^N\right]. \tag{2.67}$$

Of course, one needs to be concerned not only with *stability*, but also *consistency*—that is, the system should reproduce the continuum equations in the limit as $N \to \infty$. The penalty p on the $\dot{\psi}$ equation in Eq. (2.66) is applied throughout the domain and not only on the boundaries. Moreover, it does not scale as

N^2, so consistency might seem dubious. However, the penalty on $\dot{\pi}$ in Eq. (2.67) does scale as N^2 and is applied only on the boundaries. Therefore, the condition $\delta U_- \to 0$ on the boundary as $N \to \infty$ is enforced. This also implies $p \to 0$ in turn, so consistency follows.

Although the second-order energy argument was performed on Legendre points, the equations can be implemented on any grid, just as in the first-order system discussed in Section 2.2.1. Eigenvalues of the fully discrete system imply stability here as well, as shown in Fig. 2.3 for a representative two-domain problem. The spectral radius is somewhat larger than in the first-order spectrum in Fig. 2.1. However, we find that differences in CFL conditions essentially disappear for more general systems, including the three-dimensional wave equation in flat or curved space.

2.3 Three-Dimensional Wave Equation

Let us now consider the three-dimensional second-order in space wave equation

$$\dot{\psi} = -\pi, \tag{2.68}$$

$$\dot{\pi} = -\partial_i \partial^i \psi. \tag{2.69}$$

The characteristic modes and speeds of this system are

$$U_\psi = \psi, \qquad \lambda = 0, \tag{2.70}$$

$$U_\pm = \pi \pm n^i \partial_i \psi, \qquad \lambda = \pm 1, \tag{2.71}$$

$$U_i^0 = \partial_i \psi - n_i n^j \partial_j \psi, \qquad \lambda = 0, \tag{2.72}$$

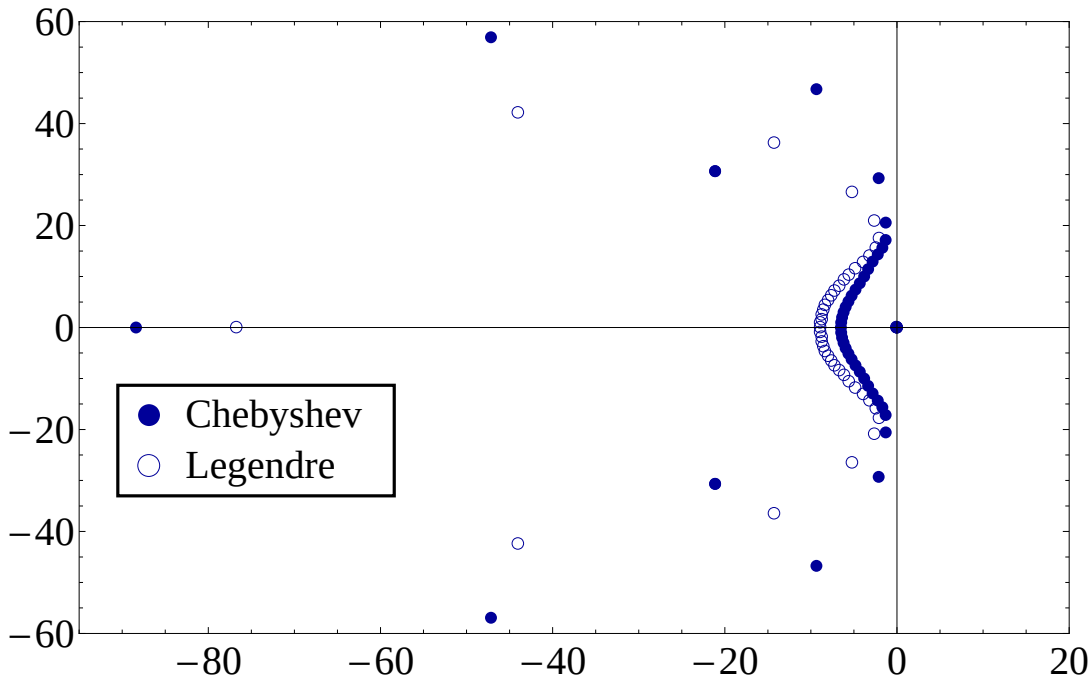

Figure 2.3: Eigenvalues in the complex plane of the second-order system Eqs. (2.66)-(2.67) on two subdomains covering $[-1, 1]$, with an inner boundary at $x = 0$, outer boundary conditions $U_{-}^{\mathrm{BC}} = 0$, and $N + 1 = 11$ grid points per subdomain. Results for Legendre- and Chebyshev-Lobatto grids are shown for comparison.

where n^i is the outward-directed unit normal to the boundary. These are the same as the characteristic variables of the first-order system obtained by defining $\phi_i \equiv \partial_i \psi$. Usually, one thinks of characteristic variables as being defined only for first-order systems, but they can be generalized to second-order systems. One way to do this is to *define* the second-order modes as those combinations U of variables $(\pi, \partial_i \psi)$ that satisfy

$$\dot{U} = -\lambda\, n^i \partial_i U + \ldots, \tag{2.73}$$

where the dots represent derivatives transverse to n^i plus lower order terms [26]. As a consequence of this definition, the transverse derivatives U_i^0 are automatically zero-speed modes (in fact, they can be given arbitrary speeds). Moreover, the characteristic variables in Eq. (2.71) are unique only up to addition of these zero-speed modes. For example, we could redefine $U_\pm$ as $U_\pm + X^i U_i^0$ for arbitrary (fixed) X^i. As discussed in Ref. [26], this ambiguity is removed for a symmetric hyperbolic system by requiring the existence of a conserved energy that is quadratic in the modes. Here, that amounts to taking the definitions in Eqs. (2.70)-(2.72) as they are. The conserved energy density for this system is

$$\epsilon = \frac{1}{2}(\pi^2 + \partial^i \psi\, \partial_i \psi). \tag{2.74}$$

Note that this energy is indeed quadratic in terms of the characteristic modes:

$$2\epsilon = \frac{1}{2}(U_+^2 + U_-^2) + U^{0i} U_i^0. \tag{2.75}$$

In analogy with the one-dimensional case in Eq. (2.17), the flux is

$$\dot{E} = \frac{1}{4} \int_{\partial\Omega} (U_-^2 - U_+^2)\, d^2x, \tag{2.76}$$

where $\partial\Omega$ represents the boundary of the domain.

Now consider the semi-discrete problem in three-dimensions. We encounter a few issues in generalizing from the one-dimensional case. For one, if the

boundary of the domain contains edges or corners, the normal vectors there (and hence characteristic modes) are not well-defined. For reasons that will become clear below, we resolve this ambiguity by defining the normal vectors as follows. We will use upper case $\mathbf{N}$ and lower case $\mathbf{n}$ to denote the unnormalized and unit normal vectors, respectively. For simplicity, suppose the domain Ω is a cube with $x, y, z \in [-1, 1]$. On boundary faces (codimension 1), one coordinate is fixed (e.g. the $x = +1$ face). We define face normals on a boundary with a fixed i^{th} coordinate as

$$\mathbf{N} = \omega_j \, \omega_k \, \mathbf{n}, \tag{2.77}$$

where ω_j, ω_k are the quadrature weights (see Appendix A) corresponding to the two free dimensions, and $\mathbf{n}$ is the usual (Cartesian) unit normal vector in the i^{th} direction. On edges and corners, the normal vector is defined to be the sum of the normals to the adjacent boundary faces. For example, the normal vector at the corner $(x, y, z) = (1, 1, 1)$ is defined to be

$$\mathbf{N} = \omega_y \, \omega_z \, \hat{\mathbf{x}} + \omega_x \, \omega_z \, \hat{\mathbf{y}} + \omega_x \, \omega_y \, \hat{\mathbf{z}}. \tag{2.78}$$

The second-order system with penalty functions p, q is

$$\dot{\psi} = -\pi + p, \tag{2.79}$$

$$\dot{\pi} = -\partial_i \partial^i \psi + q, \tag{2.80}$$

where for conciseness we have suppressed indices representing grid values (e.g. $\psi = \psi_{ijk}$). Consider the semi-discrete energy

$$E = \frac{1}{2} \left[\langle \pi, \pi \rangle + \langle \partial^i \psi, \partial_i \psi \rangle \right]. \tag{2.81}$$

The computation of $\dot{E}$ proceeds analogously to the one-dimensional case, except for complications due to the corners and edges. To see this, consider the following term that arises in taking the time derivative of Eq. (2.81), up to an overall

sign:

$$\langle \partial^l \psi, \partial_l \pi \rangle \equiv \sum_{i,j,k} \omega_i \omega_j \omega_k \, \partial^l \psi \, \partial_l \pi. \tag{2.82}$$

We use summation by parts in this expression and obtain three boundary terms—one for each l. For example, from $l = z$ we get

$$\langle \partial^z \psi, \partial_z \pi \rangle = \sum_{i,j} \omega_i \omega_j \left[\partial_z \psi \, \pi \right]_{z=-1}^{+1} - \langle \partial^z \partial_z \psi, \pi \rangle. \tag{2.83}$$

Each point on an edge receives a contribution from two such boundary terms, while points on corners get a contribution from all three. On the cube at the corner point $(1, 1, 1)$, for example, the value obtained is

$$(\omega_x \omega_y \, \partial_z \psi + \omega_x \omega_z \, \partial_y \psi + \omega_y \omega_z \, \partial_x \psi) \, \pi. \tag{2.84}$$

We would like to be able to write this in terms of a normal vector N^i and characteristic modes as

$$N^i \partial_i \psi \, \pi = \frac{|\mathbf{N}|}{4} (U_+^2 - U_-^2), \tag{2.85}$$

and this is precisely the reason for the definition of normal vectors on edges and corners given above. Thus, Eq. (2.82) can be written

$$\langle \partial^l \psi, \partial_l \pi \rangle = \frac{1}{4} \sum_{\partial\Omega} |\mathbf{N}| (U_+^2 - U_-^2) - \langle \partial^i \partial_i \psi, \pi \rangle, \tag{2.86}$$

where the sum is over all boundary points, including edges and corners. The magnitude of the normal vector $|\mathbf{N}|$ encodes the appropriate quadrature weight factors for boundaries of any codimension.

In a similar way, the terms in $\dot{E}$ due to the penalty p of Eq. (2.79) can be written

$$\langle \partial^i \psi, \partial_i p \rangle = \sum_{\partial\Omega} |\mathbf{N}| n^i \partial_i \psi \, p - \langle \partial^i \partial_i \psi, p \rangle. \tag{2.87}$$

The penalty q in Eq. (2.80) is applied only on the boundary, and it takes the value

$$q\Big|_{\partial\Omega} = \frac{1}{2}\frac{|\mathbf{N}|}{\omega_x\omega_y\omega_z}\delta U_-. \tag{2.88}$$

On a boundary face with fixed i^{th}-coordinate, this reduces to

$$q = \frac{1}{2}\frac{1}{\omega_i}\delta U_-, \tag{2.89}$$

just as in the one-dimensional system. Assuming the boundary value of p satisfies

$$p\Big|_{\partial\Omega} = -\frac{1}{2}\delta U_-, \tag{2.90}$$

the penalty contributions to $\dot{E}$ combine to give

$$\dot{E}_{\text{penalties}} = \frac{1}{2}\sum_{\partial\Omega}|\mathbf{N}|U_-\delta U_- - \langle\partial^i\partial_i\psi, p\rangle. \tag{2.91}$$

With everything included, the energy flux is

$$\dot{E} = \frac{1}{4}\sum_{\partial\Omega}|\mathbf{N}|\left(U_-^{\text{BC}2} - U_+^2 - \delta U_-^2\right) - \langle\partial^i\partial_i\psi, p\rangle. \tag{2.92}$$

We would like to eliminate the last term with an appropriate choice of bulk penalty function p, as was done in the one-dimensional case. The most obvious generalization of the one-dimensional approach would be to construct p out of polynomials θ_n satisfying $\langle\partial^i\partial_i\psi, \theta_n\rangle = 0$. Unfortunately, this cannot be done. There are in general only about $2N^2$ such functions θ_n—not enough to satisfy $6N^2+2$ boundary conditions (a proof is provided in Appendix B).

Alternatively, one could allow the penalty p to depend explicitly on the scalar field ψ. One way of doing this is to split the offending inner product term of Eq. (2.92) into contributions from the boundary and the interior of the domain:

$$\langle\Delta\psi, p\rangle = \langle\Delta\psi, p\rangle\Big|_{\partial\Omega} + \langle\Delta\psi, p\rangle\Big|_{\text{interior}}, \tag{2.93}$$

where $\Delta\psi \equiv \partial^i \partial_i \psi$. Considering the values of p on the boundary to be determined by Eq. (2.90), the first term on the right-hand of Eq. (2.93) is fixed. We can then define p on the interior of the domain to be

$$p_{\text{interior}} \equiv -\frac{\langle \Delta\psi, p \rangle\big|_{\partial\Omega}}{\langle \Delta\psi, \Delta\psi \rangle\big|_{\text{interior}}} \Delta\psi, \tag{2.94}$$

provided $\Delta\psi_{\text{interior}} \neq 0$. With this definition, the discrete sum over the interior cancels the sum over the boundary in Eq. (2.93), and the inner product $\langle \Delta\psi, p \rangle$ vanishes. If $\Delta\psi \equiv 0$, we cannot use Eq. (2.94), but in this case there would be no need since then $\langle \Delta\psi, p \rangle \equiv 0$. One way this recipe could fail is if $\Delta\psi$ vanishes on the interior of the domain, but not on the boundary. However, this is extremely unlikely in a numerical simulation. We find that methods like this (in which the penalty p depends explicitly on ψ) generally yield stability, but because of accumulation of round-off error, they suffer from lack of convergence as resolution is increased.

Abandoning any explicit dependence on ψ in the penalties, we seek instead to construct p so as to *minimize* the inner product $\langle \partial^i \partial_i \psi, p \rangle$ of Eq. (2.92). It turns out this can be done by using a penalty constructed out of the same functions f, g defined in Eqs. (2.61)-(2.62) for the one-dimensional problem. Here we will give a summary of the result; a derivation is provided in Appendix C. We define one-dimensional functions f, g along each dimension and write their grid values as $f_i = f(x_i)$, $f_j = f(y_j)$, $f_k = f(z_k)$ (and similarly for g). Assuming the values of the penalty function p on the domain boundary $\partial\Omega$ are given, the grid values on the interior of the domain are

$$\begin{aligned} p_{ijk} = {} & p_{0jk}\, f_i + p_{Njk}\, g_i + p_{i0k}\, f_j + \ldots && \text{(faces)} \\ & - p_{00k}\, f_i f_j - p_{N0k}\, g_i f_j - \ldots && \text{(edges)} \\ & + p_{000}\, f_i f_j f_k + p_{N00}\, g_i f_j f_k + \ldots && \text{(corners)} \end{aligned} \tag{2.95}$$

The bulk penalty picks up a contribution from each boundary face, edge, and corner. The assumption of a cubic domain is not a limitation, as it is straightforward to generalize this procedure to other domains. With this choice of penalty, $\dot{E}$ is again given by Eq. (2.92), and the last term in Eq. (2.92) vanishes in the limit $N \to \infty$ (see the discussion at the end of Appendix C).

Therefore, while not strictly stable, the system is *asymptotically* stable. Collecting results, we find that the second-order system is

$$\dot{\psi} = -\pi - \frac{1}{2}\delta U_{-}, \tag{2.96}$$

$$\dot{\pi} = -\partial_i \partial^i \psi + \frac{1}{2}\frac{|\mathbf{N}|}{\omega_x \omega_y \omega_z}\delta U_{-}, \tag{2.97}$$

where the penalties represent boundary values, the penalty on the first equation is applied throughout the interior of the domain via Eq. (2.95), and the normal vector $\mathbf{N}$ is defined as in Eq. (2.78).

2.3.1 Numerical Tests

The three-dimensional wave equation in Eqs. (2.96)-(2.97) with bulk penalty given by Eq. (2.95) is found to be robust, stable, and convergent in all of our tests. We have run simulations on multiple spherical shell, cylindrical shell, and cubic subdomains. As an example, Fig. 2.4 shows the L_2 error $||\psi - \psi_{\text{analytical}}||$ of a sinusoidal plane wave propagating through a domain consisting of 27 cubic subdomains. The results of an equivalent first-order evolution are plotted for comparison. The L_2 error is defined here as

$$||\psi - \psi_{\text{analytical}}|| \equiv \left[\sum |\psi - \psi_{\text{analytical}}|^2 / N\right]^{1/2}, \tag{2.98}$$

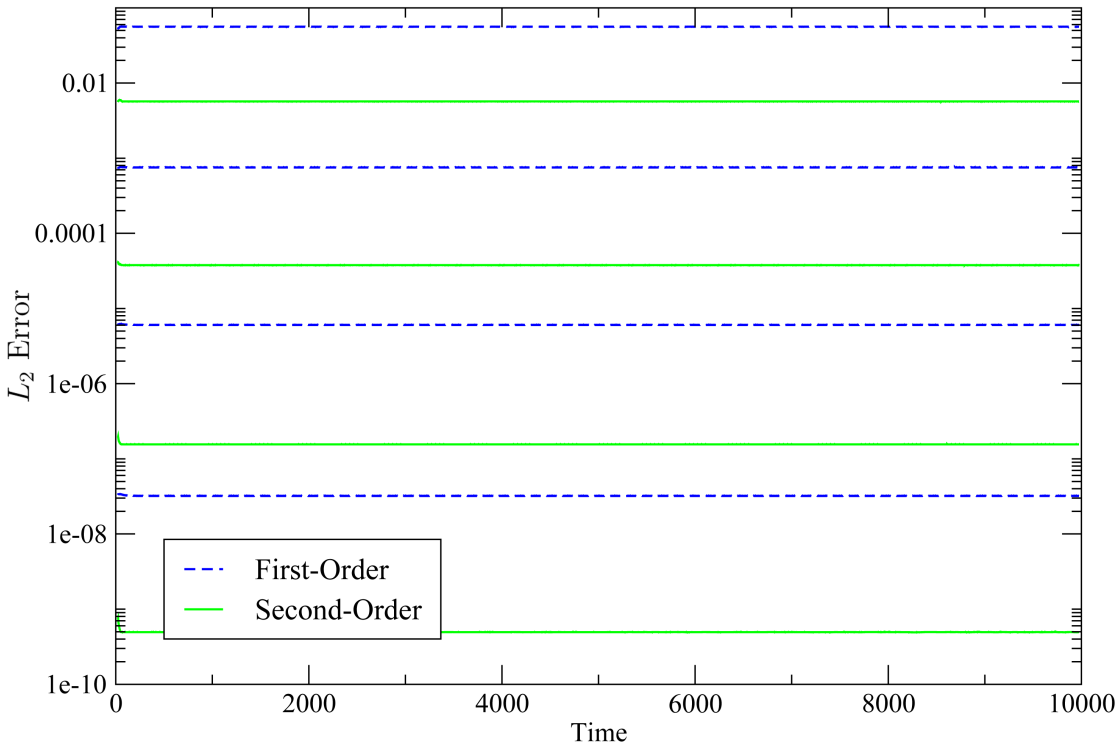

Figure 2.4: L_2 error of a plane wave $\psi(\mathbf{x}, t) = \sin(\mathbf{k}\cdot\mathbf{x} - \omega t)$ on 27 identical cubic subdomains covering the region $x, y, z \in [-3, 3]$. Results of equivalent first- and second-order evolutions are plotted for comparison. The successive resolutions have $5, 7, 9$, and 11 Legendre-Lobatto grid points per subdomain along each dimension. In this test, $\mathbf{k} = (.3, .2, .1)$ and $\omega = |\mathbf{k}|$. The L_2 error is a moving average over an interval $\Delta t = 50$, which includes 50 data points.

where the sum is over all grid points and N is the total number of points. In this example, only the boundary-face part of the bulk penalty in Eq. (2.95) is used, and normal vectors are defined as in Eq. (2.78). Empirically, we find that the bulk penalties associated with edges and corners are not needed in this example. The incoming mode at an interface boundary is supplied by the adjacent subdomain, while at outer boundaries it is computed from the analytical solution. When an edge or corner occurs at an interface, the incoming mode is supplied by the subdomain to which the normal vector points. Time-stepping is performed using an explicit fourth-order Runge-Kutta method.

A few empirical observations are worth mentioning. In practice, we find that the bulk penalty terms arising from edges and corners in Eq. (2.95) are not actually necessary to obtain a stable, convergent system. In all the tests we have performed for scalar waves in flat space, the terms due to the faces of the boundary are sufficient. However, the additional terms in Eq. (2.95) may need to be included for complicated domain decompositions or in curved space applications.

For more general systems of quasi-linear wave equations (such as Einstein's equations in generalized harmonic form [24], which will be treated in Chapter 3), we find that it is sometimes necessary to include a boundary term enforcing continuity of the field ψ in the penalty. That is, one makes the replacement $\delta U_- \to \delta U_- + \delta\psi$ in the penalties. In the tests that we have performed, this is not required for a simple wave equation in flat (or curved) space.

An alternative to defining unique normal vectors on corners and edges is to use a so-called multi-penalty method. With a multi-penalty method, boundary conditions (and hence penalties) on edges and corners are defined to be the sum of those from the adjacent boundary faces. While this has the advantage of avoiding some of the issues with corners and edges, it makes obtaining analytical results such as Eq. (2.92) more difficult. Although we have not fully tested this alternative in curved space applications, we find that the multi-penalty method performs equally well for scalar waves in flat space.

2.4 Wave Equation on Curved Background

In this section we consider the application of the new penalty method to the evolution of a scalar wave on a fixed, curved background spacetime:

$$\nabla_\mu \nabla^\mu \psi = 0, \tag{2.99}$$

where ∇_μ is the four-dimensional covariant derivative. In rewriting this equation as a first-order system, we use the standard 3 + 1 splitting of the metric:

$$ds^2 = -\alpha^2 dt^2 + \gamma_{ij}\,(dx^i + \beta^i dt)\,(dx^j + \beta^j dt), \tag{2.100}$$

where α is the lapse function, β^i is the shift, and γ_{ij} is the three-dimensional metric intrinsic to the constant time spatial hypersurfaces. It is assumed that $\alpha > 0$ and that the three-metric γ_{ij} is positive definite.

The wave equation in Eq. (2.99) can be rewritten in a standard way [35] as the first-order system

$$\dot{\psi} = -\alpha\pi + \beta^i \partial_i \psi, \tag{2.101}$$

$$\dot{\pi} = -\alpha\gamma^{ij}\partial_i \phi_j + \beta^i \partial_i \pi + \alpha K \pi + \alpha J^i \phi_i, \tag{2.102}$$

$$\dot{\phi}_i = -\alpha\partial_i \pi - \pi\partial_i \alpha + \phi_k \partial_i \beta^k + \beta^k \partial_k \phi_i. \tag{2.103}$$

Equation (2.101) is just the definition of the variable π. As usual, the spatial derivative variable is defined as

$$\phi_i \equiv \partial_i \psi. \tag{2.104}$$

The quantities K and J^i in Eq. (2.102) are purely functions of the background spacetime:

$$K \equiv -\frac{1}{\alpha\gamma^{1/2}}\Big[\partial_0 \gamma^{1/2} - \partial_i(\gamma^{1/2}\beta^i)\Big], \tag{2.105}$$

$$J^i \equiv -\frac{1}{\alpha\gamma^{1/2}}\,\partial_j(\alpha\gamma^{1/2}\gamma^{ij}), \tag{2.106}$$

where $\gamma \equiv \det \gamma_{ij}$. In deriving Eq. (2.103), the equivalence of interchanging indices in

$$\partial_i \phi_j = \partial_j \phi_i \tag{2.107}$$

has been assumed. This reduction to first-order therefore introduces two constraints to the system: $C_i = C_{ij} = 0$, where

$$C_i \equiv \phi_i - \partial_i \psi, \tag{2.108}$$

$$C_{ij} \equiv \partial_i \phi_j - \partial_j \phi_i. \tag{2.109}$$

The second-order in space equations are

$$\dot{\psi} = -\alpha\pi + \beta^i \partial_i \psi, \tag{2.110}$$

$$\dot{\pi} = -\alpha\gamma^{ij}\partial_i\partial_j\psi + \beta^i\partial_i\pi + \alpha K\pi + \alpha J^i \partial_i \psi. \tag{2.111}$$

This system avoids the introduction of the constraints in Eqs. (2.108)-(2.109) as well as the third set of evolution equations in Eq. (2.103).

The characteristic variables and speeds of the second-order system are the same as those of the equivalent first-order reduction with $\phi_i \to \partial_i \psi$:

$$U_\psi = \psi, \qquad \lambda_0 = -n^k \beta_k \tag{2.112}$$

$$U_\pm = \pi \pm n^i \partial_i \psi, \qquad \lambda_\pm = \pm\alpha - n^k \beta_k, \tag{2.113}$$

$$U_i^0 = \partial_i \psi - n_i n^j \partial_j \psi, \qquad \lambda_0 = -n^k \beta_k, \tag{2.114}$$

where n^i is the outward-directed unit normal vector to the boundary of the three-dimensional spatial domain. These are the same as the characteristic modes of the scalar wave in flat space in Eqs. (2.70)-(2.72), with the characteristic speeds modified. Note that as discussed in Section 2.3 above, the "zero-speed" modes U_i^0 can be considered to have arbitrary speeds in the second-order system [26]. The speeds λ_0 given here are chosen to be the same as those of the

corresponding first-order system. Additionally, these are the coefficients that appear in the boundary flux of the energy, and in this sense they are the preferred choice.

2.4.1 Continuum Energy Estimate

The energy density for this system is the same as that of the flat space scalar wave system given in Eq.(2.74):

$$\epsilon = \frac{1}{2}(\pi^2 + \partial^i \psi \partial_i \psi). \tag{2.115}$$

The energy flux is found by computing the time derivative of the energy

$$E = \int_\Omega \epsilon \, \gamma^{1/2} d^3x, \tag{2.116}$$

where Ω is the spatial domain under consideration and $\gamma^{1/2} d^3x$ is the volume element. In computing the flux, one obtains a boundary term in addition to multiple volume terms that depend on derivatives of the background ($\partial_i \alpha$, $\partial_i \beta_j$, or $\partial_i \gamma_{jk}$). These volume terms can all be bounded by multiples of the energy itself (or neglected in the constant-coefficient approximation), to give

$$\dot{E} \leq -\frac{1}{4} \int_{\partial\Omega} F^n \, \sigma^{1/2} d^2x \; + \; k \, E, \tag{2.117}$$

for some constant $k \geq 0$. The flux integrand is

$$F^n = \lambda_- U_-^2 + \lambda_+ U_+^2 + 2\lambda_0 \, U^{0j} U_j^0, \tag{2.118}$$

and the element of area in Eq. (2.117) is $\sigma^{1/2} d^2x$, where $\sigma \equiv \det \sigma_{ij}$ and σ_{ij} is the intrinsic metric on the boundary surface. The continuum problem is therefore well-posed with boundary conditions that control incoming modes (those with

$\lambda < 0$). For a timelike boundary, a boundary condition is needed on U_- and possibly on U_i^0, depending on the sign of λ_0. For a spacelike boundary, either all modes are incoming, or all modes are outgoing in which case no boundary conditions are required (e.g. on an excision boundary inside the horizon of a black hole).

We could also have included a term $a^2\psi^2$ in the energy density, replacing Eq. (2.115) by

$$\epsilon = \frac{1}{2}(a^2\,\psi^2 + \pi^2 + \partial^i\psi\partial_i\psi). \tag{2.119}$$

This would give an additional term in $\dot{E}$:

$$\int_\Omega a^2\psi\dot{\psi}\,\gamma^{1/2}d^3x = \int_\Omega a^2\psi\,(\beta^i\partial_i\psi - \alpha\pi)\,\gamma^{1/2}d^3x. \tag{2.120}$$

Integrating by parts in the first term on the right-hand side gives

$$\frac{a^2}{2}\int_{\partial\Omega} n_i\beta^i\,\psi^2\,\sigma^{1/2}d^2x - \frac{a^2}{2}\int_\Omega \psi^2\,\partial_i(\beta^i\gamma^{1/2})\,d^3x. \tag{2.121}$$

The second term in this expression can be bounded in terms of the energy, while the first term contributes to the boundary flux. It may seem, then, that including the term $a^2\psi^2$ in the energy density would require the flux F^n of Eq. (2.118) to be modified. However, the entire right-hand side of Eq. (2.120) can in fact be bounded in the volume as

$$\int_\Omega a^2\psi\,(\beta^i\partial_i\psi - \alpha\pi)\,\gamma^{1/2}d^3x \;\le\; a\,(\alpha_{\max} + |\beta|_{\max})\,E, \tag{2.122}$$

where we have used $(\hat{\beta}^i\partial_i\psi)^2 \le \partial^i\psi\partial_i\psi$. The constant k in Eq. (2.117) would therefore be modified, but not the flux F^n. Consequently, including a term $a^2\psi^2$ in the energy density does not affect our conclusions about well-posedness or boundary conditions. It is interesting to note, however, that the same does not hold for the first-order system in Eqs. (2.101)-(2.103), because the first-order energy

corresponding to Eq. (2.119) controls ϕ_i, but not $\partial_i\psi$ (and therefore the inequality in Eq. (2.122) does not follow).

2.4.2 Semi-discrete Energy Estimate

The penalties in the semi-discrete equations need to be slightly modified from those of the flat space scalar wave system in Eqs. (2.96)-(2.97). To see how, consider the semi-discrete equations corresponding to Eqs. (2.110)-(2.111) with penalty functions p, q:

$$\dot{\psi}_i = -\alpha\pi_i + \ldots + p, \tag{2.123}$$

$$\dot{\pi}_i = -\alpha\gamma^{jk}\partial_j\partial_k\psi_i + \ldots + q. \tag{2.124}$$

As usual, is it to be understood that the fields represent grid values (e.g. $\psi = \psi_{ijk}$), and differentiation is implemented, for example, by matrix multiplication. For simplicity, we will assume that the physical domain under consideration has been mapped to the cube Ω with $x, y, z \in [-1, 1]$. We will also assume for now that the boundary is timelike, with U_- the only incoming mode. As in the flat space scalar wave system, the penalties will thus be proportional to $\delta U_- \equiv U_-^{\mathrm{BC}} - U_-$. The semi-discrete energy is

$$E = \frac{1}{2}[\langle\pi, \pi\rangle + \langle\partial^i\psi, \partial_i\psi\rangle], \tag{2.125}$$

where the discrete inner product is now defined by, for example

$$\langle\pi, \pi\rangle \equiv \sum_{ijk} \omega_i\omega_j\omega_k\,\pi^2\gamma^{1/2} \simeq \int_\Omega \pi^2\,\gamma^{1/2} d^3x. \tag{2.126}$$

Note that because of the presence of $\gamma^{1/2}$ in the volume element, the quadrature integrals we encounter will in general no longer be exactly equal to the continuum integrals.

The time derivative of the semi-discrete energy in Eq. (2.125) separates as usual into a continuum-like part plus a contribution from the penalties:

$$\dot{E} = \dot{E}_{\text{continuum}} + \dot{E}_{\text{penalties}}, \tag{2.127}$$

where the penalty contribution is

$$\dot{E}_{\text{penalties}} = \langle \pi, q \rangle + \langle \partial^i \psi, \partial_i p \rangle. \tag{2.128}$$

Assuming the penalty q is defined as in Eq. (2.97) except for an overall factor q_0, we have

$$\langle \pi, q \rangle = \frac{1}{2} \sum_{\partial\Omega} |\mathbf{N}|\, q_0\, \pi\, \delta U_-\, \gamma^{1/2}, \tag{2.129}$$

where $|\mathbf{N}|$ is the magnitude (now with respect to γ_{ij}) of the normal vector defined as in Eq. (2.78). The second term in Eq. (2.128) gives

$$\langle \partial^i \psi, \partial_i p \rangle = \sum_{\partial\Omega} |\mathbf{N}|\, n^i \partial_i \psi\; p\, \gamma^{1/2} - \langle \nabla_j \nabla^j \psi, p \rangle, \tag{2.130}$$

where n^i is the unit normal vector to the boundary, and ∇_j is the three-dimensional covariant derivative associated with γ_{ij}. With the penalty function p constructed in the volume according to Eq. (2.95), the last term in Eq. (2.130) asymptotically vanishes as in the flat-space case, and we will therefore neglect it. Assuming that p has the same value as in Eq. (2.96) apart from an overall factor p_0, it follows that

$$\langle \partial^i \psi, \partial_i p \rangle = -\frac{1}{2} \sum_{\partial\Omega} |\mathbf{N}|\, n^i \partial_i \psi\; p_0\, \delta U_-\, \gamma^{1/2}. \tag{2.131}$$

If we choose $q_0 = p_0$, then Eq. (2.128) for the penalty contribution to $\dot{E}$ becomes

$$\dot{E}_{\text{penalties}} = \frac{1}{2} \sum_{\partial\Omega} |\mathbf{N}|\, p_0\, U_- \delta U_-\, \gamma^{1/2}. \tag{2.132}$$

Setting $p_0 = |\lambda_-|$, we obtain the semi-discrete energy estimate

$$\dot{E} \leq -\frac{1}{4} \sum_{\partial\Omega} |\mathbf{N}|\, F^n\, \gamma^{1/2} \;+\; k\, E, \tag{2.133}$$

for some constant $k \geq 0$. The flux integrand is

$$F^n = \lambda_-(U_-^{\mathrm{BC2}} - \delta U_-^2) + \lambda_+ U_+^2 + 2\lambda_0 U^{0i} U_i^0, \tag{2.134}$$

which resembles the continuum result of Eq. (2.118), with the addition of the negative term proportional to the mismatch of characteristic modes δU_-^2. Note that the sum over the boundary can be rewritten as

$$\sum_{\partial\Omega} |\mathbf{N}|\, \gamma^{1/2}\, (\,\cdot\,) = \sum_{\partial\Omega} |\tilde{\mathbf{N}}|_{\mathrm{E}}\, \sigma^{1/2}\, (\,\cdot\,), \tag{2.135}$$

where $|\tilde{\mathbf{N}}|_{\mathrm{E}}$ is the magnitude (with respect to a Euclidean metric) of the normal one-form corresponding to $\mathbf{N}$, and $(\,\cdot\,)$ represents any integrand. In this form, the similarity to the surface integral

$$\int_{\partial\Omega} (\,\cdot\,)\, \sigma^{1/2} d^2x \tag{2.136}$$

in the continuum result of Eq. (2.117) is evident.

We have assumed that U_- is the only incoming mode, and in this case Eq. (2.133) shows that the semi-discrete system is asymptotically well-posed. If $\lambda_0 < 0$, then the boundary flux in Eq. (2.134) implies that a boundary condition is required to control U_i^0 as well. Although we have been unable to see how to do this with penalties, we have found empirically that it is unnecessary to impose any boundary conditions on this mode; it is sufficient to enforce the condition on the incoming mode U_-.

For a spacelike boundary with all characteristic modes outgoing, no boundary conditions and hence no penalties are required. In that case, the boundary term in Eq. (2.133) is strictly non-positive. If on the other hand the boundary is spacelike with all characteristic modes incoming, we can enforce a boundary

condition on U_- *and* U_+ by setting

$$p\big|_{\partial\Omega} = \frac{1}{2}\Big(|\lambda_+|\,\delta U_+ - |\lambda_-|\,\delta U_-\Big), \tag{2.137}$$

$$q\big|_{\partial\Omega} = \frac{1}{2}\frac{|\mathbf{N}|}{\omega_x\,\omega_y\,\omega_z}\Big(|\lambda_+|\,\delta U_+ + |\lambda_-|\,\delta U_-\Big). \tag{2.138}$$

In this case, the flux integrand in Eq. (2.133) is

$$F^n = \lambda_-(U_-^{\mathrm{BC}2} - \delta U_-^2) + \lambda_+(U_+^{\mathrm{BC}2} - \delta U_+^2) + 2\,\lambda_0\,U^{0i}U_i^0. \tag{2.139}$$

In summary, the second-order system with penalties is

$$\dot{\psi} = -\alpha\pi + \ldots - \frac{|\lambda_-|}{2}\,\delta U_-, \tag{2.140}$$

$$\dot{\pi} = -\alpha\gamma^{ij}\partial_i\partial_j\psi + \ldots + \frac{|\lambda_-|}{2}\frac{|\mathbf{N}|}{\omega_x\,\omega_y\,\omega_z}\,\delta U_-, \tag{2.141}$$

where as usual the penalties represent boundary values, the penalty on the first equation is applied throughout the interior of the domain via Eq. (2.95), and the normal vector $\mathbf{N}$ is defined as in Eq. (2.78). Furthermore, it is to be understood that the penalties with δU_- are applied only when U_- is an incoming mode, and in the event that U_+ is also incoming, the penalties are modified according to Eqs. (2.137)-(2.138).

2.4.3 Numerical Tests

In order to compute the error with respect to an analytical solution, we consider the inhomogeneous wave equation

$$\nabla_\mu\nabla^\mu\psi = \mathcal{S}, \tag{2.142}$$

where the source $\mathcal{S}$ is computed by substituting an analytical solution for ψ into the left-hand side. With a source term, Eq. (2.110) is unchanged, while

Eq. (2.111) is modified by adding a term $\alpha \mathcal{S}$:

$$\dot{\pi} = \ldots + \alpha \mathcal{S}. \tag{2.143}$$

As an example test problem, we use the following background metric (the Schwarzschild solution in Kerr-Schild coordinates):

$$ds^2 = -\left(1 + \frac{2M}{r}\right) dt^2 + \left(1 + \frac{2M}{r}\right) dr^2 + \frac{4M}{r}\, dr\, dt + r^2 d\Omega^2, \tag{2.144}$$

and consider an analytical solution of the form

$$\psi_{\text{analytical}} = \cos(\omega t)\, e^{-(r-r_0)^2/\sigma^2}\, Y_{lm}. \tag{2.145}$$

We evolve the second-order equations Eqs. (2.140)-(2.141) with source term on a domain consisting of three concentric spherical shell subdomains. The innermost boundary is placed just inside the horizon (located at $r = 2M$), so that no boundary condition is required there (all characteristic modes are outgoing). At an interface between two subdomains the value of the incoming mode U_-^{BC} is supplied by the adjacent subdomain, while on the outermost boundary U_-^{BC} is computed from the analytical solution in Eq. (2.145). Time-stepping is performed using an explicit Runge-Kutta method.

For a spherical shell subdomain, we use a spectral basis composed of Legendre polynomials in the radial direction scaled to the appropriate radial extent and spherical harmonics in the angular directions. The numerical approximant for particular truncations N_r and L is therefore given by:

$$\psi = \sum_{i=0}^{N_r} \sum_{l=0}^{L} \sum_{m=-l}^{+l} a_{ilm}\, \tilde{P}_i(r) Y_{lm}(\theta, \phi), \tag{2.146}$$

where $\tilde{P}_i(r)$ represents the appropriately scaled Legendre polynomial, and a_{ilm} are the spectral coefficients. The L_2 error in ψ for this test problem, defined as in

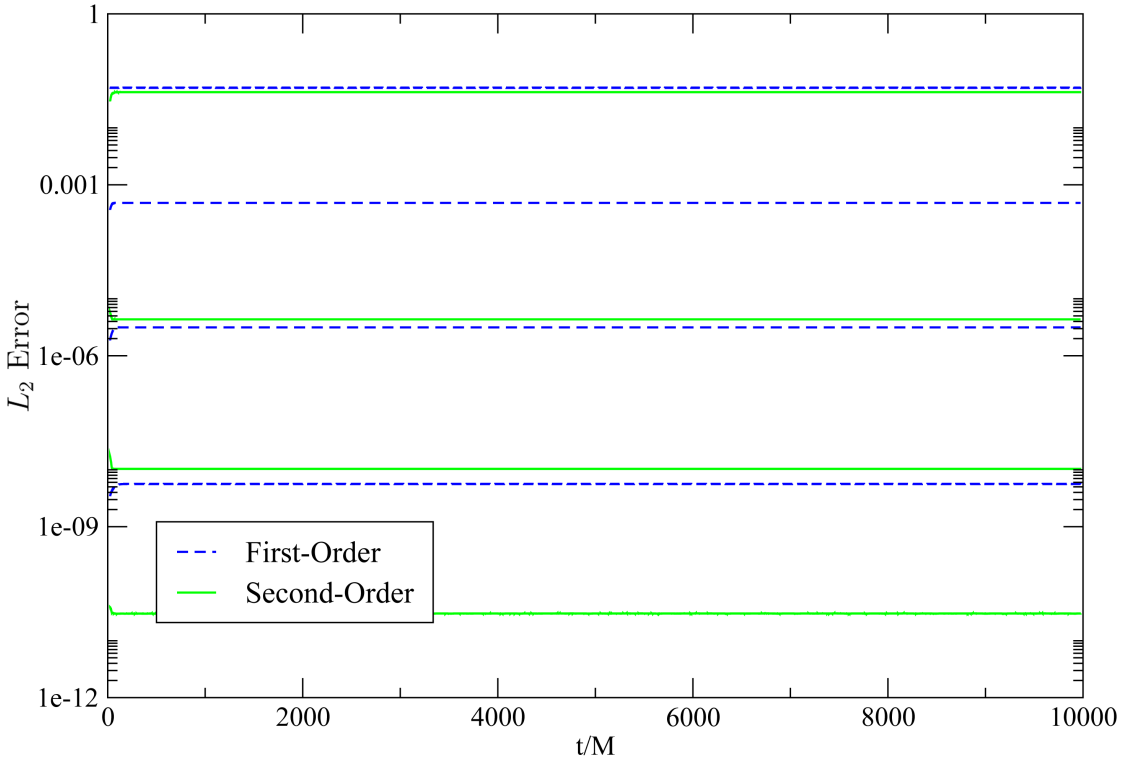

Figure 2.5: L_2 error for a scalar wave given by Eq. (2.145) on a Schwarzschild background in Kerr-Schild coordinates. The domain consists of three concentric spherical shells with radial boundaries at $r = 1.9, 11.9, 21.9, 32.9$ (in units of M). The radial and angular resolutions (N_r, L) of the runs are $(8, 4)$, $(14, 6)$, $(20, 8)$, and $(26, 10)$. In this test, the following values for the analytical solution were used: $r_0 = 17\,M$, $\sigma = 2\,M$, $\omega = 0.5\,M^{-1}$, $l = 3$, and $m = 1$. The results of an equivalent first-order evolution are plotted for comparison. The L_2 error is a moving average over an interval $\Delta t = 50$, which includes 50 data points.

Eq. (2.98), is shown in Fig. 2.5 as a function of time for various resolutions. The results from an equivalent first-order evolution are plotted for comparison.

The homogeneous second-order system of Eqs. (2.140)-(2.141) is also found to be stable and convergent in tests that we have run with arbitrary initial data for a variety of background metrics. For example, we have run simulations on a Schwarzschild background in Kerr-Schild, Painlevé-Gullstrand [36], and fully harmonic coordinates, and on a Kerr background (with a spin up to $a = 1$) in Kerr-Schild coordinates. In the event that we do not have an analytical solution to supply a condition on U_- at the outer boundary, we find good results by using a Sommerfeld condition, assuming a solution of the form

$$\psi \sim \frac{f(t-r)}{r}. \tag{2.147}$$

This translates into a condition on the incoming mode at the outer boundary:

$$U_-^{\mathrm{BC}} \sim \frac{\psi}{r}. \tag{2.148}$$

For the first-order evolutions, as discussed below Eq. (2.40), one can use Chebyshev polynomials instead of Legendre for the radial basis in Eq. (2.146), and the results are comparable (the same holds for Einstein's equations). In the second-order evolutions, while it is acceptable to use a Chebyshev basis for flat space applications, we find that the L_2 error is significantly larger (almost two orders of magnitude) in the curved background case. In the application to Einstein's equations (as will be discussed in Chapter 3), the second-order evolutions are in fact no longer stable if a Legendre basis is not used. Note, however, that we are not addressing the Chebyshev-Legendre method discussed below Eq. (2.40) here, but rather the use of a Chebyshev basis without modifying the grid values of the penalty function of Eq. (2.141) (i.e. imposing this penalty only

on the boundary for the Chebyshev grid as well). Presumably, the Chebyshev-Legendre method would perform equally well, but we have not explored this modification.

2.5 Discussion

We have not found a significant difference in efficiency between the first- and second-order forms of the equations for the simple systems considered here. Even with equal time steps, the rates of the first- and second-order codes (using explicit time-stepping) are comparable (within about 10% of each other), despite the absence of the third set of evolution equations (the $\dot{\phi}_i$ equations) in the second-order system. One reason for this is that the second derivatives are computationally more expensive than first derivatives on arbitrary domains, because of the coordinate transformations involved. Symbolically, the transformation of a first derivative to new (barred) coordinates involves a multiplication by the Jacobian J of the transformation:

$$\bar{\partial}\psi = J\partial\psi, \tag{2.149}$$

while the transformation of a second derivative requires the Hessian H and the first derivative as well:

$$\bar{\partial}^2\psi = JJ\partial^2\psi + H\partial\psi. \tag{2.150}$$

It is evident that the second-order evolutions generally have smaller errors than their first-order counterparts at given resolutions by as much as two orders of magnitude, as can be seen in Figs. 2.4-2.5. To a degree, then, this makes the second-order evolutions somewhat more efficient in the sense that for a given

accuracy goal, a smaller resolution is required in the second-order system. However, our focus has not been on comparing or analyzing code efficiencies, but rather on establishing the viability of a second-order in space spectral method. We believe the second-order system has the potential to show substantial increases in efficiency for more complicated systems than those considered here.

All of the energy arguments presented in this work have assumed a grid structure that can be mapped to a cube. While it is straightforward to apply the methods to spherical or cylindrical shells, it is assumed that any dimension with boundaries (e.g. the radial dimension on a spherical shell) has a collocation grid that contains its endpoints (Gauss-Lobatto grid). For a domain containing the origin, such as the unit disk, it is typical to use a radial grid of Gauss-Radau points, so that the endpoint at the origin is not included (see e.g. [37]). We have not considered the generalization to such domains.

We have shown how to evolve a multi-domain second order in space wave equation stably using spectral methods. In more general systems, energy arguments like those given here cannot be carried out. Nevertheless, in the most important case we consider, namely Einstein's equations in generalized harmonic form, these methods work quite well. The reason is that the *principal part* of the equations is directly analogous to the scalar wave equation on a curved background [24].

CHAPTER 3

SPECTRAL METHODS FOR EINSTEIN'S EQUATIONS IN SECOND-ORDER FORM

3.1 Introduction

One of the most likely candidates for detection by gravitational wave observatories such as LIGO is the inspiral, merger, and ringdown of a binary black hole system [5]. Because of the low expected signal-to-noise ratio for these events, it is desirable to have a template of calculated waveforms in order to use methods such as matched filtering [15], which can enhance the detection likelihood. Simulations of the full Einstein equations for such systems also facilitate the validation of Post-Newtonian methods and exploration of black hole dynamics. For these reasons, there has been a great amount of effort directed at evolving binary black holes numerically.

Recent years have seen tremendous progress in the binary black hole problem, beginning with the work of Pretorius [21] and followed by the success of the moving punctures method [22, 23]. All of these simulations have used finite difference methods. However, because the vacuum Einstein equations have smooth solutions (provided pathological coordinates are not chosen), spectral methods should be superior to finite differencing in terms of efficiency and accuracy.

Even though Einstein's equations are naturally second order, they must generally be rewritten as a first-order system when using spectral methods. The basic reason for this has been that there is little mathematical theory on the proper

formulation of second-order hyperbolic systems for spectral methods, and it is accordingly unclear how to evolve the second-order equations spectrally in a stable and consistent manner. On the other hand, there is extensive literature on first-order systems, which includes theorems concerning the well-posedness of the equations and the way to impose stable boundary conditions for hyperbolic systems [18, 19, 20]. While there have been some attempts at evolving Einstein's equations spectrally in second-order form [38], successful spectral methods to date have employed the first-order representations [16, 25].

Reducing the order of the equations is usually done by introducing new variables defined as first-order time and space derivatives. The disadvantage of this is that the definitions (at least for spatial derivatives) become constraints that the solution must satisfy and thus new possible sources of instability in the system. Furthermore, each new variable must be evolved with the system, increasing the number of equations and the computational cost of the simulations. In the case of the generalized harmonic form of the equations, for example, the reduction to first order in space requires the introduction of 30 additional variables, more than doubling the number of equations and constraints in the system [24]. Typical binary black hole simulations running on a parallel supercomputers require weeks of evolution time for even modest accuracy, so even a small fractional increase in the computational cost can be expensive.

Being able to evolve Einstein's equations spectrally in second-order form would avoid these additional constraints and equations and potentially provide more efficient and stable simulations. Recently, Gundlach and Martín-García have proposed and analyzed definitions of symmetric hyperbolicity for a general class of second order in space systems [26, 27, 28]. They have

also shown how one may define characteristic modes in the second-order system and thereby formulate stable boundary conditions at the continuum level. However, there still remains the problem of how to impose the boundary conditions in the discrete system (using spectral methods).

In Chapter 2, a new penalty method was derived for spectral evolutions of second order wave equations. The new method employs penalty functions that are constructed from Legendre polynomials. Boundary conditions are imposed by adding volume penalties to the equations everywhere—not only on the boundaries as is typical in first-order formulations. In this chapter, we investigate the application of these methods to Einstein's equations in generalized harmonic form. Since in this form Einstein's equations appear as ten nonlinear coupled wave equations, the extension of the scalar wave methods of Section 2.4 to this case is straightforward.

While some stability problems in the second-order binary evolutions remain, the results are promising and we believe the methods presented here will soon become a viable alternative to first-order spectral evolutions of Einstein's equations. It is also likely that the work presented here will ultimately allow other formulations of Einstein's equations, such as the BSSN (Baumgarte-Shapiro-Shibata-Nakamura) formulation, to be treated by spectral methods without reduction to first-order form.

In Section 3.2, we begin by reviewing some properties of the generalized harmonic form of Einstein's equations, including the first- and second-order forms of the equations. In Section 3.3, we apply the new penalty method to the evolution of single black hole initial data, and we discuss the problems that arise and how they can be overcome. In Section 3.4, we explore the application

of the new penalty method to the evolution of an equal-mass, 16 orbit black hole binary. We review some of the numerical techniques that are employed and then discuss the preliminary results.

3.2 Einstein's Equations in Generalized Harmonic Form

We will begin by briefly reviewing the important features of the generalized harmonic (GH) system. Consider a spacetime with a four-metric ψ_{ab}. We use Latin indices $a, b, c, \ldots$ from the beginning of the alphabet to represent four-dimensional spacetime indices. The GH coordinate condition is

$$\mathcal{H}^a = \nabla^b \nabla_b x^a = -\Gamma^a, \tag{3.1}$$

where $\mathcal{H}^a$ is a prescribed function specifying the gauge (coordinate) choice, x^a are the coordinates, ∇^b is the spacetime covariant derivative, and $\Gamma^a \equiv \psi^{bc}\Gamma^a_{bc}$ is the trace of the usual Christoffel symbols:

$$\Gamma^a_{bc} = \frac{1}{2}\psi^{ad}(\partial_b \psi_{dc} + \partial_c \psi_{db} - \partial_d \psi_{bc}). \tag{3.2}$$

With this choice of gauge, the vacuum Einstein equations can be written as

$$\psi^{cd}\partial_c \partial_d \psi_{ab} = 2\psi^{cd}\psi^{ef}(\partial_e \psi_{ca}\partial_f \psi_{db} - \Gamma_{ace}\Gamma_{bdf}) - 2\nabla_{(a}\mathcal{H}_{b)}, \tag{3.3}$$

where $\mathcal{H}_a = -\Gamma_a$ has been assumed [24]. In this form, the principal part of the equation is the second-order wave operator on the left-hand side, since the term containing $\mathcal{H}_b$ is considered to be a given function and not a dynamical variable. Thus, Einstein's equations are manifestly hyperbolic with the GH coordinate condition.

In a numerical solution to Einstein's equations, the gauge condition of Eq. (3.1) does not hold exactly, but instead represents a constraint $C_a = 0$ that

the system must satisfy, where

$$C_a \equiv \mathcal{H}_a + \Gamma_a. \tag{3.4}$$

Truncation error, discretization error, and imperfect boundary conditions typically cause the constraint to be violated, even when it is satisfied in the initial data. Moreover, constraint violations generally lead to instabilities, where the constraint grows exponentially during a simulation, contaminating the numerical solution.

Fortunately, there exists a modified form of the equations, originally suggested by Gundlach et al. [39], that is designed to damp the constraints. Equation (3.3) is modified by adding the following term to the right-hand side:

$$\gamma_0[2t_{(a}C_{b)} - \psi_{ab}t^c C_c], \tag{3.5}$$

where γ_0 is a constant that determines the strength of the constraint damping, and t^a is the future-directed unit timelike normal vector to the constant time hypersurfaces. It can be shown that with the addition of this term, high frequency constraint violations will be damped at the rate $e^{-\gamma_0 t}$ or $e^{-\gamma_0 t/2}$ [24]. Equation (3.5) vanishes if the constraints are satisfied ($C_a = 0$), so the vacuum solutions to Einstein's equations are not altered. Furthermore, Eq. (3.5) does not change the principal part of Eq. (3.3), so the modified system remains hyperbolic. Additional properties of the GH system, such as the relation of the gauge source function $\mathcal{H}_a$ to the usual 3+1 lapse and shift, are discussed in Ref. [24].

3.2.1 First Order Evolution System

The principal part of the system of equations in Eq. (3.3) with the constraint damping term of Eq. (3.5) is analogous to a scalar wave equation on a curved

background [35]. The same methods can therefore be employed in reducing the system to fully first-order form. One uses the standard 3+1 splitting of the metric:

$$ds^2 = -\alpha^2 dt^2 + \gamma_{ij}(dx^i + \beta^i dt)(dx^j + \beta^j dt), \tag{3.6}$$

where α is the lapse, β^i is the shift, and γ_{ij} is the three-metric intrinsic to the constant-time hypersurfaces. The first-order variables are defined as

$$\Pi_{ab} \equiv -t^c \partial_c \psi_{ab}, \tag{3.7}$$

$$\Phi_{iab} \equiv \partial_i \psi_{ab}. \tag{3.8}$$

The first-order system thus obtained is

$$\partial_t \psi_{ab} - \beta^k \partial_k \psi_{ab} = -\alpha \Pi_{ab}, \tag{3.9}$$

$$\partial_t \Pi_{ab} - \beta^k \partial_k \Pi_{ab} + \alpha \gamma^{ik} \partial_i \Phi_{kab} = \ldots, \tag{3.10}$$

$$\partial_t \Phi_{iab} - \beta^k \partial_k \Phi_{iab} + \alpha \partial_i \Pi_{ab} = \ldots, \tag{3.11}$$

where Eq. (3.9) is precisely the definition of Π_{ab}, and the dots on the right-hand sides of Eqs. (3.10)-(3.11) represent lower order algebraic terms. The definition in Eq. (3.8) amounts to the addition of a new constraint to the system. Additionally, in deriving Eq. (3.11), the equivalence of interchanging the order of differentiation in

$$\partial_k \Phi_{iab} = \partial_i \Phi_{kab} \tag{3.12}$$

has been assumed. Consequently, this first-order representation of the GH system has two additional constraints $C_{iab} = 0$ and $C_{ijab} = 0$, where

$$C_{iab} \equiv \Phi_{iab} - \partial_i \psi_{ab}, \tag{3.13}$$

$$C_{ijab} \equiv \partial_i \Phi_{jab} - \partial_j \Phi_{iab}. \tag{3.14}$$

The modified first-order GH system used by the Cornell-Caltech group contains additional constraint-damping terms designed to control the growth

of these added constraints [24]. The system (with or without the additional constraint-damping terms) is symmetric hyperbolic and therefore well-posed with boundary conditions specified on incoming characteristic variables [18].

3.2.2 Second Order Evolution System

The first order in time, second order in space GH evolution system avoids the introduction of the constraints in Eqs. (3.13)-(3.14) as well as the third set of evolution equations in Eq. (3.11). The variable Π_{ab} is defined the same way as in Eq. (3.7), and the second-order equations, including all lower-order terms and the constraint-damping term of Eq. (3.5), are given by

$$\partial_t \psi_{ab} = -\alpha \Pi_{ab} + \beta^k \partial_k \psi_{ab}, \tag{3.15}$$

$$\begin{aligned} \partial_t \Pi_{ab} = &-\alpha \gamma^{ik} \partial_i \partial_k \psi_{ab} + \beta^k \partial_k \Pi_{ab} + 2\alpha \psi^{cd} (\gamma^{ij} \partial_i \psi_{ca} \partial_j \psi_{db} - \Pi_{ca} \Pi_{db} \\ &- \psi^{ef} \Gamma_{ace} \Gamma_{bdf}) - 2\alpha \nabla_{(a} \mathcal{H}_{b)} - \frac{1}{2} \alpha t^c t^d \Pi_{cd} \Pi_{ab} - \alpha t^c \Pi_{ci} \gamma^{ij} \partial_j \psi_{ab} \\ &+ \alpha \gamma_0 [2\delta^c{}_{(a} t_{b)} - \psi_{ab} t^c] (\mathcal{H}_c + \Gamma_c). \end{aligned} \tag{3.16}$$

This system consists of ten coupled scalar wave equations, each of which has the same principal part as the scalar wave on a curved background treated in Section 2.4. The same methods can therefore be applied here, despite the presence of nonlinearity and the lower-order terms on the right-hand sides of Eqs. (3.15)-(3.16).

The characteristic modes and speeds depend only on the principal part of the equations and are the same as those of the first-order reduction in Eqs. (3.9)-

(3.11), with the replacement $\Phi_{iab} \to \partial_i \psi_{ab}$:

$$U^{\psi}_{ab} = \psi_{ab}, \qquad \lambda_0 = -n^k \beta_k \tag{3.17}$$

$$U^{\pm}_{ab} = \Pi_{ab} \pm n^i \partial_i \psi_{ab}, \qquad \lambda_{\pm} = \pm\alpha - n^k \beta_k, \tag{3.18}$$

$$U^{0}_{iab} = \partial_i \psi_{ab} - n_i n^j \partial_j \psi_{ab}, \qquad \lambda_0 = -n^k \beta_k, \tag{3.19}$$

where n^i is the outward-directed unit normal vector to the boundary of the three-dimensional spatial domain. Boundary conditions are to be imposed on the incoming characteristic modes (those with $\lambda < 0$): usually U^{-}_{ab} and possibly U^{+}_{ab}, depending on the sign of λ_+. Just as in the scalar wave system analyzed in Section 2.4, no boundary conditions are imposed on the "zero-speed" modes U^{ψ}_{ab} or U^{0}_{iab}, even when $\lambda_0 < 0$.

Boundary conditions are imposed in this system via the penalty method derived in Chapter 2: A bulk penalty function that is a constructed out of Legendre polynomials is applied to the $\partial_t \psi_{ab}$ equations, while a penalty function that is nonvanishing only on the boundary is applied to the $\partial_t \Pi_{ab}$ equations.

3.3 Single Black Hole

The most important preliminary test of the second-order GH system is the evolution of a single black hole spacetime. Being able to evolve this case in a stable and convergent way is a necessary precursor to simulating a binary black hole spacetime. We now turn to a discussion of the issues that arise and how they may be resolved.

3.3.1 Test Problem Description

We evolve the second-order GH system with initial and boundary data for a Schwarzschild black hole in Kerr-Schild coordinates. The analytical solution is given by

$$ds^2 = -\left(1 + \frac{2M}{r}\right) dt^2 + \left(1 + \frac{2M}{r}\right) dr^2 + \frac{4M}{r}\, dr\, dt + r^2 d\Omega^2. \tag{3.20}$$

For the first numerical test, we evolve the equations on a single spherical shell subdomain with radial boundaries (1.9, 11.9). All of the lengths and times given in this section are in units of the black hole mass M. The innermost boundary is placed just inside the horizon (located at $r = 2$), so that no boundary condition is required there (all characteristic modes are outgoing). The interior of the black hole is thus excised from the computational domain. On the outer boundary, $U_{ab}^{-,\mathrm{BC}}$ is computed from the analytical solution. Time-stepping is performed using an explicit Runge-Kutta method. The GH gauge function $\mathcal{H}_a$ is computed from the initial data and then fixed during the evolution:

$$\partial_t \mathcal{H}_a = 0. \tag{3.21}$$

For a spherical shell subdomain, we use a spectral basis composed of Legendre polynomials in the radial direction scaled to the appropriate radial extent and scalar spherical harmonics in the angular directions. The Cartesian components of the tensors are expanded on this basis, so that the numerical solution for particular truncations N_r and L is given by

$$\psi_{ab} = \sum_{i=0}^{N_r} \sum_{l=0}^{L} \sum_{m=-l}^{+l} a_{ilm}\, \tilde{P}_i(r) Y_{lm}(\theta, \phi), \tag{3.22}$$

where $\tilde{P}_i(r)$ represents the appropriately scaled Legendre polynomial, and a_{ilm} are the spectral coefficients.

As the equations are nonlinear, it is well-known that the spectral expansion must be filtered in order to control aliasing error [19]. However, there is another important reason that we employ filtering. Since derivatives of scalar spherical harmonics couple different values of l and m, additional errors are introduced because some (but not all) of the new terms arising from differentiation are truncated. Because these errors often lead to instabilities, some algorithm other than direct filtering of the top few scalar spherical harmonic modes must be used.

The remedy that has been used in the first-order system [40] is equally valid here: transform the variables first to a *tensor* spherical harmonic basis [41], perform the filtering, and then transform back. This works because spatial derivatives of tensor harmonics result in modes of the same index l. We utilize the rather rudimentary filtering method of simply setting the relevant components to zero, and we find that it is sufficient to filter the top three l *tensor* spherical harmonic modes after each time step.

3.3.2 Continuity Condition

Even with filtering, the single black hole evolutions turn out to be unstable. We have found empirically, however, that the system can be stabilized by including an additional term in the penalties: We find that it is necessary to impose a boundary condition that enforces continuity of the field ψ_{ab}. This is done by adding an extra term to the penalties of the form

$$\delta\psi_{ab} \equiv \psi_{ab}^{\mathrm{BC}} - \psi_{ab}. \tag{3.23}$$

The effect of this "continuity term" is displayed in Fig. 3.1, which shows the L_2 error in ψ_{ab} for an evolution both with and without the extra term. Unless

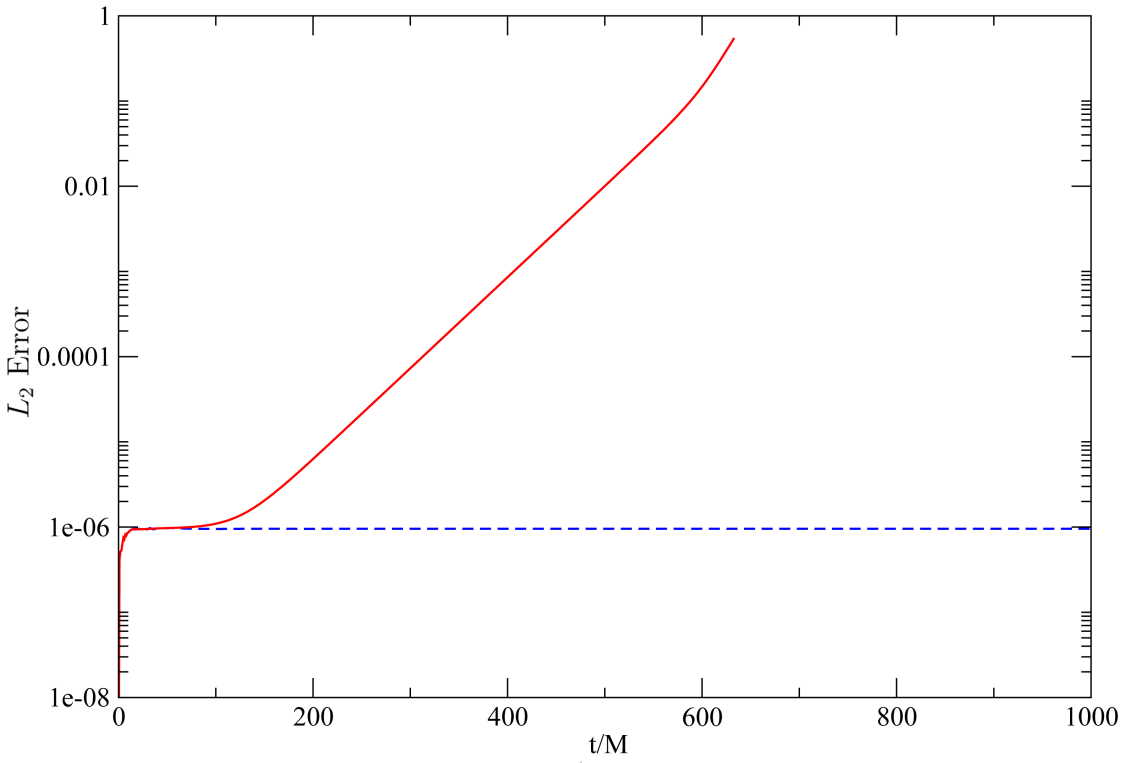

Figure 3.1: The effect of including a continuity term $\delta\psi_{ab}$ in the penalties. The plot shows the L_2 error in the spacetime metric ψ_{ab} for Schwarzschild initial data in Kerr-Schild coordinates. This evolution is on a single spherical shell subdomain with radial extents (1.9 M,11.9 M) and constraint-damping factor $\gamma_0 = 1$. The radial and angular resolutions (N_r, L) are $(18, 8)$.

otherwise stated, the L_2 norm of a (rank ≥ 1) tensor such as $\psi_{\rm err}$ is defined as

$$||\psi_{\rm err}||^2 \equiv \frac{1}{N} \sum_{\substack{\text{grid}\\ \text{points}}} \sum_{a,b} \psi^2_{ab,\rm err}, \tag{3.24}$$

where $\psi_{\rm err} \equiv \psi - \psi_{\rm analytical}$, and N is the total number of grid points.

The second-order equations with penalties, including the continuity term, are thus

$$\partial_t \psi_{ab} = -\alpha \Pi_{ab} + \ldots - \frac{1}{2}\Big(|\lambda_-|\, \delta U^-_{ab} - \delta\psi_{ab}\Big), \tag{3.25}$$

$$\partial_t \Pi_{ab} = -\alpha \partial^k \partial_k \psi_{ab} + \ldots + \frac{\tau}{2}\Big(|\lambda_-|\, \delta U^-_{ab} - \delta\psi_{ab}\Big). \tag{3.26}$$

The penalty on the first equation is applied throughout the entire domain via the

procedure detailed by Eq. (2.95) in Section 2.3, while the penalty on the second equation is applied only on the boundary. The factor τ in Eq. (3.26) represents the penalty coefficient of Eq. (2.141) in Section 2.4. The sign difference in the $\delta\psi_{ab}$ terms can be understood heuristically by thinking of the continuity term as having an appropriately signed dynamical influence and keeping in mind the negative sign in the definition of Π_{ab} in Eq. (3.7).

It could be construed that the continuity term essentially serves the purpose of imposing a boundary condition on the characteristic mode U^{ψ}_{ab}, despite the arguments given in Section 2.4.1 for the analogous scalar wave system that such a condition is unnecessary. This is true in a limited sense only, as we have found that for stability the continuity term must be included in the penalties even on those boundaries where the characteristic mode U^{ψ}_{ab} is outgoing. Note, however, that it is never imposed on a boundary where *all* characteristic modes are outgoing (i.e. an excision surface).

Notice that the continuity term in the penalties in Eqs. (3.25)-(3.26) is not multiplied by any characteristic speed, although it is multiplied by τ in Eq. (3.26). The penalty factor τ scales as N^2, where $N+1$ is the number of grid points along the dimension orthogonal to the boundary in question (radial in this example). This has the worrisome implication that the continuum boundary condition recovered in the limit as $N \to \infty$ is in fact

$$|\lambda_-|U^-_{ab} + \psi_{ab} = |\lambda_-|U^{-,\mathrm{BC}}_{ab} + \psi^{\mathrm{BC}}_{ab}. \tag{3.27}$$

It is thus possible that the coefficient of the continuity term should scale differently, so that in the continuum limit the expected boundary condition $U^-_{ab} = U^{-,\mathrm{BC}}_{ab}$ is obtained, but we have not fully explored this modification.

With the continuity term included in the penalties, the evolutions are stable

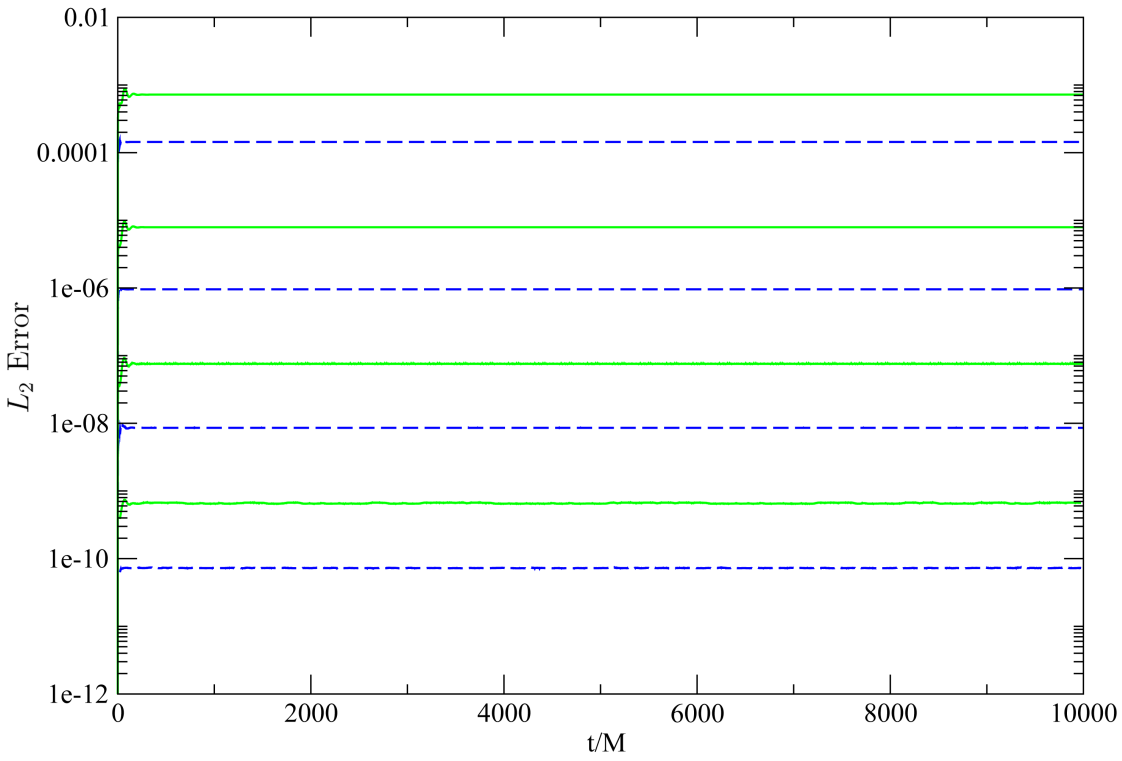

Figure 3.2: L_2 error in the spacetime metric ψ_{ab} for Schwarzschild initial data in Kerr-Schild coordinates with a continuity term $\delta\psi_{ab}$ included in the penalties of the second-order system (dashed blue). This test is performed on a single spherical shell subdomain with radial extents (1.9 M,11.9 M) and constraint-damping factor $\gamma_0 = 1$. The radial and angular resolutions (N_r, L) of these evolutions are $(12, 6)$, $(18, 8)$, $(24, 10)$, and $(30, 12)$. The results of an equivalent first-order simulation are plotted for comparison (solid green).

and convergent. Figure 3.2 shows the L_2 error in ψ_{ab} for this test problem as a function of time for several resolutions. The results from an equivalent first-order evolution (using the modified GH system of Ref. [24]) are plotted for comparison. The second-order evolutions have significantly smaller errors (about an order of magnitude) in the metric than the first-order simulations at each resolution, as was similarly observed for the scalar wave system in Figs. 2.4-2.5.

One important difference from the second order scalar wave system, however, is that there is now a constraint—namely, the gauge constraint C_a defined in Eq. (3.4). As is shown in Fig. 3.3, the L_2 gauge constraint violations in the

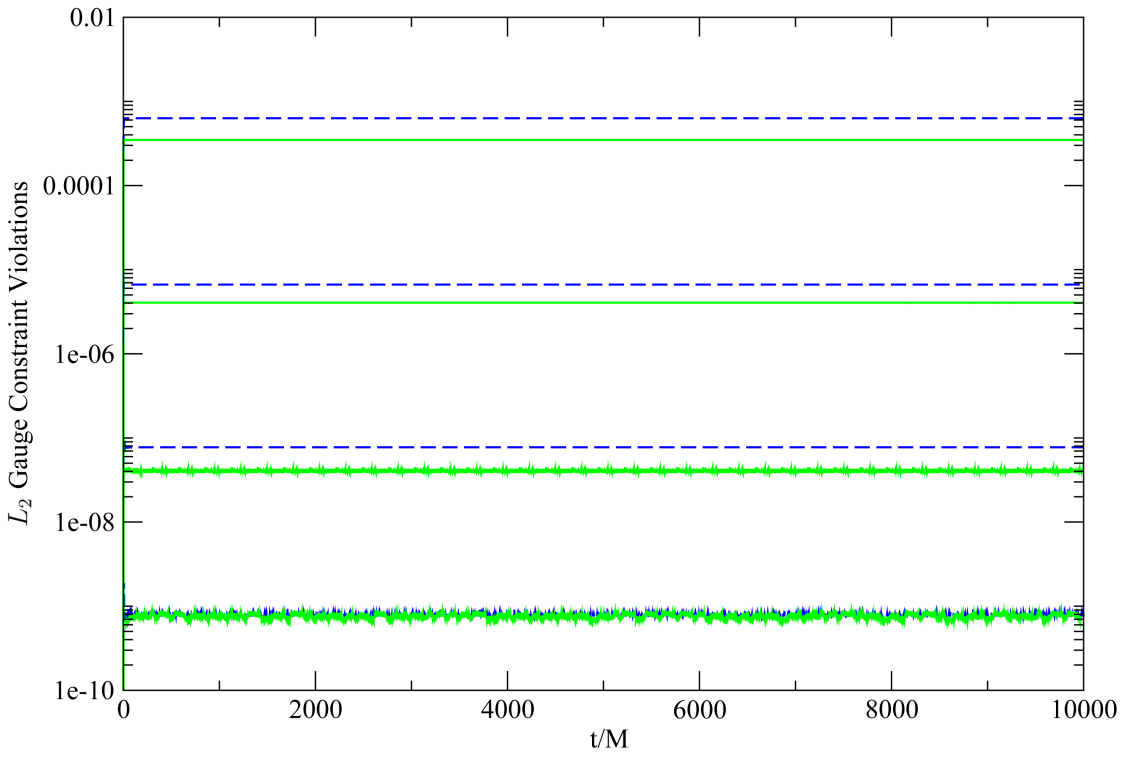

Figure 3.3: L_2 gauge constraint violations $||C_a||$ for the same evolutions as shown in Fig. 3.2. The constraints in the second-order system (dashed blue) are somewhat larger than in the equivalent first-order simulations (solid green).

second-order system are actually somewhat larger (by about a factor of two) than in the first-order evolutions, at all but the highest resolution. This may seem surprising at first, since we have just seen that the error in the metric is smaller in the second-order system.

However, the constraint C_a is computed from the trace of the Christoffel symbols Γ_a and is thus in some sense a measure of the error in the derivatives of the metric, rather than the metric itself. Moreover, the trace Γ_a in the first-order system is computed not from derivatives $\partial_i \psi_{ab}$, but from the variable Φ_{iab}. One might expect the variable Φ_{iab} to be a more accurate representation of derivatives than $\partial_i \psi_{ab}$ (computed from the numerical solution), since differentiation in effect reduces the number of basis functions in the spectral expansion by one.

Of course, the first-order system has multiple constraints, which are typically combined into a constraint norm [24], and these should be considered when comparing the two systems. In particular, a closer comparison of the constraints C_a should take into account the magnitude of C_{iab} defined by Eq. (3.13) for the first-order system, which measures the amount by which ϕ_{iab} differs from $\partial_i \psi_{ab}$. For the single black hole test problem of Figs. 3.2-3.3, the L_2 magnitude of C_{iab} is equal to or greater than the gauge constraint violations in the second-order system at every resolution. This can therefore account for the difference in $\|C_a\|$ between the two systems.

3.3.3 Effects of Constraint Damping

Now consider the same test problem on three spherical shell subdomains with radial boundaries at $(1.9, 11.9, 21.9, 31.9)$. The incoming characteristic mode $U^{-,\mathrm{BC}}_{ab}$ at an interface boundary is supplied by the adjacent subdomain, and the continuity term $\delta\psi_{ab}$ is included at all boundaries. The use of multiple subdomains serves several purposes. Perhaps most importantly, our pseudo-spectral methods are based on the use of relatively simple topologies (cubes, spherical shells, etc.) [42]. To solve a problem on a more complicated domain (as in the binary black hole case, which has two holes excised), one must therefore subdivide the domain into a combination of relatively simple subregions, so any robust code must be able to perform sufficiently well in the presence of interface boundaries. Having multiple subdomains also provides a straightforward way to balance the computational load across multiple processors, and it gives an easy way to vary the strength of the constraint damping in different regions (i.e. by having a different constant value of γ_0 on each subdomain).

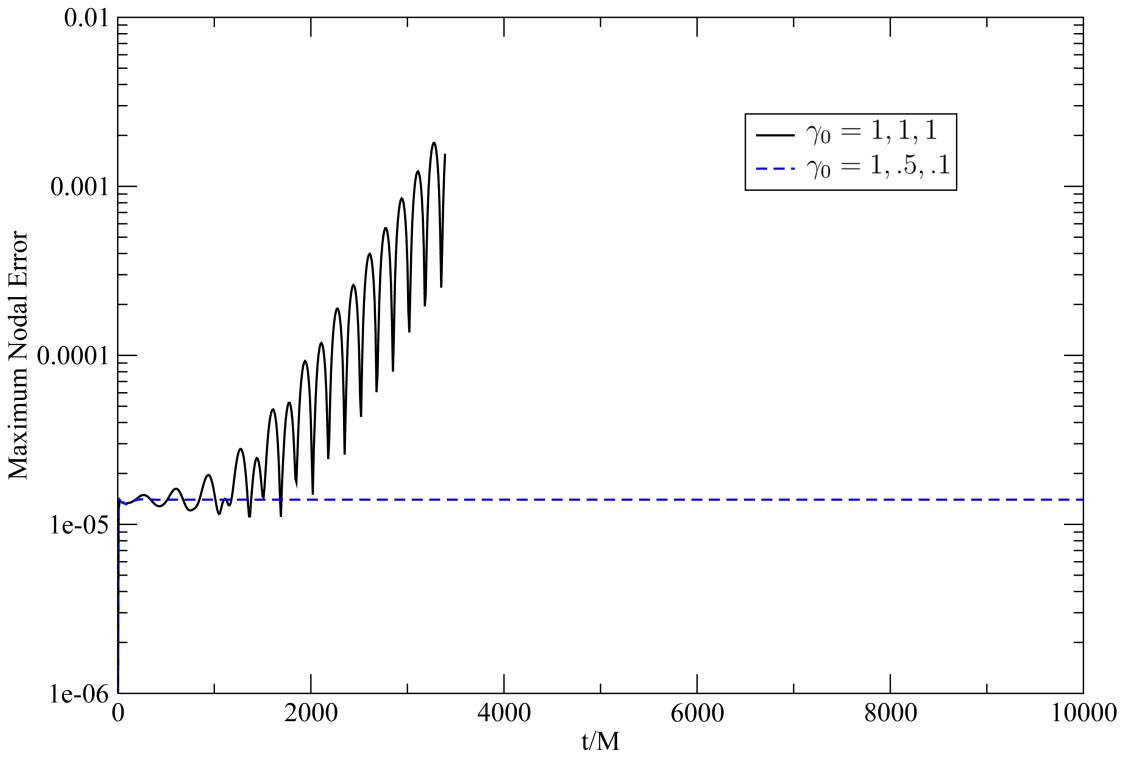

Figure 3.4: The effect of constraint damping strength on stability. In the unstable case, $\gamma_0 = 1$ on each subdomain. In the stable case, $\gamma_0 = 1, .5, .1$ on the inner, middle, and outer spherical shells, respectively. The plot shows the L_∞ error (maximum nodal error) in the spacetime metric ψ_{ab} for Schwarzschild initial data in Kerr-Schild coordinates evolved on three concentric spherical shell subdomains with radial boundaries (in units of M) at $(1.9, 11.9, 21.9, 31.9)$. The radial and angular resolutions (N_r, L) of the evolutions are $(16, 9)$ on each subdomain.

For this test problem, we find that the evolutions are unstable with a constraint-damping factor $\gamma_0 = 1$ on each subdomain. One might expect that the remedy to this would simply be to increase the strength of the constraint damping by increasing the value of γ_0. However, we observe essentially the opposite effect: the damping factor must be decreased on the outer subdomains in order to stabilize the evolutions. Figure 3.4 shows the constraint violations with two different choices of γ_0 on the three subdomains, demonstrating this effect. Note that such sensitivity to damping strength is not unique to the second-order system, but occurs in the first-order case as well.

It is important to point out that the instability associated with the choice $\gamma_0 = 1$ on each subdomain is not tied to the use of multiple subdomains in any essential way. Indeed, if we evolve the system on a single spherical shell subdomain with radial boundaries at $(1.9, 31.9)$ and $\gamma_0 = 1$, we find a similarly unstable result. Moreover, if we evolve the system on three subdomains with radial boundaries at $(1.9, \cdot, \cdot, 11.9)$, the evolutions are stable.

The instability is also not solely a result of having too large a constraint damping in any particular region, for a single subdomain evolution with $\gamma_0 = 1$ and radial boundaries at either $(1.9, 11.9)$, $(11.9, 21.9)$, or $(21.9, 31.9)$ is perfectly stable. Rather, the problem seems to be associated with the relative magnitudes of $\|C_a\|$ and $\|\psi_{\rm err}\|$ on different parts of the domain. We conjecture that the ideal choice of constraint damping is one that helps to equalize the magnitudes of the errors and constraint violations across the domain. This would be an interesting topic to explore in more detail, but for now the choice of damping factors is largely empirical.

There is typically a range of stable values for γ_0: too small and the constraints are not damped, too large and the evolutions (sometimes) become unstable. In general, the larger the value of γ_0, the stricter the time-stepping (CFL) condition. While we have tested the evolutions with sufficiently small time steps to rule this out as a cause of the instability, it does suggest that the smallest possible stable values of γ_0 should be chosen in order to achieve the most efficient evolutions.

An effective way to judge the presence and relative strength of an instability in an evolution is to examine the spectral coefficients as functions of time [19]. If an instability is present in the highest-order modes, it can usually be cured

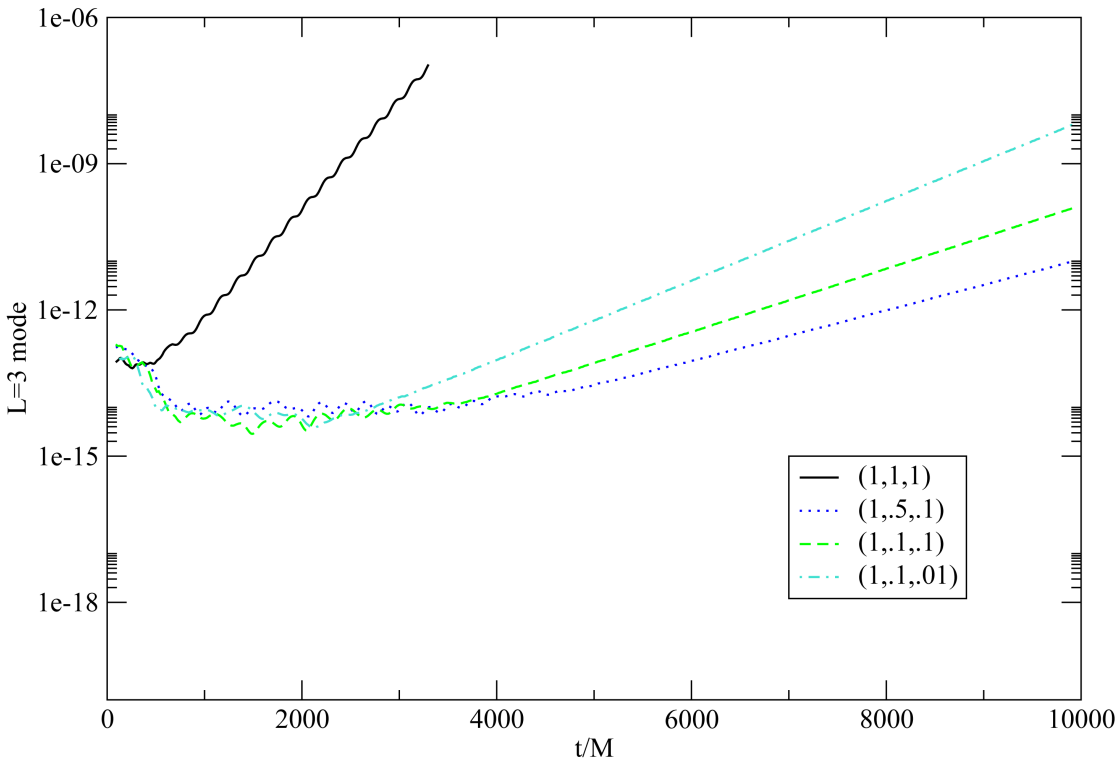

Figure 3.5: The magnitude of the $l = 3$ mode of the spacetime metric ψ_{ab} on the innermost subdomain for several sets of constraint damping factors. The values of γ_0 from innermost to outermost subdomain are displayed as triples $(\gamma_{\rm in}, \gamma_{\rm mid}, \gamma_{\rm out})$. The three concentric spherical shell subdomains have radial boundaries (in units of M) at $(1.9, 11.9, 21.9, 31.9)$, and the radial and angular resolutions (N_r, L) of the evolutions are $(16, 9)$ on each subdomain.

by additional filtering. For the unstable case shown in Fig. 3.4, however, the instability shows up in the lower order spherical harmonic modes. Figure 3.5 shows the magnitude of the $l = 3$ component of the metric (rms averaged over tensor components and values of m) on the innermost subdomain for several different sets of damping factors γ_0. The instability can be practically eliminated by proper choice of constraint damping, as evidenced in the figure.

With judicious choice of constraint damping (and with the continuity term $\delta\psi_{ab}$), the multiple subdomain Schwarzschild evolutions are stable and convergent on timescales that are more than sufficient for the binary black hole prob-

lem. We have successfully tested the evolutions on a variety of domain decompositions, including spherical shells, cylindrical shells, and blocks, and with a variety of (noisy) initial data, including flat space, Schwarzschild in Painlevé-Gullstrand coordinates [36] and Kerr (with arbitrary spin) in Kerr-Schild coordinates.

The numerical tests discussed in this section have used a spectral expansion of the form in Eq. (3.22), with a radial basis composed in particular of (scaled) Legendre polynomials. In the investigation of the second order penalty method applied to scalar waves, it was found that a basis of Chebyshev polynomials could be used almost interchangeably. In the present case, this is no longer true. Indeed, if a Chebyshev basis is used, the evolutions are no longer stable. This is in contrast to the first-order system, which performs equally well with either basis. However, we have not explored the use of the Chebyshev-Legendre method [33], in which the equations are implemented on a Chebyshev grid by evaluating (or equivalently interpolating) the Legendre penalty functions at the Chebyshev grid points.

In all of these tests, we have found it to be sufficient to include only the bulk penalty contributions from faces of the boundaries (not edges or corners), as discussed in Section 2.3.1. However, we caution that these additional terms may be needed in some cases. We have also relied on definitions of outgoing spatial normal vectors on domain boundaries of any codimension (edges and corners) as defined in Section 2.3.

3.4 Binary Black Hole

We now consider the application of the second-order GH system to the evolution of a binary black hole. For this problem, we utilize many of the same techniques as the first-order evolutions described in Ref. [16]. We first review some of these techniques and discuss the formulation of boundary conditions in the second-order system. We then briefly describe the numerical setup for this problem and turn to a discussion of the preliminary results.

3.4.1 Dual Frames Method

The system is evolved using the dual frames method [43] in which the equations are solved in an "inertial frame" that is asymptotically Minkowskian, while the numerical domain rotates in a "moving" frame. A control system measures the positions of the apparent horizons of the black holes and periodically updates the mapping between the two frames in order to keep the excised regions of the grid inside the horizons, at approximately constant locations in the moving frame. The inertial components of the tensor variables are thus evolved as functions of the moving coordinates, so the equations are modified only by a change of coordinates (not a change of basis). Here, we briefly review some of the main points of the dual frames method—the motivation and details are discussed in Ref. [43].

We consider only changes of coordinates that have the same time slicing $t = \bar{t}$, so the mapping from inertial to moving frames simply introduces an additional shift term in the equations. For example, if the mapping is a function $x^\mu = x^\mu(\bar{x}^\nu)$

that maps moving (barred) to inertial coordinates, then a change of variables on a function ψ relates the time derivatives in the two frames:

$$\partial_{\bar{t}}\psi = \partial_t\psi + \frac{\partial x^i}{\partial \bar{t}}\partial_i\psi. \tag{3.28}$$

Therefore, the system in Eqs. (3.15)-(3.16) is modified as

$$\partial_{\bar{t}}\psi_{ab} = -\alpha\Pi_{ab} + \ldots + \tilde{\beta}^i\partial_i\psi_{ab}, \tag{3.29}$$

$$\partial_{\bar{t}}\Pi_{ab} = -\alpha\partial^k\partial_k\psi_{ab} + \ldots + \tilde{\beta}^i\partial_i\Pi_{ab}, \tag{3.30}$$

where the shift in the additional terms is defined by $\tilde{\beta}^i \equiv \partial x^i/\partial\bar{t}$. Since the tensor variables are functions of moving coordinates, derivatives (which are computed with respect to the grid) must be transformed to the inertial basis, as in

$$\partial_i\psi_{ab} = \frac{\partial x^{\bar{k}}}{\partial x^i}\partial_{\bar{k}}\psi_{ab}. \tag{3.31}$$

The characteristic modes in Eqs. (3.17)-(3.19) remain the same, while the characteristic speeds are modified as

$$\bar{\lambda} = \lambda - n_i\tilde{\beta}^i, \tag{3.32}$$

where n_i represents the (inertial) components of the outgoing normal one-form on the boundary. Note that the modified speeds may result in a change of which characteristic variables are incoming on a boundary. If both U^-_{ab} and U^+_{ab} are incoming, we enforce a condition on both modes by using the form of the penalties appropriate to this case as in Eqs. (2.137)-(2.138) of Section 2.4.2.

Lastly, the filtering procedure must be modified when using the dual frames method [43]. In short, before filtering as described in Sec. 3.3.1 above, the (spatial) tensor variables must first be transformed to a *moving frame* tensor spherical harmonic basis.

3.4.2 Boundary Conditions

We turn now to a discussion of the boundary conditions imposed at the outermost boundary of the computational domain. Even though U^{ψ}_{ab} and U^{0}_{ab} may be incoming ($\lambda < 0$), recall that we do not impose any conditions on these modes in the second-order system. We will therefore assume that U^{-}_{ab} is the only incoming mode. Since we do not have an analytical solution, we cannot include a continuity term $\delta\psi_{ab}$ in the penalties as was done for the single black hole evolutions in Sec. 3.3 (although this term is included at all interface boundaries).

One of the simplest boundary conditions we can impose is a Sommerfeld condition, heuristically defined by assuming that the Cartesian components of the metric asymptotically obey

$$\psi_{ab} \sim \eta_{ab} + \frac{f(t-r)}{r}, \tag{3.33}$$

where η_{ab} is the Minkowski metric. This translates into a condition on the incoming mode:

$$U^{-}_{ab} = \frac{\psi_{ab} - \eta_{ab}}{r}. \tag{3.34}$$

While naive conditions like this one lead to qualitatively correct evolutions, constraint violations on the outermost subdomain do not converge (to zero) with increasing resolution. The constraint-damping term of Eq. (3.5) can control constraint growth that arises on the domain as a result of truncation error, for example, but it is not as effective at reducing constraint violations that enter the domain through the outer boundary. We therefore employ constraint-preserving boundary conditions that are designed to control the influx of constraint-violating modes.

Details of the derivation of constraint-preserving boundary conditions for

the first-order GH system are given in Ref. [24]. The results are the same for the second-order system, with the replacement $\Phi_{iab} \to \partial_i \psi_{ab}$, and with the first-order constraints of Eqs. (3.13)-(3.14) (which are not present in the second-order system) set to zero. Here, we briefly summarize the procedure.

One begins by writing down the evolution equations for the constraint C_a of Eq. (3.4), which can be derived from the GH form of Einstein's equations. This gives a second-order equation for C_a that can be reduced to first order in the usual way by introducing new variables defined as first order time and space derivatives (of C_a). After computing the characteristic variables of this first order constraint system, conditions on the incoming variables U^-_{ab} of the original system are obtained by requiring that the incoming constraint modes vanish.

This does not completely specify the incoming modes, but instead determines only four of the ten degrees of freedom in the symmetric tensor U^-_{ab}; there are an additional two physical and four gauge degrees of freedom that must be specified separately. The boundary conditions on the constraint, physical, and gauge degrees of freedom are combined into a single condition on the incoming mode U^-_{ab} (along with the other incoming modes of the first-order system). Setting the incoming constraint modes to zero is tantamount to a condition on the (incoming) characteristic projection of the normal derivatives of the fundamental variables. It can be shown that this is equivalent to a condition on the time derivative of the incoming mode $\partial_t U^-_{ab}$ (neglecting the derivative of the normal vector $\partial_t n^i$), which is the form that is imposed in the first-order GH system.

The final form of the boundary condition imposed in the second-order system is given by combining the right-hand sides of Eqs. (64) and (68) of Ref. [24], rewritten in the language of the second-order system (setting constraints unique

to the first-order system to zero, etc.). The remaining (gauge) degrees of freedom in U^-_{ab} are set according to a Sommerfeld condition similar to Eq. (3.34):

$$\partial_t U^-_{ab} = \mathcal{P}_{\rm gauge}\Big(\frac{\partial_t \psi_{ab}}{r}\Big), \tag{3.35}$$

where $\mathcal{P}_{\rm gauge}$ represent the projection onto the gauge degrees of freedom, defined by

$$\mathcal{P}_{\rm gauge} \equiv \mathbf{1} - \mathcal{P}_{\rm constraint} - \mathcal{P}_{\rm physical}, \tag{3.36}$$

and where the constraint and physical projection operators are defined by Eqs. (64) and (68) of Ref. [24].

Since the constraint-preserving boundary condition supplies the time derivative of the incoming mode, it cannot be imposed through the usual penalties such as in Eqs. (3.25)-(3.26). In the first-order system, these conditions are imposed by using a Bjørhus projection method [31], which enforces the boundary conditions by replacing the time derivatives of the fields on the boundary. For example, the inverse characteristic projection to the variable Π_{ab} is

$$\Pi_{ab} = \frac{1}{2}(U^-_{ab} + U^+_{ab}). \tag{3.37}$$

With the Bjørhus method, the equation of motion for $\partial_t \Pi_{ab}$ on the outer boundary is accordingly replaced by

$$\partial_t \Pi_{ab} = \frac{1}{2}(\partial_t U^{-,\rm BC}_{ab} + \partial_t U^+_{ab}), \tag{3.38}$$

where $\partial_t U^{-,\rm BC}_{ab}$ is supplied by the boundary condition and $\partial_t U^+_{ab}$ is computed as the characteristic projection of (the right-hand side of) the evolution equations.

Unfortunately, we have been unable to use the Bjørhus projection method in the second-order system. The correct way to project the boundary condition to $\partial_t \psi_{ab}$ is not clear, as discussed in Section 2.2.2 for the analogous case of a scalar

wave, and all of our attempts to employ variations of this method have resulted in quickly unstable evolutions. We have attempted to impose time derivative boundary conditions by using a penalty method with bulk penalty functions constructed especially for this purpose (see Appendix D for details). Although this approach has worked for scalar wave evolutions, we have been unable so far to generalize it to Einstein's equations in a stable way.

3.4.3 Auxiliary Boundary Variable Evolution

The most effective method that we have found for imposing time derivative boundary conditions is to evolve an auxiliary variable X_{ab} on the boundary, whose time evolution is governed by the boundary condition:

$$X_{ab}(0) = U^{-}_{ab}(0), \tag{3.39}$$

$$\partial_t X_{ab} = \partial_t U^{-,\mathrm{BC}}_{ab}. \tag{3.40}$$

The boundary conditions are then imposed according to the usual second-order penalty method of Eqs. (3.25)-(3.26) with the identification $U^{-,\mathrm{BC}}_{ab} = X_{ab}$. It should be noted that the addition of a variable that couples to the evolution equations brings the well-posedness of the system into question. While we have not analyzed this, we find that the method performs fairly well in the binary evolutions, as will be discussed below.

Care must be taken when implementing this sort of boundary condition in the context of the dual frames method discussed above. The constraint-preserving conditions are formulated in the inertial frame, but boundary conditions are imposed as functions of moving coordinates. The condition on $\partial_t U^{-}_{ab}$ must therefore be translated to a condition on $\partial_{\bar{t}} U^{-}_{ab}$ in order to evolve the vari-

able X_{ab}. A straightforward application of the change of variables from inertial to moving frames gives

$$\partial_{\bar{t}} U^- = \partial_t U^- + \tilde{\beta}^j \partial_j U^-, \tag{3.41}$$

where $\tilde{\beta}^i \equiv \partial x^i / \partial \bar{t}$, and we have omitted all tensor indices for conciseness. Expanding the last term, we obtain

$$\partial_{\bar{t}} U^- = \partial_t U^- + \tilde{\beta}^k \partial_k \Pi - n^i \tilde{\beta}^j \partial_i \partial_j \psi - \tilde{\beta}^j \partial_j n^i \partial_i \psi. \tag{3.42}$$

Note that the constraint-preserving boundary condition does not supply $\partial_t U^-$, but rather the characteristic projection of $\partial_t \Pi$ and $\partial_t \partial_i \psi$. That is, it does not contain the derivative of the normal vector $\partial_t n^i$. Using

$$\partial_{\bar{t}} n^i = \partial_t n^i + \tilde{\beta}^j \partial_j n^i, \tag{3.43}$$

we can rewrite Eq. (3.42) as

$$\partial_{\bar{t}} U^- = \partial_t U^-_{\mathrm{BC}} + \tilde{\beta}^k \partial_k \Pi - n^i \tilde{\beta}^j \partial_i \partial_j \psi - \partial_{\bar{t}} n^i \partial_i \psi, \tag{3.44}$$

where $\partial_t U^-_{\mathrm{BC}}$ represents the constraint-preserving boundary condition.

In the first-order system, the derivative of the normal vector in the last term of Eq. (3.44) can be ignored when using the Bjørhus projection method. This is allowed because such terms cancel out in the projection back to fundamental variables. For example, in Eq. (3.38) any terms involving the derivatives $\partial_t n^i$ would have opposite signs in the two characteristic modes on the right-hand side. With the evolution of an auxiliary variable X, however, these terms cannot simply be ignored.

Note that the last term in Eq. (3.44) contains the moving frame time derivative of the *inertial* components of the normal vector. Normals are defined with

respect to the domain boundary, which is fixed in the moving frame. It is therefore plausible that we may in fact neglect the moving frame time derivative of the *moving* components of the normal vector instead, and this does indeed give good results as will be shown below. The last term in Eq. (3.44) can be rewritten in terms of the moving components as

$$\partial_{\bar{t}} n^i \partial_i \psi = n^i \partial_i \tilde{\beta}^j \partial_j \psi + \partial_{\bar{t}} n^{\bar{k}} \partial_{\bar{k}} \psi. \tag{3.45}$$

Neglecting the time derivative of the moving components of the normal vector, we obtain the transformation law

$$\partial_{\bar{t}} U^- = \partial_t U^-_{\rm BC} + \tilde{\beta}^k \partial_k \Pi - n^i \tilde{\beta}^j \partial_i \partial_j \psi - n^i \partial_i \tilde{\beta}^j \partial_j \psi. \tag{3.46}$$

This relation is used to transform the constraint-preserving boundary conditions to the moving frame before evolving the auxiliary variable X_{ab}. Of course, it is possible to compute the derivatives of the normal vectors exactly during an evolution without neglecting any terms; However, we have not experimented with this variation.

3.4.4 Test Problem Description

The problem we consider is the evolution of a 16 orbit, equal mass, non-spinning binary black hole system with initial coordinate separation $d = 30$ (in code units). Most of the results given in this section will use length and time scales measured in terms of code units, which we denote as M_c. For comparison, this can be expressed in terms of the total irreducible mass m of the two black holes in the initial data, where

$$m \equiv M_{\rm irr,1} + M_{\rm irr,2}. \tag{3.47}$$

The irreducible mass of a single black hole is defined as

$$M_{\rm irr} \equiv \sqrt{\frac{A}{16\pi}}\,, \tag{3.48}$$

where A is the surface area of the event horizon (in practice this is taken to be the apparent horizon). Computing the total irreducible mass in the initial data in terms of code units, we find

$$m \simeq 2.078\, M_c. \tag{3.49}$$

The initial data set we use is the eccentricity-removed set 30c described in Ref. [16]. Most of the evolution techniques (e.g. the gauge source function evolution) that we employ are the same as those used for the first-order system, except that the evolution equations (including penalty functions) are replaced by the second-order GH system of Section 3.2.2, and the outer boundary conditions are replaced by the auxiliary variable method described above. Boundary conditions at interfaces are imposed via the penalty method described in Section 3.3, which includes the continuity term $\delta\psi_{ab}$ on all boundaries that have at least one other incoming mode. We impose boundary conditions on edges and corners by utilizing the normal vectors defined in Section (2.3), and we include the volume penalty contributions from boundary faces only. We have experimented with including the bulk penalty terms due to edges and corners as well, but have found that these neither improve nor worsen the results in any of the evolutions we have performed.

The domain decomposition used for this problem is the same as that of the evolution 30c-1 of Ref. [16], except that the innermost cylinders along the x axis connecting the centers of the two black holes are replaced by blocks, which overlap the cylindrical shells surrounding them. The reason for replacing the cylinders with blocks is that we have not yet generalized the second-order penalty

method to subdomains constructed with Gauss-Radau collocation grids—i.e. grids where one of the endpoints along a dimension is omitted, as in the half-open interval $(0, 1]$. The innermost cylinders used in the first-order binary evolutions are constructed from the unit disk, which uses a Gauss-Radau grid in the radial dimension. All one-dimensional bases in our domain decomposition use Legendre polynomials (Legendre-Lobatto grids), which includes the radial basis on cylindrical- and spherical-shell subdomains and the bases along all three dimensions on blocks.

The domain decomposition consists of a total of 66 subdomains, which initially cover the region from just inside the individual horizons (located at a distance of about $1\,M_c$ from the black hole centers) to $r_{\rm max} = 960\,M_c$ as measured from the origin of the coordinate system (i.e. the center of mass of the system). In the grid frame, the centers of the black holes are located at $x = \pm 15\,M_c$. Each hole is surrounded by a series of six concentric spherical shells that extend to about $10\,M_c$ from the black hole centers. Six blocks are located along the x axis, with two between the holes and two on either side. Around these are a series of 28 cylindrical shells, placed in such a way that the domain becomes roughly spherical in shape with a radius of $r \sim 100\,M_c$. Finally, the blocks and cylinders are surrounded by 20 additional spherical shells, which extend out to $r_{\rm max} = 960\,M_c$. The innermost 'outer spherical shell' overlaps the blocks and cylinders so that there are no gaps in the computational domain. We consider the low, medium and high resolutions that are denoted as N2, N4, and N6, respectively, and are described in Ref. [16] for the first-order system.

Constraint-damping factors γ_0 are given values ranging from roughly 1 on the innermost spherical shells surrounding each black hole to about .01 on the

outer spherical shells (γ_0 is a constant on each subdomain). On the outermost few spherical shells we increase the damping for reasons that will be discussed below. No filtering is performed on blocks or on the radial components on spherical- and cylindrical-shell subdomains. On spherical shells we filter the top four l components of the variables in the moving-frame tensor spherical harmonic basis, while on cylindrical shells we filter the top two angular Fourier modes. In the results below, whenever we compare the second-order binary results to the 'equivalent' first-order case, we are referring to the corresponding first-order evolutions described in Ref. [16]. These are of course not entirely equivalent, because they use cylinders along the x axis (instead of blocks) and different constraint damping parameters.

3.4.5 Numerical Results

The second order binary simulations unfortunately exhibit stability problems that have not yet been completely resolved. However, the evolutions perform well for a significant fraction of the inspiral phase, as will be discussed below. First, we will comment on the effectiveness of the outer boundary conditions and how they relate to the choice of constraint damping strength.

The constraint violations on the outermost spherical shell depend significantly on the magnitude of the damping factor γ_0 there. Figure 3.6 shows the L_2 magnitude of the constraint C_a on the outermost spherical shell for an evolution at resolution N2, with γ_0 ranging from .01 to 5. The initial rise of constraint violations occurring after roughly one light-crossing time, or about $t \sim r_{\max} \sim 1000\, M_c$, is due to the 'junk radiation' that results from imperfect

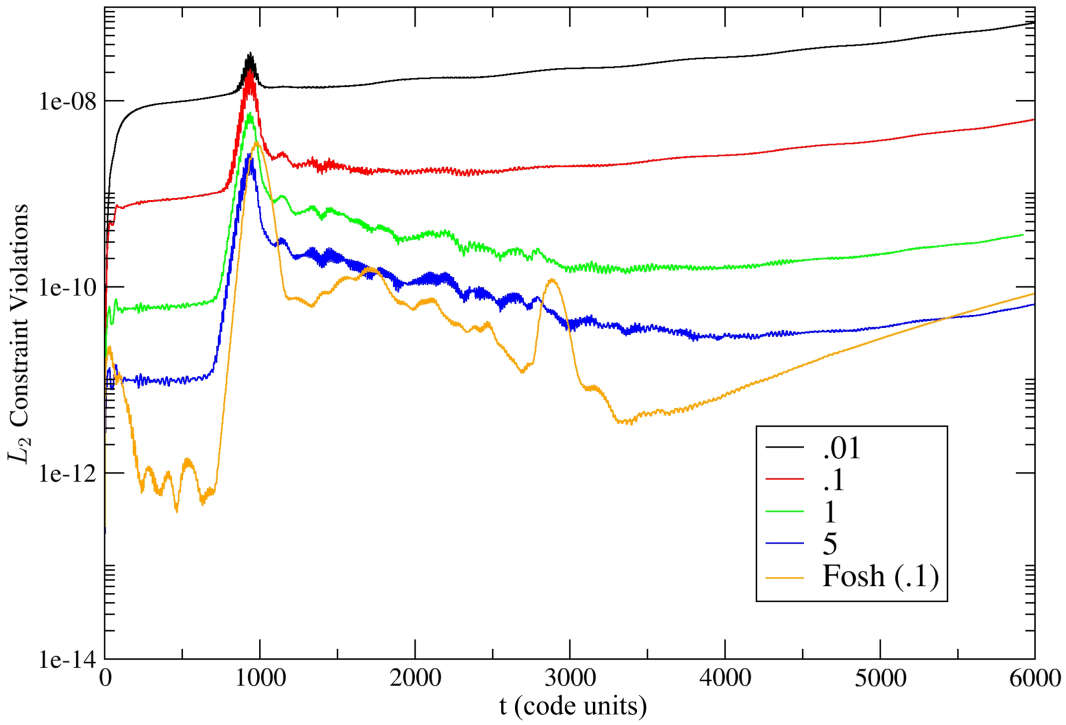

Figure 3.6: The effectiveness of constraint-preserving boundary conditions imposed with an auxiliary boundary variable in a second order binary evolution. This plot shows the L_2 constraint violations on the outermost spherical shell subdomain for a range of damping factors γ_0 versus time (in code units). The (gauge) constraint violations on the same subdomain for an equivalent first-order (Fosh) evolution (in which $\gamma_0 = .1$ on the outermost spherical shell) are plotted for comparison.

(i.e. not precisely quasi-equilibrium) initial data [16]. Increasing the constraint damping beyond that shown in the figure has very little effect on reducing the constraint violations further.

It is clear, however, that we can achieve roughly the same magnitude of (gauge) constraint violations on the outer spheres as in the first-order evolutions, albeit with a greater damping factor (the first-order evolution uses $\gamma_0 \sim .1$ on the outer spheres). Unless otherwise stated, we set $\gamma_0 \simeq 5$ on the outer few subdomains for all the binary evolutions discussed in this section. Note that with a non-constraint-preserving boundary condition such as the Sommerfeld

condition of Eq. (3.34), constraint violations on the outermost subdomain are no less than about $\|C_a\| \sim 10^{-7}\, M_c$ (which occurs in that case for $\gamma_0 \gtrsim .001$), regardless of the magnitude of the damping factor.

The second order binary evolutions crash at late times as a result of instabilities arising on the blocks along the x axis (connecting the centers of the two black holes). For the low resolution N2 case, this occurs around $t \sim 7500\, M_c$, or about 12 orbits into the inspiral. For comparison, the merger would occur at a code time of $t \sim 8190\, M_c$. We have found that this instability is related to the changing signs of the characteristic speeds on the edges and corners of the blocks. Because the speeds are modified in the moving frame by Eq. (3.32), the characteristic modes become outgoing (all speeds positive) on particular boundaries when the orbital frequency in the dual frames coordinate mapping increases beyond a certain extent. When this happens, no penalties (including the continuity condition) are imposed on these boundaries, and instabilities appear to arise on particular edges and corners of the blocks shortly after this occurs. Since normal vectors on boundaries of codimension > 1 are defined according to the procedure in Section 2.3 to be resolution-dependent weighted sums of adjacent face normals, the time at which the characteristic speeds change signs depends not only on the boundary in question, but also on the resolution.

While we do not yet fully understand this problem, we have found empirically that the lifetimes of the evolutions can be extended by modifying the coefficients of the penalties on the corners and edges of the subdomains so that boundary conditions (including the continuity term) are imposed even after the characteristic speeds change sign. Recall that the magnitudes of the characteristic speeds enter into the penalty coefficients as in Eq. (3.25)-(3.26). The ad hoc

modification we impose sets the minimum characteristic speed for U^-_{ab} entering the penalties to 0.1, even after $|\lambda_-| < 0.1$. Note that this condition is imposed only on edges and corners of the subdomains, which in our domain decomposition are not present on either the excision surfaces or the outer boundary of the domain. In the discussion that follows, it will be assumed that this modification has been imposed.

The second-order evolutions with this penalty modification perform well and exhibit good convergence in constraint violations for roughly the first six orbits, after which convergence and stability problems begin to arise at high resolution. Figure 3.7 shows the 'volume' L_2 constraint violations over the entire domain for the three resolutions N2, N4, and N6, along with the corresponding (gauge) constraint violations from the equivalent first-order evolutions. The volume L_2 norm of C_a is defined as

$$\|C_a\|^2_{\mathrm{vol}} \equiv \frac{1}{V}\int_\Omega \sum_a C_a^2\,\gamma^{1/2}\,dV, \tag{3.50}$$

where Ω is the domain, V is the total volume of the domain, $\gamma \equiv \det \gamma_{ij}$, and the integral is evaluated numerically using quadrature [19]. This definition, which is closer to the usual continuum L_2 norm, generally yields smaller constraint violations than the pointwise sum of Eq. (3.24). This is because the largest errors normally occur near boundaries, which is where the grid spacing is smallest (as with any Gauss-Lobatto grid). The values at these points therefore contribute less to the volume integral. Since the constraint violations depicted in Fig. 3.7 are unnormalized, however, it is of little importance which norm is used. We are primarily concerned only with the relative magnitudes at different resolutions (and with respect to the same quantity from the first-order code).

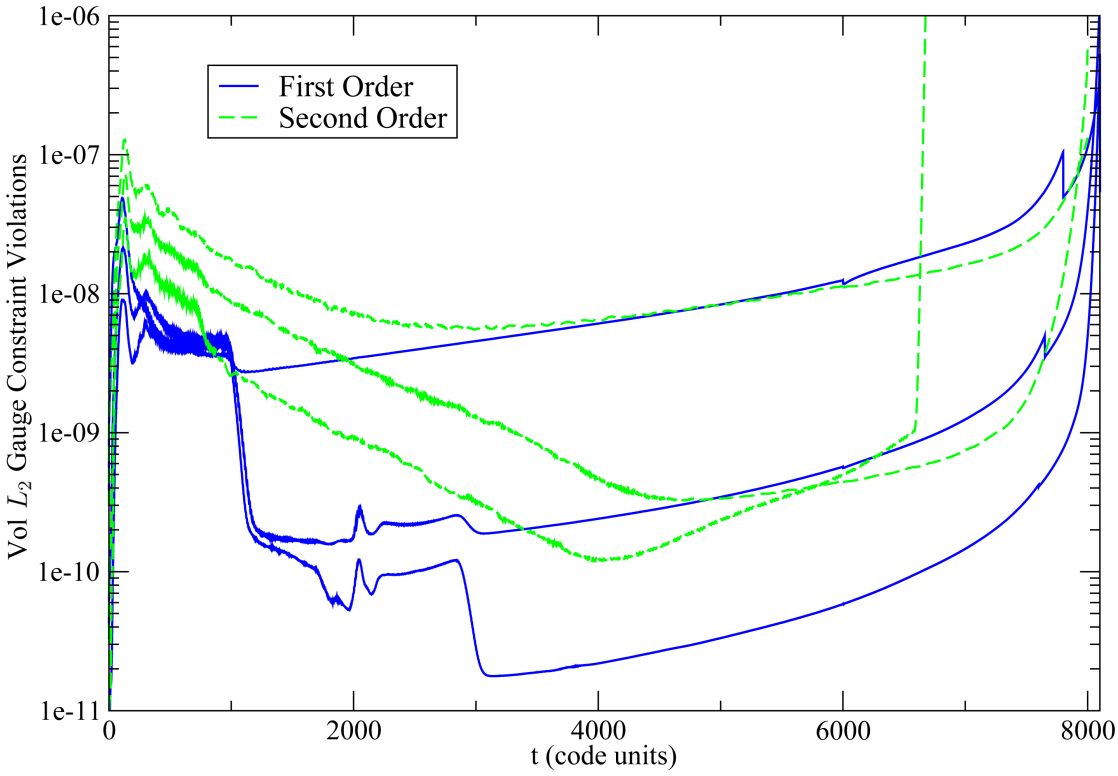

Figure 3.7: The (unnormalized) volume L_2 gauge constraint violations on the entire domain as a function of code time for the three different resolutions N2, N4, N6. Equivalent results for the first-order evolutions are also shown.

The second-order system crashes as a result of instability at the highest resolution N6 around $t \sim 6600\,M_c$ (about 10 orbits into the inspiral), with a non-convergent growth of constraint violations beginning around $t \sim 4000\,M_c$ (after about six orbits). The low and medium resolutions N2 and N4 crash around $t \sim 8000\,M_c$, which is about one orbit from merger. This is close enough that one could try adjusting the gauge conditions in order to evolve until a common horizon forms, as is done in the first-order system [25]. We will examine the high resolution instability in more detail below. First, we will make a few remarks about other features in Fig. 3.7 that are immediately apparent.

The cusps in the first-order curves in Fig. 3.7 at times $t \sim 6000\,M_c$ and again at $t \sim 7500\,M_c$ are the result of dropping the innermost spherical shell subdomains around the black holes from the computational domain. The dual frames coordinate mapping keeps the positions of the black holes fixed in the moving frame. Consequently, the size of the subdomains shrinks in the inertial frame as the black holes spiral closer to each other. This causes the size of the individual apparent horizons to grow in the moving frame, eventually to the point that the innermost spherical shells are completely inside the black holes. When this occurs, the innermost subdomains become decoupled from the remainder of the computational domain and can thus be dropped. Because the magnitude of the constraint violations is greatest near the black holes, this accounts for the sharp decreases in the curves in Fig. 3.7 at the aforementioned times. The occasional discarding of the innermost spheres is also performed in the second-order system for the same reasons. However, the lack of similar cusps in the constraint violations when this is done implies that the greatest constraint violations in the second-order evolutions do not occur on the innermost spheres.

Another obvious difference between the first- and second-order evolutions in Fig. 3.7 is the significant drop in constraint violations in the first-order code at $t \sim 1000\,M_c$ and again at $t \sim 3000\,M_c$, which does not occur in the second-order evolutions. This is a consequence of the junk radiation leaving the domain at a time roughly equal to the light-crossing time of the entire domain. The second drop occurs around three light-crossing times and can be understood on the basis of reflections reaching the outer boundary for the second time.

The fact that the second-order constraints do not similarly decrease suggests that the violations are in some sense trapped in the domain and then slowly damped away. However, it should be remembered that the gauge constraint violations in the two systems are not entirely equivalent, since they are computed from Φ_{iab} in the first-order system and from $\partial_i \psi_{ab}$ in the second-order code. As discussed in the single black hole case in Section 3.3.2, this can account for the initial ($t \lesssim 1000\,M_c$) difference in magnitude of the constraints, which are larger in the second-order system. Figure 3.8 shows the gauge constraint violations in the first- and second-order systems for the medium resolution N4 case, along with the volume L_2 norm of the 'three-index' constraint C_{iab} of Eq. (3.13) for the first-order system. It is clear that the difference in the way the gauge constraints are computed (using Φ_{iab} versus $\partial_i \psi_{ab}$) can explain the difference in magnitude of $||C_a||$ between the two systems.

The instability that occurs in the high resolution second-order evolution shown in Fig. 3.7 around $t \sim 6600\,M_c$ is the result of rapid constraint growth arising first on the blocks. However, the slower constraint growth that is evident beginning around $t \sim 4000\,M_c$ occurs on the cylinders and 'innermost' outer spheres. Figure 3.9 shows the volume L_2 constraint violations for this evo-

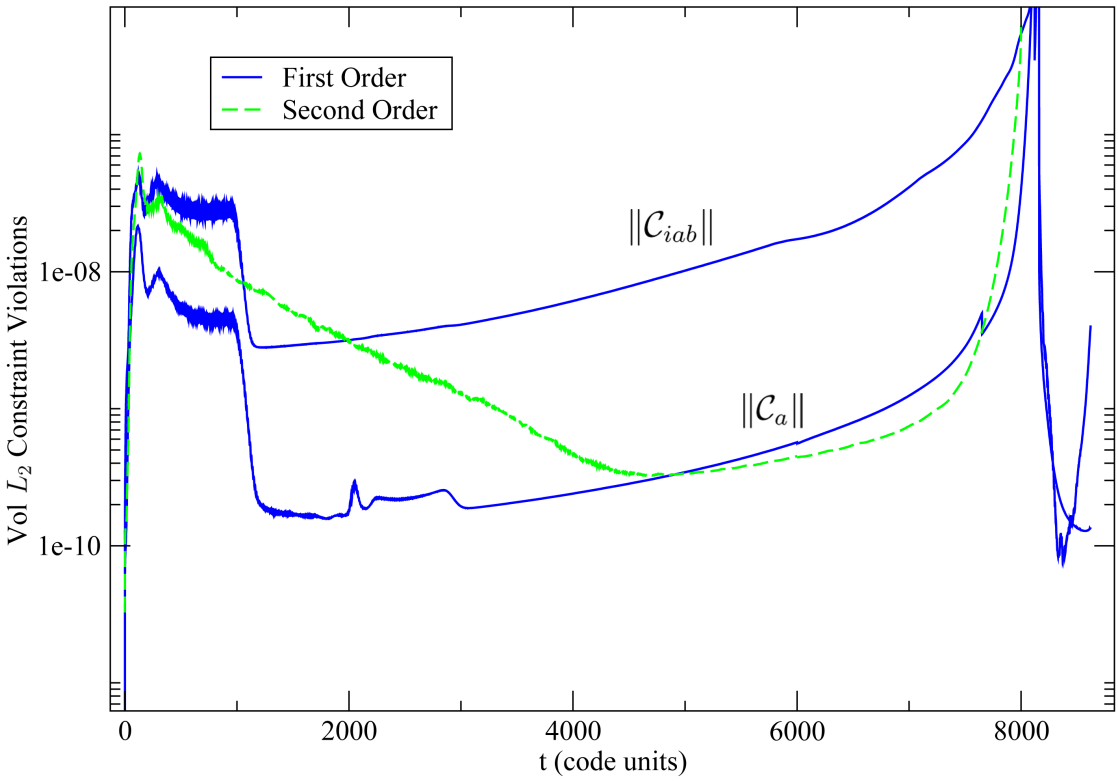

Figure 3.8: The volume L_2 gauge constraint violations $||C_a||$ for the first- and second-order systems along with the three-index constraint violations $||C_{iab}||$ for the first-order system on the entire domain as a function of code time for the medium resolution N4 binary evolution.

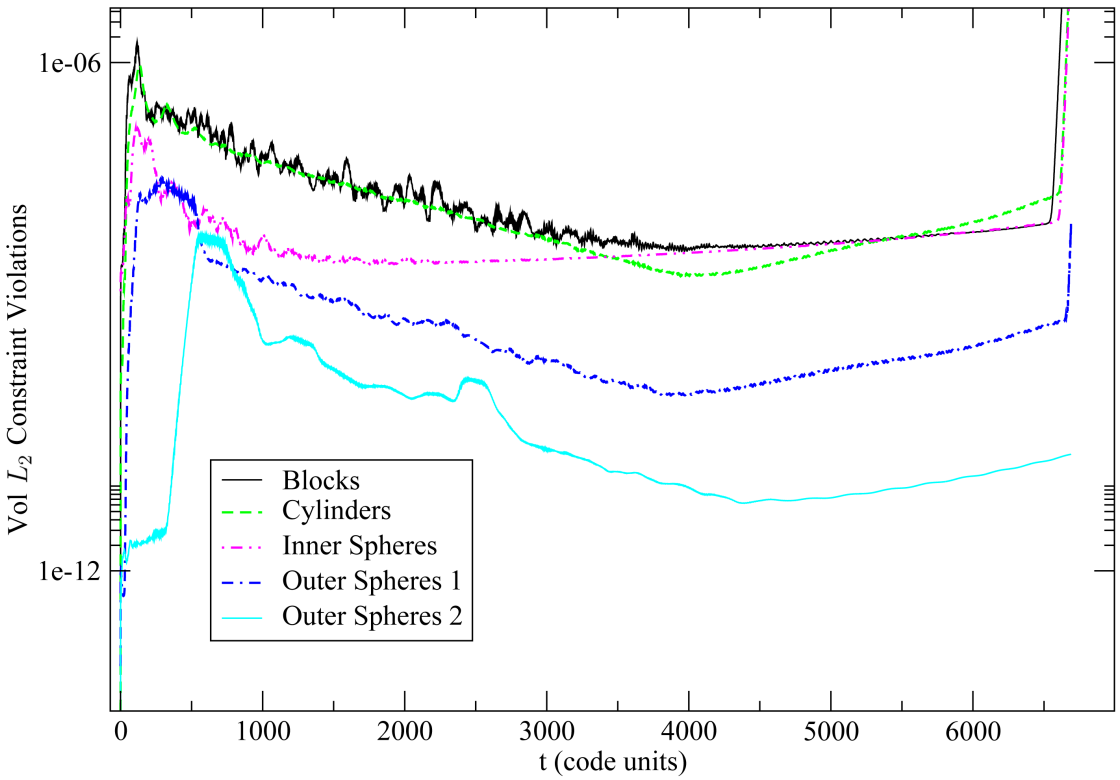

Figure 3.9: The volume L_2 gauge constraint violations $\|C_a\|$ for the high resolution N6 second order binary evolution on various parts of the domain. Outer spheres 1 and 2 refer to the first and second 10 of the 20 outer spherical shells, respectively.

lution on various parts of the domain. Recall that there are 20 'outer' spherical shells. The constraint magnitudes on the inner 10 of these are presented separately from those on the outer 10 shells. The innermost of the 20 spherical shells overlaps the outermost cylinders and blocks, so it is no surprise that constraint violations growing on the cylinders would appear in the spherical shells as well. The fact that this constraint growth is not apparent on the blocks is understandable as well, because the constraint violations there are significantly larger and hence the small increase would not be noticeable.

We do not yet understand the cause of the constraint growth beginning around $t \sim 4000\,M_c$ on the cylinders, although upon closer inspection it is clear

that it occurs on the outermost cylinders. We believe the likely cause of this is in fact the penalty characteristic speed modification discussed above, which was imposed empirically in order to control late time instabilities occurring on the blocks at lower resolutions. Recall that the modification is imposed when the characteristic speed of U^-_{ab} on an edge drops below 0.1, which indeed occurs on the outermost cylinders as early as about 4000 M_c.

Although we have not yet attempted a high resolution evolution without the speed modification to verify this as the cause of the initial constraint growth, it does not explain the instability that occurs later at $t \sim 6600\, M_c$, or rather why the penalty modification eliminates the instabilities at low but not high resolution. As mentioned above, the time at which the characteristic speeds on edges or corners of the subdomains change signs is resolution dependent, because the normal vectors there are defined as weighted sums of adjacent face normals. As the resolution of the domain decomposition is increased from N2 to N6, the number of grid points along different dimensions of the subdomains does not increase by the same proportion. Therefore, the normal vectors on edges and corners change direction as the resolution is increased, which could explain why the instability on the blocks occurs earlier at higher resolution.

We have examined the spectral coefficients on the subdomains where the constraints blow up, including the outer cylinders in the high resolution case. The unstable modes are predominantly lower order, which implies that additional filtering of the spectral expansion would be of no help. However, this is reminiscent of the instabilities related to constraint damping discussed in Section 3.3.3 for the single black hole case. Therefore, it is plausible that the problem could be alleviated by adjusting the domain decomposition, subdomain resolu-

tions, and constraint damping factors. Clearly, much remains to be explored in this problem, but for now we will turn to a discussion of how well the second-order method performs during the first 10 orbits, prior to the high resolution instabilities.

Despite the problems at higher resolution, the second-order results are fairly good for a significant fraction of the inspiral. Figure 3.10 shows the proper separation (in code units) of the black hole horizons for the first- and second-order low resolution N2 evolutions. The proper separation is computed by numerically integrating the line element $\sqrt{\gamma_{xx}}\,dx$ along the x axis connecting the centers of the black holes from the point where the axis intersects one apparent horizon to the other. It is evident from the figure that the low resolution second-order evolution yields a similar inspiral rate to the first-order case and gets essentially as close to merger prior to crashing.

The medium resolution N4 case gives similar results. Figure 3.11 shows the convergence of the proper separation as compared with the first-order N6 resolution. It is clear that the second order lower resolutions N2 and N4 perform equally as well as the first-order code (N2 is a little worse, while N4 is a little better). As is expected based on the high resolution convergence and stability problems, the N6 second-order evolution does no better than the N4 case after $t \sim 3000\,M_c$ (the curve ends at $6600\,M_c$ when the code crashes).

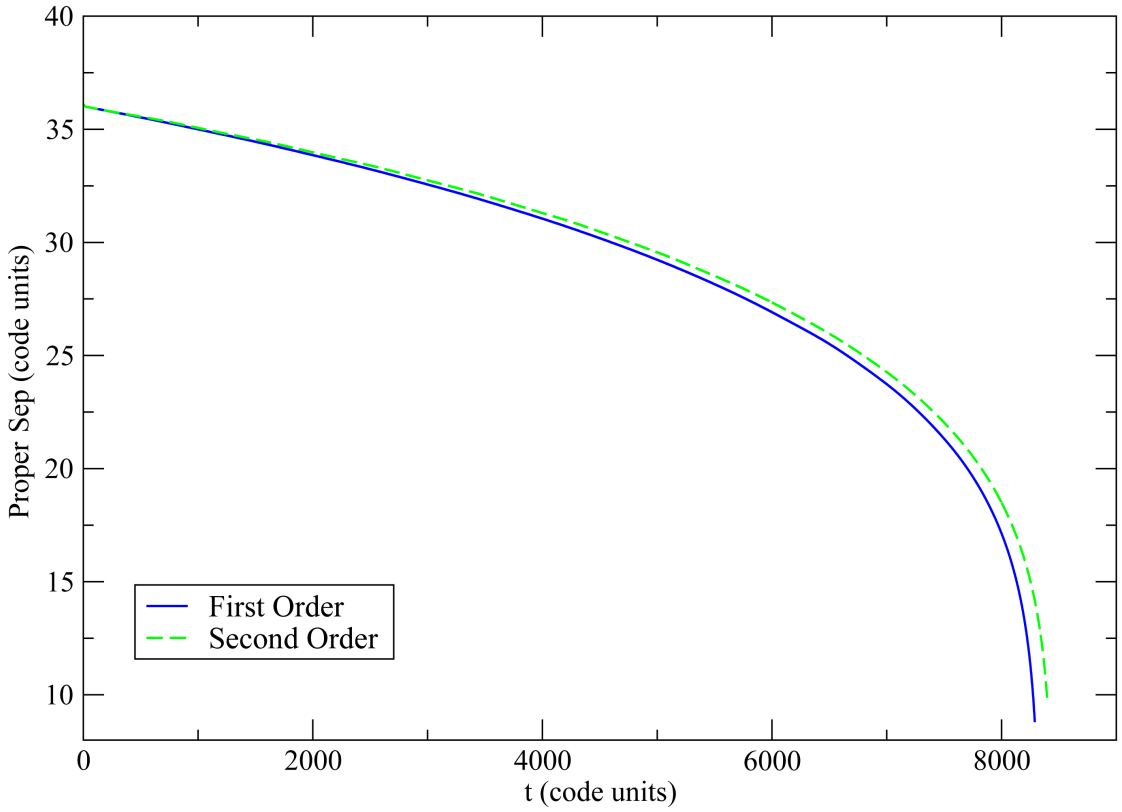

Figure 3.10: Proper separation of the black hole apparent horizons for the first- and second-order low resolution N2 evolutions in code units (M_c).

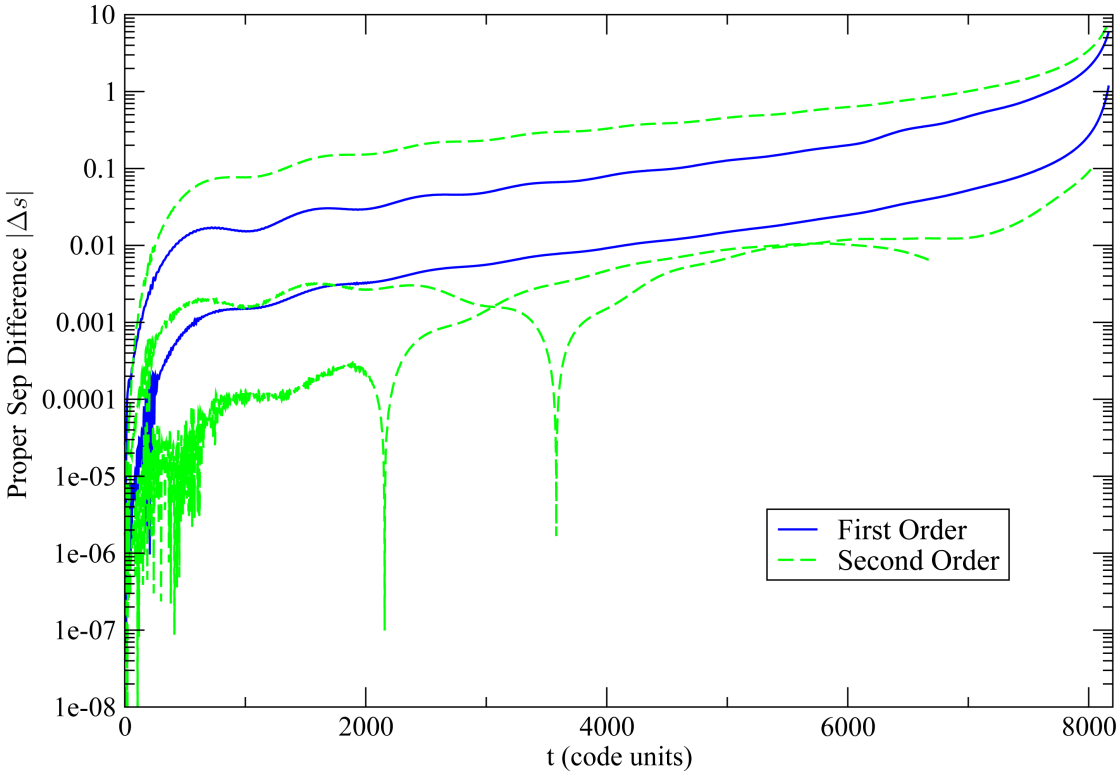

Figure 3.11: The difference $|\Delta s|$ in proper separation (in code units M_c) of the black hole apparent horizons for various resolutions compared with the high resolution N6 first-order evolution. The plot shows results for the first-order N2 and N4 and the second-order N2, N4, and N6 resolutions.

We have also compared gravitational waves extracted at a fixed coordinate radius in the first- and second-order systems. This is done using the Newman-Penrose scalar Ψ_4. The procedure is identical to that described in Ref. [16], which we now summarize. The scalar Ψ_4 is defined as the component of the Weyl curvature tensor

$$\Psi_4 \equiv -C_{abcd}\, l^b\, l^d\, \bar{m}^a \bar{m}^c, \tag{3.51}$$

where the null vectors l^a and m^a are defined as

$$l^a \equiv \frac{1}{\sqrt{2}}(t^a - r^a), \tag{3.52}$$

$$m^a \equiv \frac{1}{\sqrt{2}\, r}\Big(\partial_\theta + i\, \frac{1}{\sin\theta}\partial_\phi\Big)^a, \tag{3.53}$$

and where the bar in Eq. (3.51) represents complex conjugation. Here, t^a is the future-directed timelike unit normal vector to the constant time hypersurfaces, and r^a is the outgoing radial unit vector. The variables (r, θ, ϕ) in Eq. (3.53) represent the usual spherical coordinates in the inertial frame.

The quantity Ψ_4 is computed on a fixed coordinate radius 'extraction sphere' and then expanded on a basis of spin-weighted spherical harmonics:

$$\Psi_4 = \sum_{lm} \Psi_4^{lm}(t, r)\, {}_{-2}Y_{lm}(\theta, \phi). \tag{3.54}$$

We compute the dominant mode $\Psi_4^{(2,2)}$ and calculate the amplitude and phase according to

$$\Psi_4^{(2,2)} = A(r, t)\, e^{-i\phi(r,t)}. \tag{3.55}$$

Figure 3.12 shows the waveform for the medium resolution N4 second-order evolution, extracted at a radius $r = 200\, M_c$. The spike in the waveform at early times is caused by the initial pulse of the junk radiation.

Figure 3.13 shows the convergence of the phase defined by Eq. (3.55) for the waveform extracted at $r = 200\, M_c$ compared with the same waveform extracted

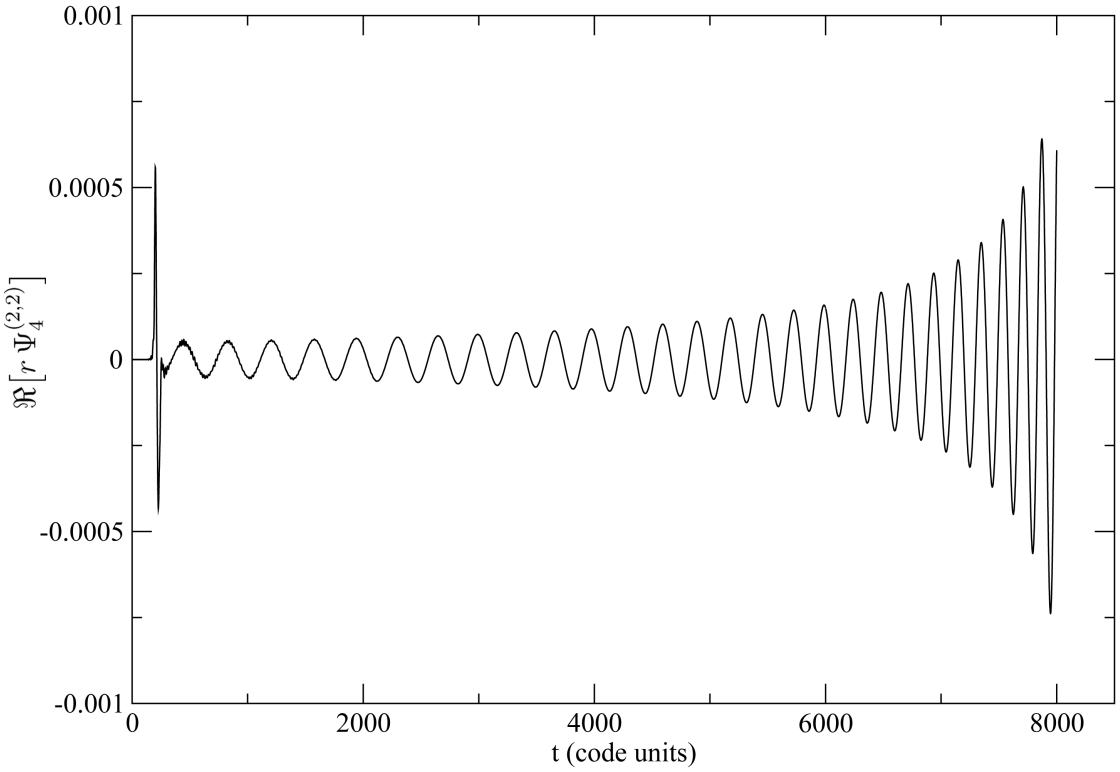

Figure 3.12: Gravitational waveform (real part of $r\,\Psi_4^{(2,2)}$) extracted at $r = 200\,M_c$ in the medium resolution N4 second-order evolution.

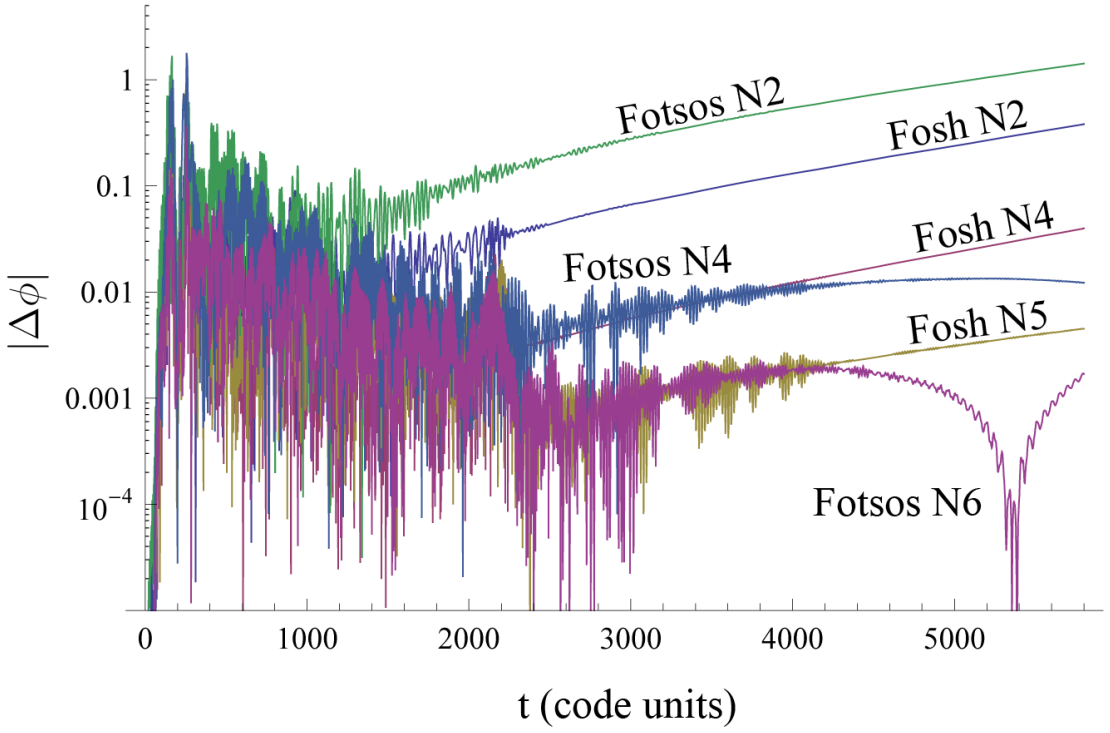

Figure 3.13: Phase difference of $r\,\Psi_4^{(2,2)}$ extracted at $r = 200\,M_c$ compared with the high resolution N6 first-order evolution for several resolutions of the first-order (Fosh) and second-order (Fotsos) systems.

from the high resolution N6 first-order evolution. Included on the plot are results for lower resolution first-order evolutions as well. In this figure, no time or phase shift has been performed. The noise at early times is a result of junk radiation, which takes several crossing times to completely leave the domain.

It is evident that the second-order waveforms are somewhat noisier, particularly at the medium resolution N4. However, it is equally clear that the second-order waveform convergence is comparable to that of the first-order system, at least for the time interval presented in the figure. By time $t \sim 6000\,M_c$ (about 10 orbits), the accumulated phase difference in the second-order system compared with the high resolution first-order evolution is $\Delta\phi \lesssim .01$ at medium and $\Delta\phi \lesssim .001$ at high resolution.

3.5 Discussion

The single black hole evolutions show significant speed increase, by as much as a factor of two over the equivalent first-order simulations. In contrast, the binary evolutions show only a 20−25% speed increase in the second-order system. Since we evolve the equations using adaptive explicit time-stepping, however, the efficiency of the code is largely dependent on the CFL limit. Moreover, this limit is not necessarily the same in the first- and second-order systems, even with identical domain decompositions. As discussed in Section 3.3.3, the choice of constraint damping factors γ_0 on multiple subdomains has a significant impact on the stability, and we have found the same to be true of the CFL limit: the efficiency can be optimized through appropriate choice of damping factors and relative resolutions of the subdomains. How these optimized CFL limits would compare between the first- and second-order systems remains to be seen.

As discussed in Section 3.4.5, the instabilities in the second order binary evolutions at high resolution seem to be related to the penalties on edges and corners of the subdomains. Alternative methods of dealing with these boundaries may therefore present possible solutions to the problem. The multi-penalty method is an example of such an alternative. This could potentially sidestep many of the issues by avoiding the need to define normal vectors on subdomain edges and corners. In a multi-penalty method, the penalties that are added to the equations on edges and corners are defined to be the (weighted) sum of penalties at the same points on the adjacent boundary faces. Unfortunately, implementing such a method in the second-order system has been unsuccessful: all attempts to date have become unstable before $t \sim 4000\, M_c$ for reasons that are not yet understood. Another potential solution to the problems on edges and

corners (in particular on blocks) is to use cylinders along the x axis instead of blocks, as is done in the first-order domain decomposition. However, the second order method must first be generalized to the appropriate form for Gauss-Radau grids as discussed in Section 3.4.4, and this has not yet been done.

There are of course a number of other things that could be related to the instabilities in the binary evolutions. For example, it is possible that the continuity term $\delta\psi_{ab}$ discussed in Section 3.3.2 should scale with resolution in some way. Also, the auxiliary boundary variable method of imposing outer boundary conditions may have impacted the well-posedness of the scheme. This is unlikely, however, since the constraint violations on the outermost spheres in Fig. 3.9 do not display significant growth. We believe that the most promising course of action is to adjust the domain decomposition and constraint damping factors. Based on our experience with the single black hole evolutions discussed in Section 3.3, we feel that it is likely that the second order binary system could be stabilized by suitably modifying these parameters.

We have successfully evolved the second order in space Einstein equations spectrally for single black hole initial data, obtaining good stability and convergence. This relied on including the continuity term $\delta\psi_{ab}$ in the penalties and selecting appropriate constraint damping factors. The second order binary black hole evolutions at low and medium resolution show remarkably good agreement with the first-order results for as much as 15 orbits. At high resolution though, there remain stability and convergence issues that we do not yet fully understand. We are actively exploring the possible solutions to these problems, however, and we are confident that they can be overcome.

APPENDIX A

GAUSS-LEGENDRE-LOBATTO QUADRATURE

Here we provide some of the properties of Gauss-Legendre-Lobatto quadrature [19]. The basis functions on $[-1, 1]$ are the Legendre polynomials $P_n(x)$. This is a convenient choice for obtaining analytical results because the Legendre polynomials are orthogonal with a weighting function of unity:

$$\int_{-1}^{1} \rho(x) P_n(x) P_m(x)\, dx = \frac{2}{2n+1}\, \delta_{nm}, \tag{A.1}$$

with $\rho(x) = 1$. The $(N + 1)$-point quadrature rule,

$$\int_{-1}^{1} u(x)\, dx \simeq \sum_{i=0}^{N} \omega_i\, u(x_i), \tag{A.2}$$

is exact if $u(x)$ is a polynomial of degree $2N-1$ or less. The $N+1$ nodes x_i are

$$x_0 = -1, \tag{A.3}$$

$$x_N = +1, \tag{A.4}$$

$$x_i = \text{the roots of } P'_N(x) \text{ for } 0 < i < N, \tag{A.5}$$

and the weights ω_i are given by

$$\omega_i = \frac{2}{N(N+1)[P_N(x_i)]^2}. \tag{A.6}$$

Note that there is no known explicit formula for the roots of $P'_N(x)$—they must be found numerically. A function $\psi(x)$ is approximated by an N^{th}-order interpolating polynomial $\psi_N(x)$, which can be written

$$\psi_N(x) = \sum_{i=0}^{N} \psi(x_i) C_i(x), \tag{A.7}$$

where $C_i(x)$ are cardinal functions satisfying $C_i(x_j) = \delta_{ij}$. They are given by

$$C_i(x) = \frac{-(1-x^2)P'_N(x)}{N(N+1)P_N(x_i)(x-x_i)}. \tag{A.8}$$

Differentiation can be computed via matrix multiplication from

$$\psi'_N(x_i) = \sum_{j=0}^{N} D^{(1)}_{ij} \psi(x_j), \tag{A.9}$$

where $D^{(1)}_{ij} \equiv C'_j(x_i)$ is the first-order differentiation matrix. The second-derivative matrix is defined similarly and satisfies $D^{(2)} = D^{(1)}D^{(1)}$. An efficient algorithm for computing pseudo-spectral differentiation matrices is given in Ref. [20].

If f, g are two N^{th}-order polynomials, summation by parts follows naturally because the product fg' is a polynomial of order $2N-1$ or less:

$$\langle f, g' \rangle = \sum_{i=0}^{N} \omega_i f_i \, g'_i \tag{A.10}$$

$$= f_i \, g_i \Big|_{i=0}^{N} - \langle f', g \rangle. \tag{A.11}$$

Summation by parts generalizes to higher dimensional inner products in a straightforward way. For example, if f and g are 2-d polynomials in x and y:

$$\langle \partial_x f, g \rangle = \sum_{i,j=0}^{N} \omega_i \omega_j (\partial_x f)_{ij} \, g_{ij} \tag{A.12}$$

$$= \sum_{j=0}^{N} \omega_j (fg) \Big|_{i=0}^{N} - \langle f, \partial_x g \rangle. \tag{A.13}$$

APPENDIX B

PROOF OF INABILITY TO GENERALIZE 1D PENALTY FUNCTION

In this section we will show that in two or more dimensions the inner product

$$\langle \partial^i \partial_i \psi, p \rangle \tag{B.1}$$

arising in the energy arguments cannot be made to vanish in general with a penalty function p that satisfies the boundary conditions. We will argue by counting degrees of freedom. For simplicity, consider the two-dimensional case and let our domain be a square with $N+1$ grid points along each dimension.

Instead of using a basis of Legendre polynomials, we will consider a (non-orthogonal) basis of functions $x^i y^j$. A scalar field is thus approximated on the grid as a two-dimensional interpolating polynomial of the form

$$\psi = \sum_{0 \le i,j \le N} a_{ij} x^i y^j. \tag{B.2}$$

There are $(N+1)^2$ basis functions and hence the same number of degrees of freedom in the function ψ. The penalty function p must satisfy $4N$ boundary conditions on the square.

Now consider operating on the expansion of ψ in Eq. (B.2) with the Laplacian $\partial_x^2 + \partial_y^2$. The effect of this operation on a term $x^i y^j$ is essentially

$$x^i y^j \to x^{i-2} y^j + x^i y^{j-2}. \tag{B.3}$$

Since we are only interested in counting the degrees of freedom that remain in $\nabla^2 \psi$, we only need to retain one of the terms in Eq. (B.3):

$$x^i y^j \to x^{i-2} y^j. \tag{B.4}$$

By doing this, we will at worst undercount the degrees of freedom in $\nabla^2\psi$. We are left with terms of the form $x^{i-2}y^j$ for $2 \le i \le N$ and $0 \le j \le N$, which implies that there are at least $(N+1)(N-1)$ degrees of freedom remaining in the Laplacian.

There are thus at most $(N+1)^2 - (N+1)(N-1) = 2N+2$ degrees of freedom for constructing a penalty function that is orthogonal to $\nabla^2\psi$, which is not enough to satisfy the $4N$ boundary conditions. The same argument can be applied in any number of dimensions. In particular, in the three-dimensional case we find that there are at most $2(N+1)^2$ degrees of freedom for constructing the penalty function—not enough to satisfy the $6N^2+2$ boundary conditions, which proves the assertion made below Eq. (2.92).

APPENDIX C

DERIVATION OF 3D PENALTY FUNCTION

In this section the form of the three-dimensional bulk penalty given by Eq. (2.95) will be derived. The goal is to minimize the inner product

$$\langle \partial^i \partial_i \psi, p \rangle, \tag{C.1}$$

with the values of the penalty function p on the boundary given. First, we will revisit the one-dimensional problem on the interval $[-1, 1]$ from a new point of view. In Section 2.2.3 it was shown that the one-dimensional inner product vanishes when p is constructed out of the functions f, g defined in Eqs. (2.61)-(2.62). The functions f and g were constructed out of P_N and P_{N-1} so that they would automatically be orthogonal to ψ''.

Let us start over and consider the penalty function p to be unspecified, except on the boundaries. Suppose also that there is no boundary condition at $x_N = +1$, so the penalty function satisfies $p_N = 0$. The boundary condition at $x_0 = -1$ fixes the value p_0, and we can view the values p_i for $0 < i < N$ as free parameters for minimizing the inner product:

$$\langle \psi'', p \rangle = \omega_0 \psi_0'' p_0 + \sum_{i=1}^{N-1} \omega_i \psi_i'' p_i. \tag{C.2}$$

This will vanish if and only if

$$\psi_0'' = \sum_{i=1}^{N-1} \Big(\frac{-\omega_i p_i}{\omega_0 p_0} \Big) \psi_i'', \tag{C.3}$$

where it is safe to assume $p_0 \neq 0$ (if $p_0 = 0$, then $p = 0$ as there would be no need for a penalty function). Since $\psi''(x)$ is an *arbitrary* $(N-2)$-order polynomial, this equation defines the ideal interpolation weights $c_0(x_i)$ for approximating a

function at $x_0 = -1$ based on its values over a stencil of points x_i for $0 < i < N$:

$$\psi_0'' = \sum_{i=1}^{N-1} c_0(x_i)\, \psi_i''. \tag{C.4}$$

Assuming the grid points are Gauss-Legendre-Lobatto points, we can therefore make the identification

$$c_0(x_i) = -\frac{\omega_i p_i}{\omega_0 p_0} = -\frac{\omega_i}{\omega_0} f_i, \tag{C.5}$$

where f_i are the grid values for $0 < i < N$ of the function f defined in Eq. (2.61) and we have used the fact that Eq. (C.3) holds when the penalty p is defined by Eq. (2.63).

The case with a boundary condition at $x = +1$ and no boundary condition at $x = -1$ ($p_0 = 0$) is similar, and we can thus conclude that the interpolation weights $c_N(x_i)$ for approximating a function at $x_N = +1$ based on its values over a stencil of points x_i for $0 < i < N$ are given by

$$c_N(x_i) = -\frac{\omega_i}{\omega_N} g_i, \tag{C.6}$$

where g_i are the grid values for $0 < i < N$ of the function g defined in Eq. (2.62).

Now let us consider the two-dimensional problem on the square $[-1, 1] \times [-1, 1]$. In the following we will use the index i exclusively for summing over x values and j for y. Our goal is to construct the values of p on the interior of the domain so as to minimize the inner product

$$\langle \Delta\psi, p \rangle = \sum_{ij} \omega_i \omega_j \Delta\psi_{ij} p_{ij}, \tag{C.7}$$

where Δ represents the Laplacian operator $\partial^i \partial_i$, and we consider the values of p on the boundary to be given. Consider a point on the edge at (x_0, y_j), for example. The term in the inner product due to this point is

$$\omega_0 \omega_j \Delta\psi_{0j} p_{0j}. \tag{C.8}$$

Now define p on the interior along the j^{th} row to be

$$p_{ij} = p_{0j} f_i, \tag{C.9}$$

just as in one dimension. Using the identification of f as interpolation weights from Eq. (C.5), the contribution to the inner product from the interior of this row is

$$\langle \Delta\psi, p \rangle \Big|_{j^{\text{th}}\text{row}} = \sum_{i=1}^{N-1} \omega_i \omega_j \Delta\psi_{ij} p_{ij} \tag{C.10}$$

$$= -\omega_0 \omega_j p_{0j} \sum_{i=1}^{N-1} \Delta\psi_{ij}\, c_{0i} \tag{C.11}$$

$$\simeq -\omega_0 \omega_j \Delta\psi_{0j} p_{0j}, \tag{C.12}$$

which approximately cancels the term from the point on the edge in Eq. (C.8). In Eq. (C.11) we have written c_{0i} for the interpolation weights $c_0(x_i)$ defined in Eq. (C.5). Next, consider a point at a corner, say (x_N, y_0). The term in the inner product due to this point is

$$\omega_N \omega_0 \Delta\psi_{N0}\, p_{N0}. \tag{C.13}$$

Define p on the interior of the domain to be

$$p_{ij} = -p_{N0}\, g_i f_j. \tag{C.14}$$

The contribution from this term to the inner product on the interior of the square is therefore

$$\langle \Delta\psi, p \rangle \Big|_{\text{interior}} = \sum_{i,j=1}^{N-1} \omega_i \omega_j \Delta\psi_{ij}\, p_{ij} \tag{C.15}$$

$$= -\omega_N \omega_0\, p_{N0} \sum_{i,j=1}^{N-1} \Delta\psi_{ij}\, c_{Ni} c_{0j} \tag{C.16}$$

$$\simeq -\omega_N \omega_0 \Delta\psi_{N0}\, p_{N0}, \tag{C.17}$$

which approximately cancels the contribution from the point on the corner in Eq. (C.13). Following this procedure, we construct p on the interior by adding a contribution from each boundary segment: 4 edges and 4 corners on this 2-d domain. Explicitly, we obtain

$$\begin{aligned} p_{ij} = p_{0j} f_i + p_{Nj}\, g_i + p_{i0} f_j + p_{iN}\, g_j \\ - p_{00} f_i f_j - p_{0N} f_i g_j - p_{N0}\, g_i f_j - p_{NN}\, g_i g_j. \end{aligned} \tag{C.18}$$

This generalizes to three or more dimensions in a straightforward way. Each term in p_{ij} has a number of products of f or g equal to the codimension of the boundary segment it depends on. The only caveat is that the sign of the terms added to p should be $(-1)^{m+1}$, where m is the codimension of the boundary piece producing the term. This is evident in the 2-d example above where the terms in Eq. (C.18) due to the corners are negative. The sign difference arises simply because of the negative sign in the relation between the interpolation weights c_0, c_N and the functions f, g in Eqs. (C.5)-(C.6).

We have therefore shown that with p constructed according to this procedure, the inner product of p with *any* analytic function h (hence $\Delta\psi$) satisfies

$$\langle h, p \rangle \to 0, \quad \text{as} \quad N \to \infty. \tag{C.19}$$

In particular, we have shown that the last term in Eq. (2.92) asymptotically vanishes as claimed below Eq. (2.95). Moreover, while we have not bounded the error for a given resolution, the inner product in Eq. (C.19) will be as small as possible in the sense that it vanishes for the polynomial approximations to h up to order $N - 2$.

APPENDIX D

PENALTIES FOR TIME DERIVATIVE BOUNDARY CONDITIONS

In this section we describe the use of penalties to impose a type of Bjørhus boundary condition in the second-order system. For simplicity, we will illustrate the idea for the one-dimensional scalar wave on the interval $[-1, 1]$ with $1 + N$ collocation points. The case with a condition on the incoming mode $U_- = U_-^{\mathrm{BC}}$ at both boundaries was treated in Section 2.2.3, where we derived the bulk penalty p in terms of functions $f(x)$ and $g(x)$ defined by Eqs. (2.61)-(2.62).

Now suppose that we have the usual boundary condition at $x = -1$, but that at $x = +1$ we have a condition on the time derivative of the incoming mode:

$$U_-(-1) = U_-^{\mathrm{BC}}, \tag{D.1}$$

$$\dot{U}_-(+1) = \dot{U}_-^{\mathrm{BC}}. \tag{D.2}$$

The projection to fundamental variables at $x = +1$ gives

$$\dot{\psi}' = \frac{1}{2}(\dot{U}_+ - \dot{U}_-^{\mathrm{BC}}), \tag{D.3}$$

$$\dot{\pi} = \frac{1}{2}(\dot{U}_+ + \dot{U}_-^{\mathrm{BC}}). \tag{D.4}$$

The usual Bjørhus method simply sets the time derivatives of the fundamental variables on the boundary according to these conditions. In the second-order system, however, equation (D.3) determines $\dot{\psi}'$ instead of $\dot{\psi}$. In the first-order system this would be a condition on $\dot{\phi}$, and there would be no difficulty.

The idea is to define a penalty function p whose derivative p' allows Eq. (D.3) to be satisfied via

$$\dot{\psi}' = -\pi' + p'. \tag{D.5}$$

Following the arguments of Section 2.2.3, we wish to construct p out of Legendre polynomials P_N and P_{N-1} in order to satisfy $\langle \psi'', p \rangle = 0$. We define the functions $\bar{f}$ and $\bar{g}$, analogous to f and g of Eqs. (2.61)-(2.62), such that

$$\bar{f}(-1) = 1, \qquad \bar{f}'(+1) = 0, \tag{D.6}$$

$$\bar{g}(-1) = 0, \qquad \bar{g}'(+1) = 1. \tag{D.7}$$

These conditions uniquely determine the functions. We can then use $\bar{f}$ to enforce the boundary condition at $x = -1$ without interfering with the derivative at $x = +1$. Similarly, $\bar{g}$ can be used for the derivative condition at $x = +1$. The penalty function p is thus defined to be

$$p = p(-1)\,\bar{f}(x) + p'(+1)\,\bar{g}(x). \tag{D.8}$$

With the boundary values

$$p(-1) = -\frac{1}{2}\,\delta U_-, \tag{D.9}$$

$$p'(+1) = \pi' + \frac{1}{2}\,(\dot{U}_+ - \dot{U}_-^{\mathrm{BC}}), \tag{D.10}$$

the energy argument of Section 2.2.3 is unchanged with respect to terms at $x = -1$, and the Bjørhus condition of Eq. (D.3) is satisfied.

The functions $\bar{f}$ and $\bar{g}$ can easily be found from derivatives of f and g defined in Eqs. (2.61)-(2.62) along with the conditions of Eqs. (D.6)-(D.7). We obtain

$$\bar{f}(x) = f(x) - \frac{(-1)^N}{N}\,g(x), \qquad \bar{g}(x) = \frac{2}{N^2}\,g(x). \tag{D.11}$$

The generalization of this idea to three dimensions is straightforward. In our tests, this method performed well for the three-dimensional scalar wave in flat space, but was quickly unstable in the binary black hole case.

BIBLIOGRAPHY

[1] B.C. Barish and R. Weiss, LIGO and the Detection of Gravitational Waves, Physics Today **52** (Oct.), 44 (1999).

[2] S.J. Waldman, Status of LIGO at the start of the fifth science run, Class. Quantum Grav. **23**, S653 (2006).

[3] F. Acernese et al., The Virgo status, Class. Quantum Grav. **23**, S635 (2006).

[4] K.S. Thorne, Gravitational Radiation – A New Window Onto the Universe, arXiv:gr-qc/9704042v1 (1997).

[5] C. Cutler and K.S. Thorne, An Overview of Gravitational-Wave Sources, arXiv:gr-qc/0204090v1 (2002).

[6] M. Campanelli, C.O. Lousto, Y. Zlochower, B. Krishnan, and D. Merritt, Spin Flips and Precession in Black-Hole-Binary Mergers, Phys. Rev. D **75**, 064030 (2007).

[7] M. Campanelli, C.O. Lousto, Y. Zlochower, Spin-orbit interactions in black-hole binaries, Phys. Rev. D **74**, 084023 (2006).

[8] J.G. Baker, J. Centrella, D.-I. Choi, M. Koppitz, J.R. van Meter, and M.C. Miller, Getting a kick out of numerical relativity, Astrophys. J. **653**, L93 (2006).

[9] J.A. Gonzalez, M.D. Hannam, U. Sperhake, B. Brugmann, and S. Husa, Supermassive recoil velocities for binary black-hole mergers with antialigned spins, Phys. Rev. Lett. **98**, 231101 (2007).

[10] M. Koppitz, D. Pollney, C. Reisswig, L. Rezzolla, J. Thornburg, P. Diener, and E. Schnetter, Recoil Velocities from Equal-Mass Binary-Black-Hole Mergers, Phys. Rev. Lett. **99**, 041102 (2007).

[11] M. Campanelli, C.O. Lousto, Y. Zlochower, and D. Merritt, Maximum gravitational recoil, Phys. Rev. Lett. **98**, 231102 (2007).

[12] T.W. Baumgarte and S.L. Shapiro, Numerical Relativity and Compact Binaries, Phys. Rept. **376**, 41 (2003).

[13] E. Berti, V. Cardoso, J.A. Gonzalez, U. Sperhake, M. Hannam, S. Husa, and B. Bruegmann, Inspiral, merger and ringdown of unequal mass black hole binaries: a multipolar analysis, Phys. Rev. D **76**. 064034 (2007).

[14] Y. Pan, A. Buonanno, J.G. Baker, J. Centrella, B.J. Kelly, S.T. McWilliams, F. Pretorius, and J.R. van Meter, A data-analysis driven comparison of analytic and numerical coalescing binary waveforms: nonspinning case, arXiv:0704.1964v1 [gr-qc] (2007).

[15] L.S. Finn, Detection, Measurement and Gravitational Radiation, Phys. Rev. D **46**, 5236 (1992).

[16] M. Boyle, D.A. Brown, L.E. Kidder, A.H. Mroué, H.P. Pfeiffer, M.A. Scheel, G.B. Cook, and S.A. Teukolsky, High-accuracy comparison of numerical relativity simulations with post-Newtonian expansions, Phys. Rev. D **76**, 124038 (2007).

[17] P. Ajith et al., Phenomenological template family for black-hole coalescence waveforms, Class. Quant. Grav. **24**, S689 (2007).

[18] B. Gustafsson, H.-O. Kreiss, and J. Oliger, *Time Dependent Problems and Difference Methods*, Pure and Applied Mathematics (Wiley, New York, 1995).

[19] J.P. Boyd, *Chebyshev and Fourier Spectral Methods* (Springer-Verlag, Berlin, Germany, 1989).

[20] B. Fornberg, *A Practical Guide to Pseudospectral Methods* (Cambridge University Press, 1998).

[21] F. Pretorius, Evolution of Binary Black-Hole Spacetimes, Phys. Rev. Lett. **95**, 121101 (2005).

[22] J.G. Baker, J. Centrella, D.-I. Choi, M. Koppitz, and J. van Meter, Gravitational-Wave Extraction from an Inspiraling Configuration of Merging Black Holes, Phys. Rev. Lett. **96**, 111102 (2006).

[23] M. Campanelli, C.O. Lousto, P. Marronetti, and Y. Zlochower, Accurate Evolutions of Orbiting Black-Hole Binaries without Excision, Phys. Rev. Lett. **96**, 111101 (2006).

[24] L. Lindblom, M.A. Scheel, L.E. Kidder, R. Owen, and O. Rinne, A New Generalized Harmonic Evolution System, Class. Quant. Grav. **23**, 447 (2006).

[25] M.A. Scheel, M. Boyle, T. Chu, L.E. Kidder, K.D. Matthews, and H.P. Pfeiffer, High-accuracy waveforms for binary black hole inspiral, merger, and ringdown, Phys. Rev. D **79**, 024003 (2009).

[26] C. Gundlach and J.M. Martín-García, Hyperbolicity of second-order in space systems of evolution equations, Class. Quant. Grav. **23**, 387 (2006).

[27] C. Gundlach and J.M. Martín-García, Symmetric hyperbolic form of systems of second-order evolution equations subject to constraints, Phys. Rev. D **70**, 044031 (2004).

[28] C. Gundlach and J.M. Martín-García, Symmetric hyperbolicity and consistent boundary conditions for second-order Einstein equations, Phys. Rev. D **70**, 044032 (2004).

[29] D. Funaro and D. Gottlieb, A New Method of Imposing Boundary Conditions in Pseudospectral Approximations of Hyperbolic Equations, Math. Comp. **51**, 599 (1988).

[31] M. Bjørhus, The ODE Formulation of Hyperbolic PDEs Discretized by the Spectral Collocation Method, SIAM J. Sci. Comput. **16**, 542 (1995).

[32] L. Lehner, O. Reula, and M. Tiglio, Multi-block simulations in general relativity: high order discretizations, numerical stability, and applications, Class. Quant. Grav. **22**, 5283-5322 (2005).

[33] W.S. Don and D. Gottlieb, The Chebyshev-Legendre Method: Implementing Legendre Methods on Chebyshev Points, SIAM J. Numer. Anal. **31**, 1519 (1994).

[34] J.S. Hesthaven and D. Gottlieb, A Stable Penalty Method for the Compressible Navier-Stokes Equations: I. Open Boundary Conditions, SIAM J. Sci. Comput. **17**, 579 (1996).

[35] M.A. Scheel, A.L. Erickcek, L.M. Burko, L.E. Kidder, H.P. Pfeiffer, and S.A. Teukolsky, 3D simulations of linearized scalar fields in Kerr spacetime, Phys. Rev. D **69**, 104006 (2004).

[36] K. Martel and E. Poisson, Regular coordinate systems for Schwarzschild and other spherical spacetimes, Am. J. Phys. **69**, 476 (2001).

[37] T. Matsushima and P.S. Marcus, A Spectral Method for Polar Coordinates, J. Comp. Phys. **120**, 365-374 (1995)

[38] W. Tichy, Black hole evolution with the BSSN system by pseudo-spectral methods, Phys. Rev. D **74**, 084005 (2006).

[39] C. Gundlach, G. Calabrese, I. Hinder, and J.M. Martín-García, Constraint damping in the Z4 formulation and harmonic gauge, Class. Quant. Grav. **22**, 3767 (2005).

[40] L.E. Kidder, L. Lindblom, M.A. Scheel, L.T. Buchman, and H.P. Pfeiffer, Boundary Conditions for the Einstein Evolution System, Phys. Rev. D **71**, 064020 (2005).

[41] K.S. Thorne, Multipole expansions of gravitational radiation, Rev. Mod. Phys. **52**, No. 2, Part I (1980).

[42] L.E. Kidder, M.A. Scheel, S.A. Teukolsky, E.D. Carlson, and G.B. Cook, Black hole evolution by spectral methods, Phys. Rev. D **62**, 084032 (2000).

[43] M.A. Scheel, H.P. Pfeiffer, L. Lindblom, L.E. Kidder, O. Rinne, and S.A. Teukolsky, Solving Einstein's Equations With Dual Coordinate Frames, Phys. Rev. D **74**, 104006 (2006).